Emilie Udnæs

Antenna Design for UHF Satellite Communication from Sensor Nodes in the Arctic

Master's thesis in Electronics Systems Design and Innovation
Supervisor: Egil Eide
June 2019

Master's thesis

NTNU
Norwegian University of Science and Technology
Faculty of Information Technology and Electrical Engineering
Department of Electronic Systems

NTNU
Norwegian University of
Science and Technology

Emilie Udnæs

Antenna Design for UHF Satellite Communication from Sensor Nodes in the Arctic

Master's thesis in Electronics Systems Design and Innovation
Supervisor: Egil Eide
June 2019

Norwegian University of Science and Technology
Faculty of Information Technology and Electrical Engineering
Department of Electronic Systems

NTNU
Norwegian University of
Science and Technology

Summary

The objective of this thesis has been to evaluate whether a feasible and practical antenna can be designed and implemented for the retrieval of 2-200GB/year of data from sensor nodes in the Arctic, using small satellites at Ultra High Frequency. Two use cases were selected to define the design constraints. The first use case is HYPSO (HYPer-spectral Smallsat for ocean Observation), the small satellite that NTNU will be launching in 2020 into a Low Earth Orbit. Its secondary payload is a Software Defined Radio that aims to provide better communication systems in the Arctic. The second use case is Arctic ABC, a research program that develops sensor nodes in the Arctic generating large amounts of data. Different antenna types were evaluated considering that they should weigh less than 50kg, be less than $1 \times 1 \times 1 m^3$ in size, stay mechanically fixed (i.e. antenna pointing mechanism is not possible) and have a gain of 2-10dBi. It was concluded that an array of four Inverted-F Antennas with a feed system such that it generates circular polarization, has the potential to fulfill the requirements of the project. The antenna array was designed for 400MHz and the results of the simulations show that the antenna has a maximum realized gain of 4dBi in the direction of a satellite appearing 45° above the horizon. The radiation pattern has a conical shape with a dip in zenith where the gain decreases to -3dBi. Based on the link budget and the results of the simulations, it was concluded that in a year, a total of $\sim$10GB of data can be collected from sensor nodes located north of Longyearbyen, using HYPSO. However, because of ionospheric activity in the atmosphere as well as other loss factors, the data throughput can be expected to be between 2GB and 11GB. A prototype of the antenna was fabricated and tested using facilities and equipment available at NTNU. The test results show that the radiation pattern is not as similar to the simulations as expected. Future work to test the gain, temperature tolerance and polarization characteristics of the antenna prototype is suggested in order to validate whether the antenna is suitable for implementation in the Arctic.

Sammendrag

Målet med denne avhandlingen har vært å vurdere om en praktisk antenne kan designes og implementeres til innsamling av 2-200GB data i løpet av et år, fra sensornoder i Arktis. Dataen vil sendes via småsatellitt på Ultra Høy Frekvens. To spesifikke brukstilfeller definerer designbegrensningene. Første brukstilfelle er HYPSO (HYPer-spectral Smallsat for ocean Observation), en småsatellitt NTNU skal skyte opp i en lav jordbane i 2020. Satelitten har en programvare-definert radio som sekundær nyttelast. Den skal sørge for bedre kommunikasjonsmuligheter i Arktis. Det andre brukstilfelle er Arctic ABC, et forskningsprogram som utvikler sensornoder i Arktis som genererer store menger data. Ulike antennetyper ble vurdert med tanke på at de burde veie mindre enn 50kg, være mindre enn $1\times1\times1\text{m}^3$ i størrelse, være låst mekanisk (dvs. mekanisk styring er ikke mulig) og ha en antennevinning på 2-10dBi. Det ble konkludert at en antennegruppe på fire inverted-F antenner med et matningssystem slik at det genererer sirkulær polarisasjon, har potensialet til å oppfylle kravene i prosjektet. Antennen ble designet for 400MHz, og resultatene av simuleringene viser at den har en maksimal realisert antennevinning på 4dBi i retning av en satellitt som kommer til syne 45° over horisonten. Strålingsdiagrammet har en konisk form med et lavpunkt i senit hvor antennevinningen reduseres til -3dBi. Basert på linkbudsjettet og simuleringsresultatene ble det konkludert at totalt $\sim$10GB/år med data kan hentes ut fra sensornoder nord for Longyearbyen, ved hjelp av HYPSO. Grunnet ionosfærisk aktivitet i atmosfæren, samt andre tapsfaktorer, kan datautbyttet imidlertid forventes å være et sted mellom 2GB og 11GB. En prototype av antennen ble produsert og testet ved hjelp av utstyr tilgjengelig på NTNU. Testresultatene viser at strålingsdiagrammet ikke svarer til simuleringene slik som forventet. Fremtidig arbeid for å teste antennevinning, temperaturtoleranse og polariseringsegenskaper av antenneprototypen er foreslått for å validere om antennen er egnet for implementering i Arktis.

Preface

This thesis marks the end of my 5-years Electrical Engineering degree at the Norwegian University of Science and Technology. It has been a great final year, especially because my fellow classmates and other scholars at NTNU have taken their time to share their experiences and knowledge with me. The project has been part of the NTNU SmallSat Lab which aims to bring more of the space-related activities at NTNU together and make them more visible. It has been a real pleasure to be part of the team. A special thanks to Gara Quintana Diaz, Ph.D. candidate at NTNU, for great teamwork on the SDR mission of HYPSO.

The thesis has given me practical experience on the design and fabrication of antennas. I would like to thank Christer Nesset and his team at the "Teleteknisk Verksted" at NTNU for helping me realize my ideas. You have taught me that creativity is the only limit. I have also had the chance to develop expertise on test engineering and antenna measurements. I would like to thank Jens Abraham, Ph.D. candidate at NTNU, for guiding me on measurement techniques and how to use NTNU's anechoic chamber.

Finally, I would like to thank my supervisor, Egil Eide, for his continuous support and feedback. He has inspired me to develop practical experience as well as to use my creativity combined with theoretical knowledge in my designs. With a perfect combination of cheering and critique, I have been able to stay focused and motivated.

Emilie Udnæs
Trondheim, 06.06.2019

Table of Contents

Abbreviations

AIS	=	Automatic Identification System
AR	=	Axial Ratio
ASK	=	Amplitude-Shift Keying
AUT	=	Antenna Under Test
BER	=	Bit Error Rate
CP	=	Circular Polarization
CST	=	Computer Simulation Technology
Cubesat	=	U-class spacecraft
dB	=	Decibel
DEG	=	Degrees
EIRP	=	Effective Isotropic Radiated Power
FEC	=	Forward Error Correction
FIT	=	Finite Integration Technique
FSK	=	Frequency-Shift Keying
GB	=	Gigabyte
HYPSO	=	HYPer-spectral Smallsat for ocean Observation
IFA	=	Inverted-F Antenna
LEO	=	Low Earth Orbit
LNA	=	Low Noise Amplifier
LP	=	Linear Polarization
LTAN	=	Local Time of Ascending Node
MIN	=	Minutes
NKOM	=	Norwegian Communications Authority
NTNU	=	Norwegian University of Science and Technology
PSK	=	Phase-Shift Keying
QHA	=	Quadrifilar Helix Antenna
QPSK	=	Quadrature Phase Shift Keying
RF	=	Radio Frequency
RFID	=	Radio Frequency Identification
SDR	=	Software Defined Radio
SNR	=	Signal-to-noise ratio
STK	=	Systems Tool Kit
UAV	=	Unmanned Autonomous Vehicle
UHF	=	Ultra High Frequency
VDES	=	VHF Data Exchange System
VNA	=	Vector Network Analyzer
YRS	=	Years

Symbols

d	=	Distance between satellite and sensor nodes *or* between shorting and feed of Inverted-F Antenna
f	=	Frequency
e / e_{min}	=	elevation angle / minimum elevation angle
H	=	Orbit height *or* height of Inverted-F Antenna
L_{FS}	=	Free-space path loss
L_{ax}	=	Axial length of Quadrifilar Helix Antenna
N	=	Number of turns of Quadrifilar Helix Antenna
T	=	Temperature
R	=	Earth's radius
θ	=	Angle between two unit vectors *or* phase *or* transformation in elevation plane
G_r/G_t	=	Gain of receiving / transmitting antenna
L_{tot}	=	Total propagation loss
L_p	=	Length of "patch"
W_p	=	Width of "patch"
W_g	=	Width of ground plane
L_g	=	Length of ground plane
T_p	=	Thickness of "patch"
$P_{r_{ant}}$	=	Received power at input of antenna
$P_{r_{rec}}$	=	Received power at input of receiver
L_{fr}	=	Loss between antenna and receiver
$T_{sys,RI}$	=	System noise temperature with reference to the input of the receiver
T_A	=	Antenna temperature
L_F	=	Attenuation factor of feed (cable)
T_F	=	Temperature of feed
T_R	=	Effective input noise temperature of receiver
F_{LNA}	=	Noise factor of Low Noise Amplifier
T_{LNA}	=	Noise temperature of Low Noise Amplifier
T_0	=	290 Kelvin
k	=	Boltzmann's constant *or* design parameter of Quadrifilar Helix Antenna
p	=	Design parameter of Quadrifilar Helix Antenna
r_0	=	Radius of Qaudrifilar Helix Antenna in wavelength
R	=	Distance between receiver and transmitter in a radio system
D_c	=	Distance between element and center of ground plane
G_{min} / G_{max}	=	Minimum / maximum gain
v	=	Velocity
λ	=	Wavelength
Ω	=	Ohm
C/N_0	=	Carrier-to-noise-density ratio
C/N	=	Carrier-to-noise ratio

Chapter 1

Introduction

1.1 Background and Motivation

The marine ecosystem of the Arctic is one of the least known and understood ecosystems of the planet (Vogedes, 2019). The harsh climate is making it difficult to conduct research over long periods of time. Autonomous observational platforms have been developed over the years to make it easier to collect data from isolated Arctic environments. Amongst them are the Ice-Tethered Profiler (ITP), the Autonomous Ocean Flux Buoy (AOFB) and the Ice-Tethered Mooring (ITM) (Zolich, Torre, Rodwell, Geoffroy, Johnsen, and Berge, 2018).

A major challenge for these observational platforms, or sensor nodes, is data retrieval. Typically, satellites are used for communication in remote locations, but above 75 degrees latitude even satellite coverage is limited (Birkeland, 2014). In January 2019, Roger Birkeland published his Ph.D. that evaluates the possibility of using a swarm of microsatellites for communication in polar regions (Birkeland, 2019). He proposes three mission concepts: I) Based on dedicated small satellites, II) Integration with VDES (next generation AIS) mainly intended for maritime traffic purposes and III) Based on Mega Constellations such as OneWeb and Starlink by SpaceX.

In the proposed space mission architecture of concept I, Birkeland (2019) defines two types of ground sensor nodes: a powerful node and a simple node. The powerful node is required to have an antenna gain of 10dBi for the link budget to reach a bit rate of 100kbit/s. The simple node is required to have a gain of 2dBi for the link budget to reach a bit rate of 19.2kbit/s. These calculations assume that the antenna onboard the satellite has a gain of 10dBi.

The design of the ground terminal antenna proposed by Birkeland (2019) forms the baseline of the work presented in this master thesis. Two use cases have been chosen to define the necessary requirements of the design, and they will be presented in section 1.2.1 and

1.2.2. An overview of the overall system is illustrated in Figure 1.1. Only the uplink communication between the nodes and the satellite is studied.

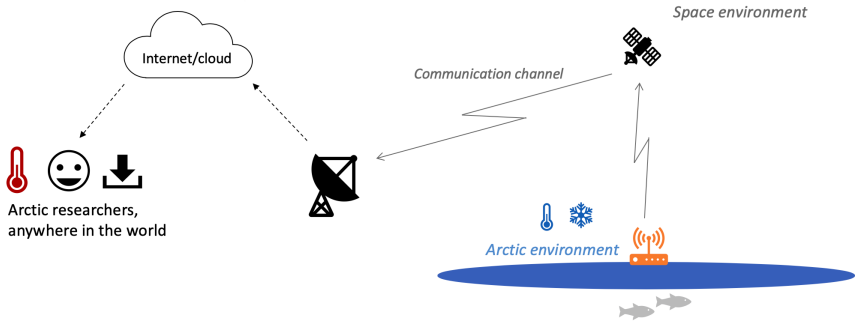

Figure 1.1: System overview of Concept I as presented by Birkeland (2019)

1.2 Introducing the Use Cases

1.2.1 Arctic ABC

Arctic ABC is a programme that started in 2015, lead by the Arctic University of Norway (UiT) in cooperation with the Norwegian University of Science and Technology, the University Centre in Svalbard (UNIS) and the Scottish Association of Marine Sciences (SAMS). It aims to build a set of autonomous observational platforms for optical, physical and ecological sensors, namely POPEs as shown in Figure 1.2. The novelty of this new set of buoys is the data-retrieval mechanism which includes flying either a manned aircraft or an unmanned aerial vehicle (UAV) close to the buoy to establish a radio link and collect the data (Zolich et al., 2018).

Some of the sensors will generate only a few bytes of data, and this is currently planned to be transmitted over Iridium SDB (Short Data Burst). The other sensors will generate 2-3GB of data per year, although this is expected to increase to hundreds of GB per year as new generations of sensors are developed. Publicly available satellite links that exist today are considered either very expensive or almost unfeasible for such extensive amounts of data (Birkeland, 2014). Considering that the throughput of the link is to a great extent determined by the antenna performance and the link budget, this master thesis will evaluate whether a feasible antenna can be designed and implemented for the retrieval of ”big-data” from sensor nodes in the Arctic, using small satellites.

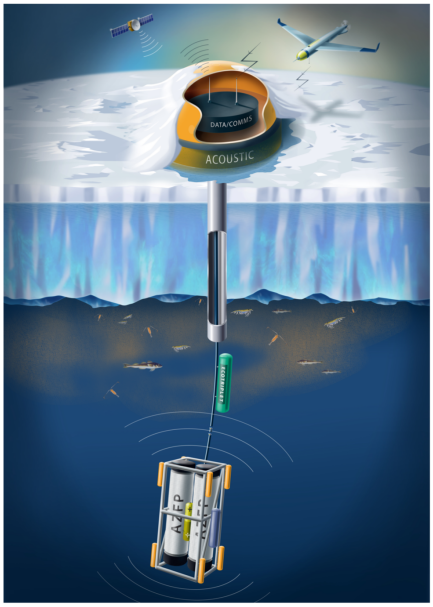

Figure 1.2: Arctic ABCs bio-acoustical ice-tethered platform for optical, physical and ecological sensors (POPE) (Zolich et al., 2018)

1.2.2 HYPSO

The NTNU SmallSat Lab is an initiative that aims to bring more of the space-related activities at NTNU together and make them more visible (Birkeland, 2018). A small satellite under the name HYPSO is currently being developed with two main missions:

1. To observe oceanographic phenomena with a hyperspectral camera onboard.
2. To provide better communication systems in the Arctic using Software Defined Radios (SDRs).

The work of this master thesis is concerned only with the second mission which more specifically will *provide Arctic researchers easier and faster access to scientific data products and prove concept and system viability by acquiring sensor data where there are harsh environments that induce high operational risk and costs.* The mission is divided into two sub-missions: 1) the spacecraft shall measure the communication channel, interference environment and noise in UHF when communicating with sensor nodes, flying nodes and ground stations in the polar regions and 2) the spacecraft shall gather data from different types of ground sensor nodes in the Arctic.

The orbital characteristics of HYPSO must be taken into account when making design choices for the antenna. The orbital parameters have been simulated in Systems Tool Kit (STK) and are listed in Table 1.1 (Grøtte, 2018).

Orbit parameters	Value
Type	Sun Synchronous Low Earth Orbit
Mean altitude (km)	500
Semi-major axis (km)	6878.14
Earth angular radius (deg)	1.1834
Inclination (deg)	97.4
Eccentricity (-)	0.00015
Argument of perigee (deg))	0
Launch LTAN	10:00 AM 01/03/20
Orbit duration (min)	94.62
Orbits/day	15.22
Repeat cycle (days)	7.032
Lifetime (yrs)	7.4 (5.92)

Table 1.1: HYPSO orbit parameters (Grøtte, 2018)

STK is also used to evaluate access times, meaning the duration of time that the sensor nodes will ”see” the satellite and be able to establish a communication link. This assumes a certain minimum elevation angle as shown in Figure 1.3. An example of minimum and maximum access times between April-September and May-June, assuming minimum elevation of 10°, is shown in Table 1.2 (Grøtte, 2018).

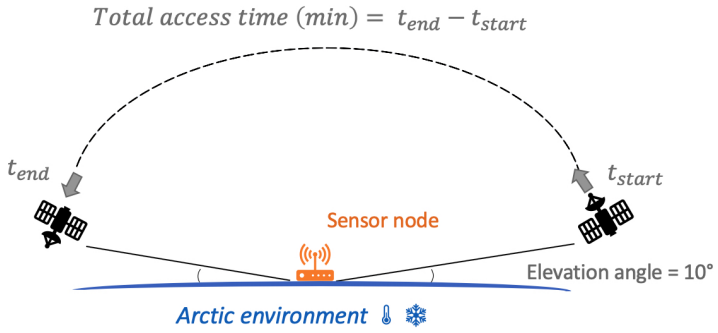

Figure 1.3: Illustration of elevation angle and total access time

Access times starting at different elevation angles for different locations in the Arctic are presented in Table 1.3. A map of the four locations is shown in Figure 1.4. The results show that the farther north the buoys are placed, the greater the access time.

Location	Period	Avg # passes / day	Min. contact (min)	Mean contact (min)	Max. contact (min)	Avg dur./day (min)
Longyearbyen	1 Apr - 1 Sep	11	0.181	6.532	7.657	78.12
Longyearbyen	1 may - 1 Jun	11	0.778	6.447	7.578	69.67

Table 1.2: Access times between Longyearbyen and HYPSO, assuming 10° elevation angle (Grøtte, 2018)

	Access time from 01.05.2020 - 01.05.2021 (in min)			
Elevation (deg)	Longyearbyen	Rossøya	GR_South	GR_North
30	8201	8482	6624	8478
45	3140	4189	2200	4187
60	998	1921	752	1927
75	216	374	164	380
90	0	0	0	0

Table 1.3: Access time in a year between Longyearbyen, Rossøya, GR_South, GR_North and the HYPSO satellite for different minimum elevation angles

Figure 1.4: Longyearbyen (yellow), Rossya (green), GR_South (pink) and GR_North (blue). (Source: Google Maps)

The UHF antenna mounted on the small satellite is a monopole with a radiation pattern as shown in Figure 1.5. The length of the simulated monopole is 172mm. At maximum, it has a gain of 2.52dBi. However this can drop to -19dBi depending on direction. Since it is a rigorous process to predict where the ground terminals will be located with respect to the HYPSO monopole at all times, it has been assumed that the monopole is isotropic with a gain of 2dBi. The monopole radiation pattern was known very late in the design process (in May), thus the previous simplification was required to complete the master thesis.

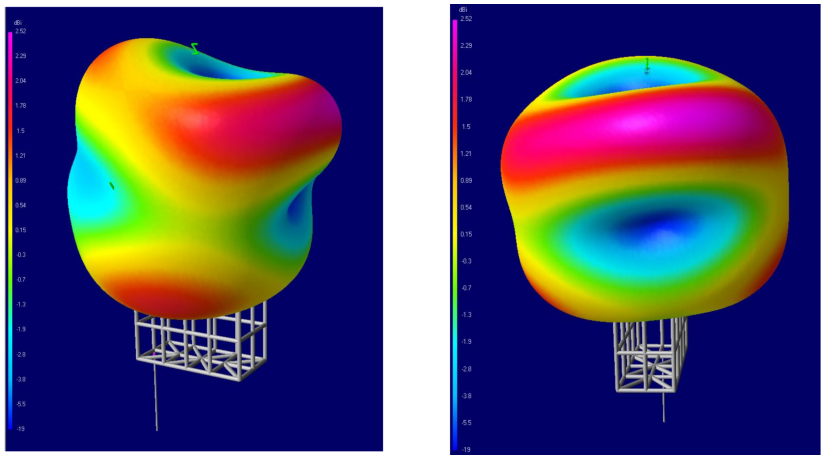

(a) View A **(b)** View B

Figure 1.5: Simulated radiation pattern of monopole onboard HYPSO, f=402MHz

1.2.3 Design Constraints Imposed by the Use Cases

With the chosen use cases comes a set of constraints that restricts the design of the antenna. These constraints are listed in Table 1.4.

Description	**Requirement**	**Use Case**
Transmit power at sensor nodes	$<$ 1Watt	Arctic ABC
Weight of ground antenna	$<$ 50kg	Arctic ABC
Yearly volume of data	2-200GB	Arctic ABC
Mechanical design of ground antenna	Stationary/fixed (no rotating elements, no mechanical steering)	Arctic ABC
Environmental caution, ground antenna	Protect from polar bears, Arctic fox and seals. Non polluting and safe for animal life	Arctic ABC
Receiving satellite antenna	Monopole, 2dBi gain, linear polarization	HYPSO
Signal modulation	QPSK	HYPSO
Bit Error Rate	10^{-4}	HYPSO
Satellite orbit	See Table1.1	HYPSO
Link direction	Uplink	HYPSO/Arctic ABC

Table 1.4: Design constraints imposed by Arctic ABC and HYPSO

1.3 Objectives and Outline for Thesis

The main objective of this master thesis is: **To evaluate whether a feasible and practical antenna can be designed and implemented for the retrieval of large volumes of data, >100GB/year, from sensor nodes in the Arctic using small satellites, at Ultra-High Frequencies**. Secondary objectives include:

1. Assess the link budget of the communication link and clarify the requirements for the antenna.
2. Make a general evaluation of antenna types that could be suitable for UHF satellite communication from the Arctic.
3. Design, simulate and optimize an antenna specifically designed for the use case presented. Target antenna gain: 2-10dBi.
4. Test a prototype of the antenna and present the results in an organized manner.
5. Do the necessary calculations to determine how much data could be retrieved and evaluate whether this is good enough for the use cases presented.

After the introduction, the link budget is presented step by step in Chapter 2. Results of the research on antenna types that could be relevant are presented and discussed in Chapter 3. The design and simulations of the chosen antenna type are presented and discussed in Chapter 4. The manufacturing of the prototype is presented in Chapter 5, and the results of the prototype tests in Chapter 6. The discussion in Chapter 7 and conclusion in Chapter 8 mark the end of the thesis.

1.4 Previous Work

Some work has already been performed on the topic of UHF LEO satellite communication at NTNU. First of all, Birkeland's Ph.D. (Jan 2019) proposes a link budget and a list of requirements and constraints for small satellite communication systems in the Arctic. However, this must be revised considering that specific use cases have been chosen.

In 2015, Erik Fremming Aurbakken studied the link budget of a remote sensor system that can be deployed in the Arctic area (Aurbakken, 2015). Nevertheless, there was no specific use case presented for the smallsat nor the sensor nodes. The antenna was presented in very theoretical means without considering any practicalities.

In 2008, Lars Løge studied a satellite system suitable for broadband communication with bit rates exceeding 1Mbps in the Arctic regions above 65 degrees northern latitude (Løge, 2008). Only the space component of the system was studied with little analysis of the ground terminal. The antenna gain for the ground terminal was set to 44dBi in the link budget, without an evaluation of how this antenna could actually be implemented for the Arctic. In general, there seems to be a lack of studies on ground-based antenna solutions for an Arctic communication system, from a more practical perspective. That is what this

master thesis seeks to address.

A pre-thesis project (15 Credits) was conducted previous to the master thesis, with the same use cases. A link budget was established and an Inverted F-Antenna was proposed as a possible solution (Udnaes, 2018). The work was continued in this thesis in more detail.

Chapter 2

Link Budget

The purpose of the link budget in this thesis is to give an indication of the level of performance required by the ground terminal antenna, as well as estimating the potential of the link in terms of data rate. The reasoning behind the calculations and assumptions are explained in this chapter.

2.1 Frequency Allocation

The antenna is designed for Ultra High Frequencies (UHF) as suggested by Roger Birkeland in his Ph.D. "On the Use of Micro Satellites as Communication Nodes in an Arctic Sensor Network" (Birkeland, 2019). He argues that UHF is seemingly a good choice for narrow-band, low power applications. The free-space loss will be lower than it would have been at higher frequencies. A small satellite Arctic communication system that supports environmental sensor data will, according to Norwegian Communications Authority (NKOM), allow classification in the Earth Exploration Satellite Service (EESS) category. The band 400.15-401MHz is to be allocated to the downlink to sensors and 401-402MHz is to be allocated to the uplink from sensors. For simplicity, and since the exact frequency was not known at the beginning of this project, the antenna has been designed and optimized for 400MHz.

2.2 Distance and Elevation Angle

The shortest distance between the small satellite and the sensor nodes is when the small satellite is at zenith. The distance to the nodes at this point is approximately 500km according to the HYPSO orbit specifications in Table 1.1. As the small satellite approaches the horizon, the distance increases and is calculated using equation (2.1) (Maini and Agrawa, 2010).

$$d = \sqrt{R^2 + (R+H)^2 - 2R(R+H)sin(e + sin^{-1}(\frac{R}{R+H}cos(e)))} \tag{2.1}$$

d is the distance, R is the Earth's radius, H is the orbit height and e is the elevation angle as illustrated in Figure 1.3. When the HYPSO satellite is 30° above the horizon ($e = 30°$), the distance between the sensor and the satellite is 909km. This means it almost doubles compared to when it is at zenith. The gain of the antenna must account for this increase in distance and path loss by having a suitable radiation pattern.

2.3 Transmission

The amount of power reserved for communication on the buoys will affect the battery lifetime. The Arctic ABC research team use on average 28dBm or 630mW for radio link transmission on 2402-2462MHz. If satellite communication is to be implemented, it is assumed that the transmit power can be increased to 1W.

Between the radio and the antenna, there will be a feed system which adds a certain loss factor. The RG58 coax cable used in the antenna prototype has a nominal attenuation of 0,31dB/m at 400MHz and 25° Celcius. The power splitter used also adds a loss factor. From measurements described in section 6.2, it was found that each of the four cables from the power splitter to the antenna elements contributes with on average 0.2dB of loss. The power splitter adds 0.7dB to the loss. Assuming the output of the radio will be connected directly to the input of the power splitter, a total feed loss of L_{ft} =1dB is estimated.

The gain of the transmitting antenna is a critical parameter for the performance of the system because it affects the data rate. The antenna design is therefore heavily concentrated on maximizing this value. Since gain and directivity are trade-off characteristics, the gain will not be equal in all directions but maximized in the most critical directions. This is discussed in section 2.9. The Effective Isotropic Radiated Power (EIRP) is the transmit power available after the feed line loss, times the gain of the transmit antenna (linear units).

2.4 Propagation

2.4.1 Free Space Loss

The radiated electromagnetic power decreases inversely to the square of the distance from the transmitter. This is referred to as free-space path loss (Maini and Agrawa, 2010). It assumes the absence of any material source of attenuation, meaning no reflection, scattering or diffraction along the path. It depends solely on the distance of the link d and the frequency f, as shown in equation 2.2. λ is the wavelength.

$$L_{FS} = \Big(\frac{4\pi R}{\lambda}\Big)^2 = 20\log\Big(\frac{4\pi R}{\lambda}\Big) \text{ dB} \tag{2.2}$$

When the satellite is at 30° elevation angle and distance equals 910km:

$$L_{FS} = 20\log(\frac{4\pi \times 910 \times 10^3 \times 400 \times 10^6}{3 \times 10^8}) = 144\text{dB}$$

When the satellite is in zenith and distance equals 500km:

$$L_{FS} = 20\log(\frac{4\pi \times 500 \times 10^3 \times 400 \times 10^6}{3 \times 10^8}) = 138\text{dB}$$

2.4.2 Atmospheric Loss

Previous research (Mendez, 2013; Marholm, 2012a) on the topic of attenuation due to rain and clouds in the troposphere, has taken into account how atmospheric loss varies with elevation angle. For elevation angles above 30°, this variation is only in the order of half a dB, and is therefore not included in the link budget. As was discussed in Udnaes (2018) and as can be seen in Figure 2.1, the gaseous absorption loss and rain attenuation at 400MHz is low and can be considered negligible.

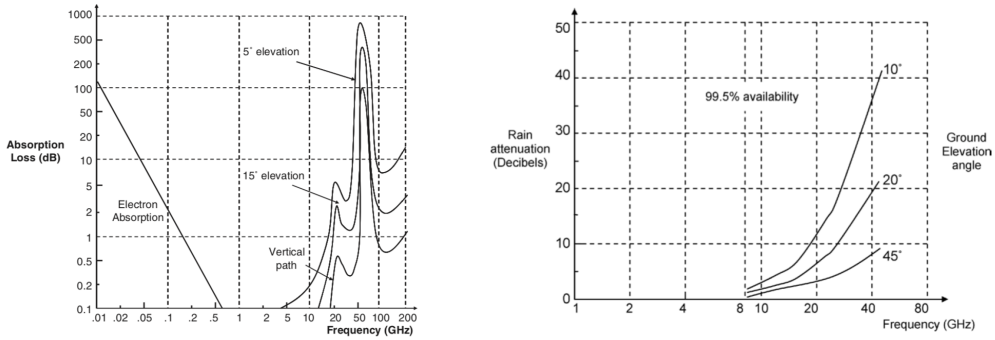

(a) Attenuation caused by gaseous absorption

(b) Attenuation caused by rain

Figure 2.1: Atmospheric attenuation as a function of frequency and elevation angle (Maini and Agrawa, 2010)

Ionospheric effects occur in regions of the atmosphere where the electron content is high. It can cause rapid fluctuations of the signal amplitude, phase, polarization or angle of arrival, as well as propagation delay, dispersion, etc. (Maini and Agrawa, 2010). Since it has a $1/f^2$ dependence, these effects cannot be ignored at 400MHz.

Ionospheric loss is a difficult parameter to estimate in the link budget because it fluctuates heavily. Marholm (2012b) proposes an estimate of 0.4dB at 438MHz, Mendez (2013) a loss varying from 0.95dB to 1.30dB at 438MHz, Aurbakken (2015) presents a graph reprinted in Figure 2.2 and Birkeland (2019) estimates a loss of 7dB based on a STK simulation. Birkeland (2019) used a very similar case study to the HYPSO case presented in this thesis, consisting of a small satellite in a 500km-altitude polar orbit with ground terminals placed at different locations in the Arctic ice.

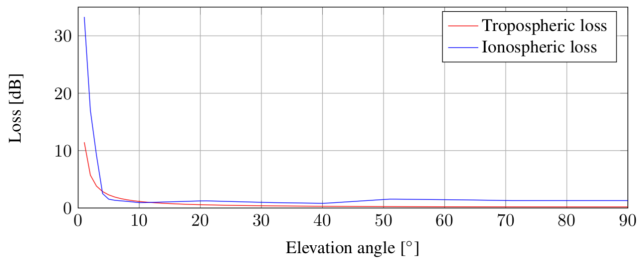

Figure 2.2: Estimate of how ionospheric and troposphere loss changes with elevation angle at Ultra-High Frequencies (Aurbakken, 2015)

Due to the difficulty of properly estimating the loss caused by ionospheric effects, there are two link budgets where one is a "best case" scenario with 1dB ionospheric loss and the other is a "worst case" scenario with 7dB ionospheric loss.

2.4.3 Polarization Mismatch Loss

The polarization of a wave is defined as "that property of an electromagnetic wave describing the time-varying direction and relative magnitude of the electric-field vector; specifically, the figure traced as a function of time by the extremity of the vector at a fixed location in space, and the sense in which it is traced, as observed along the direction of propagation" (Balanis, 2016).

Circular polarization happens when the components of the electric and magnetic fields have a phase-time difference that is odd multiples of $\pi/2$. If their magnitude also differs, the polarization becomes elliptical. For example, consider a wave defined by equation 2.3 (Balanis, 2016). E_{x0} and E_{y0} are the maximum magnitudes of the x and y components respectively. The wave is travelling in the negative z direction.

$$\mathbf{E}(z,t) = \hat{\boldsymbol{e}}_{\boldsymbol{x}} E_{x0}\cos(wt + kz + \phi_x) + \hat{\boldsymbol{e}}_{\boldsymbol{y}} E_{y0}\cos(wt + kz + \phi_y) \tag{2.3}$$

If $\Delta\phi = \phi_y - \phi_x = \big(\frac{1}{2} + 2n\big)\pi, \quad n = 0, 1, 2, ...$
Then the wave rotates in a clockwise direction (assuming it travels in -z direction).

If $\Delta\phi = \phi_y - \phi_x = -\big(\frac{1}{2} + 2n\big)\pi, \quad n = 0, 1, 2, ...$
Then the wave rotates in a counter-clockwise direction (assuming it travels in -z direction).

The polarization of the receiving antenna is often different to that of the transmitting antenna. A horizontally polarized antenna will not be able to communicate with a vertically polarized antenna. This mismatch is defined by the Polarization Loss Factor (PLF) in equation 2.4 (Balanis, 2016).

$$PLF = \mid cos\theta^2 \mid \tag{2.4}$$

θ is the angle between two unit vectors. If the angle between the received and transmitted wave is zero, then there is no polarization loss and the PLF is equal to unity. The receiving antenna will extract maximum power from the incoming wave. If there is a 90° difference between the waves, the PLF is equal to zero and no power is extracted from the receiving antenna.

Since the polarization state of the receiver antenna on the satellite will not be perfectly matched to that of the incoming wave, a polarization mismatch loss needs to be included in the link budget. The transmitting antenna will be circularly polarized and the HYPSO antenna is linearly polarized. Circular polarization occurs when the field vector has two orthogonal linear components that are 90° out of phase. The monopole on the satellite will extract only the in-phase component of the circularly polarized wave. The PLF is then 0.5, meaning a loss of 3dB must be included in the link budget.

2.5 Reception

The receiving end of the communication link is the HYPSO satellite. Since the small satellite is currently under development, it is not certain what kind of loss there might be between the antenna and the receiver. It is therefore assumed that this will be at approximately 1dB. The radiation pattern of the receiving monopole antenna is shown in Figure 1.5. For simplicity, the gain G_r has been averaged to 2dBi.

The power level of the signal at the input of the HYPSO satellite antenna is the EIRP plus the gain of the HYPSO antenna G_r, minus the total propagation loss L_{tot} as stated in equation 2.5 (Maini and Agrawa, 2010).

$$P_{r_{ant},dB} = EIRP_{dB} + G_{r,dB} - L_{tot,dB} \tag{2.5}$$

The power level at the input of the receiver is the power level at the input of the antenna minus the loss between the antenna and the receiver $L_{fr,dB}$.

$$P_{r_{rec},dB} = P_{r_{ant},dB} - L_{fr,dB} \tag{2.6}$$

2.5.1 System Noise Temperature

The noise level at the input of the receiver is calculated based on the cascaded system shown in Figure 2.3. The system noise temperature with reference to the input of the receiver is given by equation 2.7 in linear units (Maini and Agrawa, 2010). T_A (K) is the antenna temperature, L_F is the attenuation factor of the feeder, typically a cable, T_F (K) is the temperature of the feeder and T_R (K) is the effective input noise temperature of the receiver.

$$T_{sys,RI} = \frac{T_A}{L_F} + T_F\Big(\frac{L_F - 1}{L_F}\Big) + T_R \tag{2.7}$$

It has been assumed in this link budget that $T_F = T_A = T_0 = 290$K which according

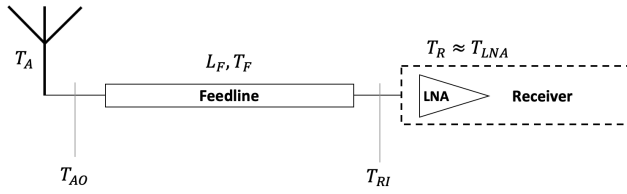

Figure 2.3: Cascaded arrangement of the antenna, the feeder connecting the antenna to the receiver and the receiver

to Mendez (2013) is a good approximation for simple onboard antennas. In addition, the noise of the receiver is approximated to the noise temperature of the LNA which according to Birkeland (2019) is valid as long as the gain of the LNA is high. It is assumed that the LNA in the HYPSO satellite is of good quality with a noise factor of 1dB. The effective input noise temperature of the receiver thus becomes

$$T_r = T_0(F_{LNA} - 1) = 290(10^{1/10} - 1) = 75\text{K} \tag{2.8}$$

Using equation 2.7, the system noise temperature at the input of the receiver becomes

$$T_{sys,RI} = \frac{T_0}{L_F} + T_0\Big(\frac{L_F - 1}{L_F}\Big) + T_R = T_0 + T_R = 290 + 75 = 365\text{K} \tag{2.9}$$

2.6 Signal Modulation

To transmit binary data over a satellite channel, the signal is modulated onto a RF carrier wave at a much higher frequency range. At the receiving end of the channel, the signal is demodulated to extract the binary data. The modulation is performed by switching or keying the amplitude (ASK), frequency (FSK) or phase (PSK) of the carrier between values corresponding to binary symbols 0 and 1 (Haykin and Moher, 2010). In binary phase-shift keying (BPSK), the carrier is shifted by 180° to change from a digital one to a digital zero and vice versa. The two states that represent the binary data can be plotted on a constellation diagram as seen in Figure 2.4(a). The I-axis represents the in-phase component of a cosine wave and the Q-axis represents the quadrature component of a sine wave. For BPSK, the Q-axis marks the decision boundary that separates a one from a zero.

The SDR communication system of the HYPSO small satellite is not fully developed yet and will most likely be using adaptive modulation, meaning the modulation scheme can be changed as the conditions of the radio link changes. Nonetheless, it has been decided that quadrature phase shift keying (QPSK) will be used as a baseline. QPSK uses four phase states to represent the binary data, and as seen in Figure 2.4(b) both the I and Q axes form the decision boundaries. This means there is more room for misinterpretation of the symbols, and thus the carrier-to-noise ratio must be higher. On the other hand, QPSK carries twice as many bits of information as BPSK and therefore requires half the transmission bandwidth with the same error rate performance (Haykin and Moher, 2010).

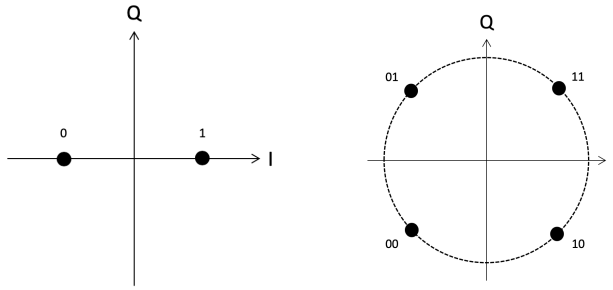

(a) BPSK **(b)** QPSK

Figure 2.4: Constellation diagram

A certain level of carrier-to-noise ratio is required to be able to interpret each symbol correctly. This level depends on how much bit error the user of the system accepts. A Bit Error Rate of 10^{-4} means that one or less errors will occur every 10000 bits. Depending on the BER and the type of modulation chosen, the required carrier-to-noise ratio (C/N) can be determined using for example graphical analysis.

An alternative measure to C/N is energy per bit to noise power spectral density ratio, E_b/N_0. The two are linked by equation 2.10 where f_b is the channel data rate and B is the channel bandwidth (Thompson, 2013).

$$\frac{C}{N} = 10\log\Big(\frac{E_b}{N_0}\Big) + 10\log\Big(\frac{f_b}{B}\Big) \qquad [\text{dB}] \tag{2.10}$$

The equation assumes that the noise environment of the satellite communication link can be described as Additive White Gaussian Noise (AWGN). It is a simple model that does not take fading, frequency selectivity, interference, non-linearity or dispersion into account. With thermal white noise power defined by $N = kTB$ and thermal noise by $N_0 = kT$, equation 2.10 can be expressed as equation 2.11.

$$\frac{C}{N_0} = 10\log\Big(\frac{E_b}{N_0}\Big) + 10\log f_b \qquad [\text{dBHz}] \tag{2.11}$$

With a BER in the order of 10^{-4}, the required (E_b/N_0) equals 8.4dB based on Figure 2.5 (Haykin and Moher, 2010). Increasing the BER to the order of 10^{-5} increases the required (E_b/N_0) by 1dB to 9.4dB. The reliability of a communication link can be determined by measuring the link margin as expressed in equation 2.12. $(E_b/N_0)_{req}$ is the required E_b/N_0 for a given BER.

$$LM = \frac{E_b}{N_0} - \Big(\frac{E_b}{N_0}\Big)_{req} \qquad [\text{dB}] \tag{2.12}$$

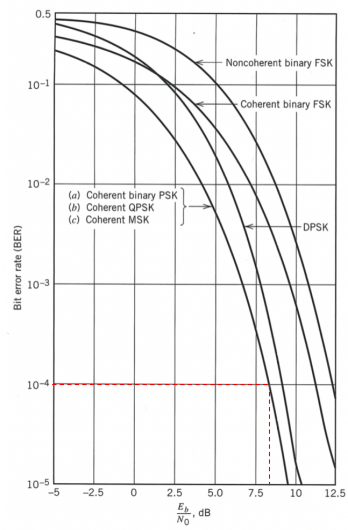

Figure 2.5: BER for different E_b/N_0 depending on type of modulation (Haykin and Moher, 2010)

2.7 Link Quality

The performance of the antenna is evaluated by the gain-to-noise temperature ratio, G/T, at the input of the receiver (Maini and Agrawa, 2010).

$$(G/T)_{dB} = G_{r,dB} - L_{fr,dB} - 10\log(T_{sys}) \tag{2.13}$$

The RF link performance is evaluated by the carrier-to-noise-density ratio, C/N_0, at the input of the receiver, calculated using equation 2.14 where k is Boltzmann's constant (Paxal, 2016).

$$\left(\frac{C}{N_0}\right)_{dB} = EIRP_{dB} + \left(\frac{G}{T}\right)_{dB} - L_{tot,dB} - 10\log(k) \tag{2.14}$$

The data rate is found using equation 2.11 where the required E_b/N_0 in dB is subtracted from the C/N_0 in dB. This calculation assumes a link margin equal to zero. Alternatively, the E_b/N_0 can be found knowing the required data rate. Since this study seeks to evaluate antenna types that would be the most effective in an Arctic satellite communication system, finding the maximum possible data rate is considered a more appropriate performance measure.

The data rate is converted from dBHz to kbit/s using equation 2.15.

$$f_b[\text{dBHz}] = \frac{10^{\frac{f_b[\text{dBHz}]}{10}}}{1000}[\text{kbit/s}] \tag{2.15}$$

2.8 Link Budget Example

An example of the link budget is shown in Figure 2.6. Elevation angle is 30° and G_t=5dBi. The following assumptions or simplifications have been made:

- 1dB loss between satellite antenna and receiver
- 1dB total loss in transmit antenna feed line
- Temperature of the transmitting antenna feed line $T_F = T_A = T_0 = 290$K
- Effective input noise temperature of the satellite receiver $T_R = T_{LNA}$
- $F_{LNA} = 1$dB (high quality LNA in receiver)
- Ionospheric loss is 7dB or 1dB
- Atmospheric loss assumed zero
- E_b/N_0 = required E_b/N_0 (margin=0 when calculating datarate)

		Uplink (worst case)	Uplink (best case)
General parameters			
Orbit height *(H)*	*km*	500,0	500,0
Elevation angle *(e)*	*degrees*	30,0	30,0
Frequency *(f)*	*MHz*	400,0	400,0
Distance *(d)*	*km*	909,4	909,4
Modulation and code			
Modulation		QPSK	QPSK
Bit/symbol		2	2
Required BER		0,0001	0,0001
Required E_b/N0 for required BER	*dB*	8,4	8,4
Transmission			
Power input to antenna *(Pt)*	*dBW*	0,00	0,00
Connector/cable/filter loss *(Lft)*	*dB*	1,00	1,00
Antenna Gain *(Gt)*	*dBi*	5	5
EIRP	*dBW*	4,0	4,0
Propagation			
Free space Loss *(Lfs)*	*dB*	143,7	143,7
Atmospheric loss	*dB*	0,0	0,0
Ionospheric loss	*dB*	7,0	1,0
Polarization loss	*dB*	3,0	3,0
Total propagation loss *(Ltot)*	*dB*	153,7	147,7
Reception			
Power input, antenna	*dB*	-147,7	-141,7
Antenna Gain *(Gr)*	*dBi*	2,0	2,0
Connector/cable/filter loss *(Lfr)*	*dB*	1,0	1,0
Antenna Noise Temp *(Ta)*	*K*	290,0	290,0
Power input, receiver *(Pr)*	*dB*	-148,7	-142,7
Receiver Noise *(Tr)*	*K*	75,0	75,0
Noise			
Equivalent Noise Temperature *(Tsys)*	*K*	365	365
Link Quality			
Receiver G/T	*dB/K*	-24,6	-24,6
C/N0	*dBHz*	54,3	60,3
Datarate (margin=0)	*dBHz*	45,9	51,9
Datarate (margin=0)	*kbit/s*	39,0	155,3

Figure 2.6: Example of link budget when gain of transmitting antenna is 5dBi and elevation angle is 30°

2.9 Discussion

The link budget example in Figure 2.6 presents both a worst case and a best case. In the worst case, the ionospheric loss is 7dB and in the best case the ionospheric loss is 1dB. The distance d is the distance from the sensor node to the satellite for a given elevation angle, which in the example is 30°. The results show a data rate of 39kbit/s in the worst case and 155kbit/s in the best case. It should be noted however, that this assumes that the gain of the transmitting antenna is 5dBi in the direction of the satellite appearing 30° above the horizon. And that the receiving antenna has a gain of 2dBi in that direction also.

Since it is difficult to predict how significant the ionospheric loss actually will be, it also becomes difficult to predict the data throughput. Nevertheless, an estimate is possible. The data rate is multiplied with the access time (see Table 1.3) in seconds, and divided by 8000000 to convert from kilobit to Gigabyte (1 GB = 8000000 kbit). Table 2.1 shows the total data throughput in GB that the system would support assuming constant data rate during the orbital pass, $e_{min} = 30°$ and high ionospheric loss (7dB). With a constant data rate of 155kbit/s, the data throughput is 7.7GB at Rossya and 9.9GB at GR_South, a difference of almost 2GB. If the data rate is only 40kbit/s, this difference is only in the order of half a GB. Data throughput varies with location because access time varies with location.

	Data throughput (GB)			
Datarate (kbit/s)	**Longyearbyen**	**Rossøya**	**GR_South**	**GR_North**
40	2.5	2.0	2.5	2.5
155	9.5	7.7	9.9	9.9

Table 2.1: Data throughput for different data rates at different locations, assuming constant data rate during the orbital pass, $e_{min} = 30°$ and high ionospheric loss (7dB)

The results given in table 2.1 assume that the data rate remains constant for the entire orbital pass. This is not true in practice. Since the distance between the satellite and the buoy changes from 910km to 500km, the data rate will also change. The graph in Figure 2.7 shows how the data rate changes as the distance changes, assuming the gain of the antennas stays constant. When the ionospheric loss is low, the data rate increases more rapidly than when the ionospheric loss is high. With a ground terminal antenna gain of 5dBi and a receiving antenna gain of 2dBi, it can be estimated that the data rate will vary between 40kbit/s and 500kbit/s throughout the orbital pass, depending on the location of the satellite and the level of ionospheric activity.

The antenna will most likely not radiate isotropically, meaning equally in all directions. In fact, it does not make sense to have such an antenna because as was shown in Table 1.3, the satellite is never present in zenith. The satellite will in a time period of 12 months, be seen in total 5062 min when between the elevation angles 30° and 45°, 2142 min when between 45° and 60°, 782 min when between 60° and 75°, and 216 min when between 75° and 90°. See Figure 2.8 to better understand at what elevation angles the satellite will be seen more often. It makes more sense to build an antenna that maximizes gain not at

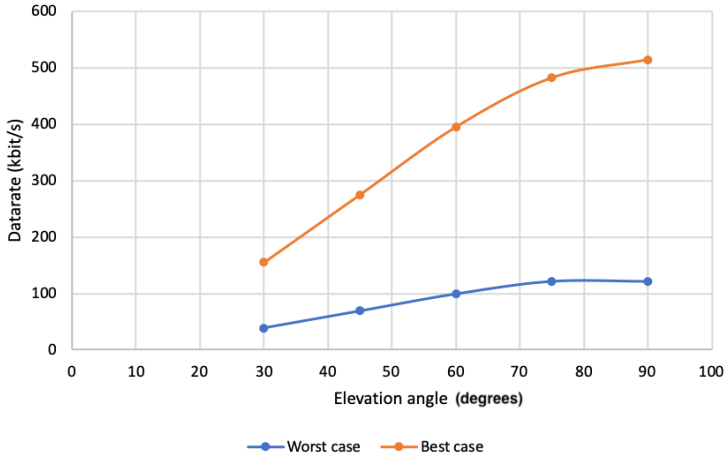

Figure 2.7: Data rate versus elevation angle. Assumes constant transmit antenna gain of 5dBi. Worst case: ionospheric loss=7dB, best case: ionospheric loss=1dB.

90°, but at around 45°. It is complicated to say in what exact direction the gain should be maximized because there is a trade-off between distance and access time. The ideal radiation pattern to keep the data rate constant at 20kbit/s is shown in Figure 2.9. It indicates that the antenna gain should be greater at lower elevation angles, and lower at higher elevation angles.

It is concluded that the antenna must be designed to have a higher gain towards lower elevation angles and a smaller gain at zenith. Exact gain values are difficult to give because there is an uncertainty regarding ionospheric loss as well as a trade-off between distance to satellite and access time.

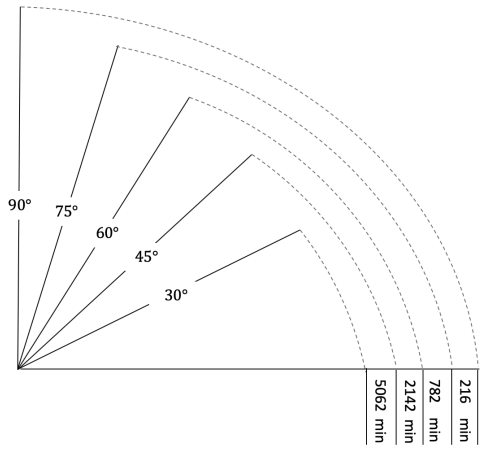

Figure 2.8: HYPSO total access time in a year for different elevation angle ranges (data source: Mariusz Grøtte, NTNU HYPSO)

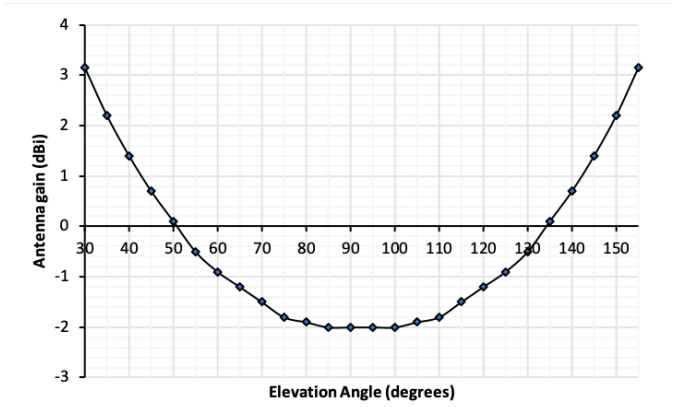

Figure 2.9: Minimum antenna gain versus elevation angle to keep a fixed bit rate of 20kbit/s

Chapter 3

Evaluation of Antenna Types

The purpose of this chapter is to present the research that was done prior to the design of the antenna. It consisted of finding what antennas have been used previously in other similar projects. For example antennas for UHF and satellite communication projects that require small and practical antennas, university and research projects, etc. The results are classified into four types of antennas: linear wire antennas, Inverted-F Antennas (IFAs), helical antennas and microstrip antennas. Only the most relevant results are presented. In the discussion in section 3.7 it is concluded to design a 4-element array of IFAs.

Satellite communication systems that require high data throughput typically use large, mechanically steered dish antennas. There is for example the Svalbard Satellite Station located 78°N with more than 31 antenna systems in C-, L-, S- and X-band (Blues, 2019). These are huge antenna installations that require extensive maintenance. They are clearly not suitable for small sensor nodes drilled into the Arctic ice and therefore only simple, lightweight and small antennas will now be presented.

3.1 Electronics in the Arctic

The antenna will be placed in an Arctic environment, and therefore a better understanding of how this might affect the antenna and the electronics is useful. Marius Bratrein works with electrical equipment and instruments used by the Norwegian Polar Institute when they do field work in the Arctic. In an email exchange, he mentions that temperatures rarely reach below -45°C. During winter, the temperature is on average between -25°C to -35°C and in summer it is usually around 0°C.

Marius also mentions that equipment is often buried under the snow to keep the temperature up and to hide it from animals as long as possible. However this varies, because the amount of snow changes from year to year and depends on location. What is covered by snow or drilled into the ice will experience heat from the ocean under the ice, unlike what lies on top of the snow that is prone to cold winds. This raises concern for very tall

antennas that will experience a temperature difference in the metal that is high up in the cold air compared to that which might be hidden under the snow. In addition, it will be seen from animals many miles away. Marius suggests painting components in white to make them less visible. He also says the Arctic fox will gnaw on loose cables and therefore these should be protected in hard shields.

According to Marius, there has never been any issues with GNSS and Iridium antennas being buried under snow. Cables can be problematic in low temperatures, but these problems are mechanic rather than electric. The shield of the cables are at risk of breaking around -20°C, some even earlier, which might cause a short circuit. He recommends using rubber, or even better - silicone. In general, he also recommends keeping the bending radius large to prevent the cables from breaking.

In terms of material, Marius has good experiences with steel, aluminum, wood and plastic. Aluminium is a popular material to use in field work in the Arctic because it is easy to work with. Although it has a reputation to become brittle at low temperatures, he has not experienced this. He says metals do shrink in cold temperatures, but not significantly enough to cause any greater problems. It might be something to consider when designing the antenna. The most popular material to use is polyethylene as it has proven strong and pliable at temperatures down to -80°C.

The insights given by Marius at the Norwegian Polar Institute suggest that there will not be too many constraints on the design posed by the Arctic environment. To sum it up; tall antennas are to be avoided, care should be taken when choosing materials and the antenna should be protected under a rigid, white radome.

3.2 Antenna Performance Indicators

To find the right type of antenna for a specific project, performance indicators must be identified and prioritized. Based on the link budget and the use cases previously presented, they have been listed in Table 3.1.

Type	**Specification**	**Priority**
Gain	$\sim$10dBi	High
Polarization	Circular	Medium
Radiation pattern	See Figure 2.9	Medium
Size	As small as possible, max $1 \times 1 \times 1\text{m}^3$	Low

Table 3.1: Performance indicators for antenna design

The gain has the highest priority as this significantly impacts the performance of the system. The higher it is, the more data can be sent over the channel. The polarization of the antenna system should be circular in order to avoid additional loss in the propagation of the signal. The reason for it being set to medium priority is that a slightly elliptical

polarization is acceptable. Perfectly circular polarization can be difficult to achieve and is not considered critical for the performance of the system. The indicator for the radiation pattern is a result of the discussion in section 2.9. Since it is difficult to define exactly how the pattern should look, an approximation is given but it is not considered highly critical that it is perfectly met.

The antenna should be small in size to hide it from curious animals such as polar bears and Arctic fox. It should also be small enough to make it possible to integrate it with the Arctic ABC sensor buoy. After talking with the Arctic ABC team, it seemed that the size of the buoys is flexible and can be arranged to fit the antenna. Therefore this indicator is marked as low priority.

3.3 Linear Wire Antennas

3.3.1 Dipole

A dipole antenna is composed of two metal wire-rod conductors spaced a small distance apart. In between, the antenna is excited by a radio frequency voltage (Balanis, 2016). The antenna resonates when the total length of the dipole is half a wavelength. For an operating frequency of 400MHz, the dipole length would be 75cm/2=37.5cm. The current distribution is maximum at the centre and minimum at the endpoints. The radiation pattern is maximum perpendicular to the antenna as shown in Figure 3.1. The gain can be expected to be around 2dBi (Vita, 2012).

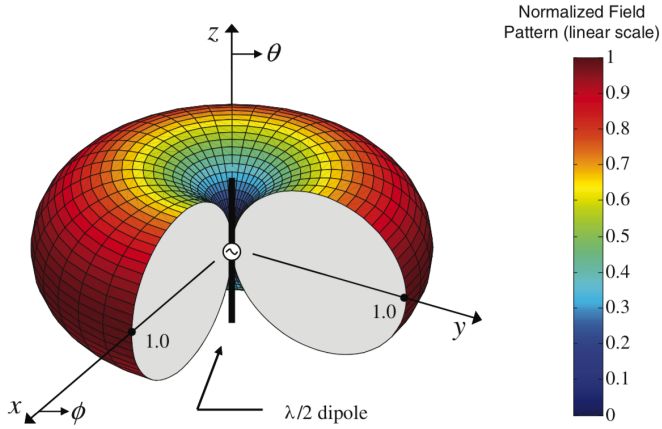

Figure 3.1: Radiation patter of a $\lambda/2$ dipole (Balanis, 2016)

Schraml, Narbudowicz, Chalermwisutkul, Heberling, and Ammann (2017) propose a UHF $\lambda/2$ dipole for a 1U ($10 \times 10 \times 10\text{cm}^3$) small satellite. Their antenna design is, in fact, dual-band and is loaded with an LC-circuit acting as a notch filter in the UHF band and as a passband in the VHF band when the full length of the antenna is to be excited. The model of the dipole is shown in Figure 3.2. For f=435MHz, the length of the inner arm is

17.65cm and the total length 35.3cm. The simulated gain pattern of the design is shown in Figure 3.3. The maximum gain is 3.91dBi when ϕ=45°and 135°, and the minimum gain is -8dBi when $\phi = 90°$. The radiation pattern is highly relevant from a ground station point of view since most of the gain is directed towards a lower elevation angle. The gain is higher than what could be expected from a dipole, but still not high enough according to the performance indicators. The dipole does not produce circular polarization and this is a major disadvantage.

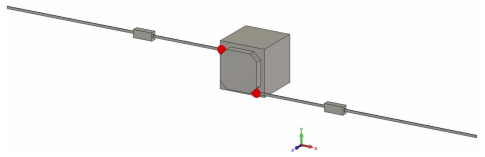

Figure 3.2: Dual-band dipole by Schraml et al. (2017)

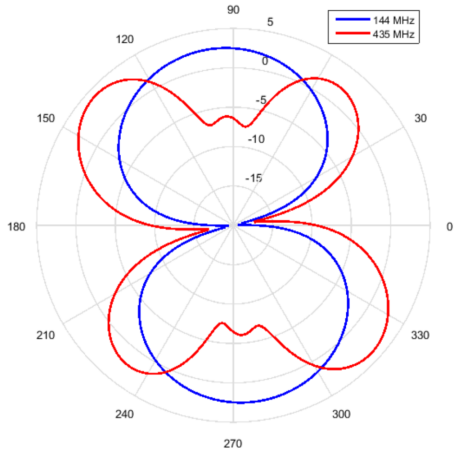

Figure 3.3: Radiation pattern of dual-band dipole simulations by Schraml et al. (2017)

3.3.2 Monopole

The monopole antenna is a single metal wire-rod conductor placed perpendicular to a ground plane. The ground plane can theoretically be replaced by an identical imaged element, and the equivalent antenna becomes similar to that of a dipole as shown in Figure 3.4 (Balanis, 2016). The ground plane should ideally spread out at least a quarter wavelength which at 400MHz would be 75cm/4=19cm. Making the ground plane smaller will affect the performance of the antenna. The length of the monopole is usually one-quarter of the wavelength and the gain is 3dBi greater than that of the dipole. The radiation pattern resembles that of the dipole for $\theta = -90°$ to $\theta = 90°$. The monopole is ideal for communication in any direction except zenith (Vita, 2012).

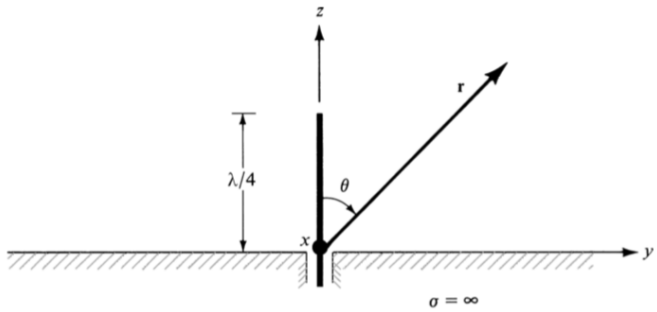

(a) $\lambda/4$ monopole on infinite electric conductor

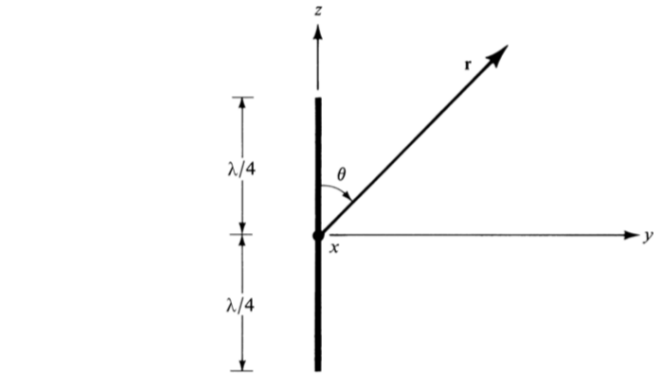

(b) Equivalent of $\lambda/4$ monopole on infinite electric conductor

Figure 3.4: $\lambda/4$ monopole (Balanis, 2016)

A compact and thin J-shaped monopole for terrestrial digital broadcasting at UHF band was developed by Kashihara and Kuroki (2009). The objective was to make a small and compact antenna for mobile TV terminals. The antenna is an array of 20 monopoles that are a quarter-wavelength long and resonate at frequencies between 440MHz and 770MHz. Each monopole is bent in a J-shape as shown in Figure 3.5(a). The feed network consists of an open-ended slotted line and a high impedance step section. The antenna is printed on a $91 \times 62 \times 1.6\text{mm}^3$ paper phenol substrate, making it a small and practical antenna for integration with the sensor buoys. However, the gain was only -10dBi which is not satisfactory. The radiation pattern shown in Figure 3.5(b) is not ideal.

Even though the J-shaped monopole array is linearly polarized, it is possible to make an array of monopoles circularly polarized (CP). For example, Cao, Cheung, and Yuk (2014) designed a CP antenna consisting of two monopole elements where one was fed with a 90° phase difference. It was implemented using a 90°-phase shifter and a Wilkinson power divider. The issue is again that the gain reaches only 2dBi which is not high enough for the application considered in this thesis.

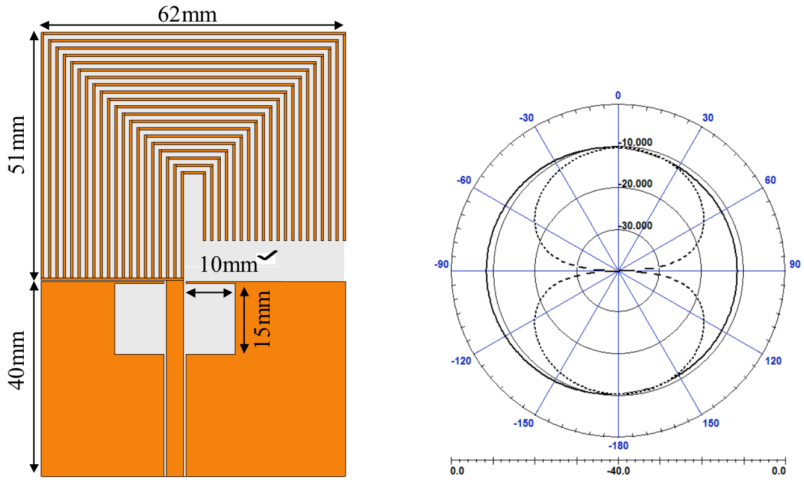

(a) Plane view

(b) Radiation pattern of Ey on the x-z plane and E on the y-z plane

Figure 3.5: J-shaped monopole antenna array (Kashihara and Kuroki, 2009)

3.4 Inverted-F Antennas

The Inverted-F Antenna (IFA) is a variant of the monopole. The name comes from the fact that it looks like a downward facing F when seen from the side. A wire-rod conductor is bent towards a ground plane to save vertical space as shown in Figure 3.6. This creates a capacitance at the input of the antenna that is compensated by adding a short circuit stub. If the bent arm is brought closer to ground, the feed point must be moved to compensate for the change in impedance. By moving the feed point away from the short circuit stub, the impedance is increased (Balanis, 2016).

Although the IFA is linearly polarized, it is possible to arrange an array of IFA elements such that it generates circular polarization. For example, two antennas can be orthogonally arranged with one being fed 90° out of phase, or four antennas can be arranged as seen in figure 3.7. When there are only two elements, the CP becomes very poor at more than 5° off broadside direction. It is therefore considered better to use the 2×2 arrangement. It is also worth noting that the arrangement in figure 3.7b is preferred over 3.7a because the axial ratio bandwidth can be increased substantially (Huang, 1986). Although the example by Huang (1986) uses patch antennas, the method can also be applied to IFAs.

The IFA is small and compact in size, which makes it a popular antenna choice for mobile communications (Zhang, 2011). If the width of the IFA is increased, it becomes a Planar IFA (PIFA) as is shown in Figure 3.8. Its design is defined by equation 3.1 (Balanis, 2016).

$$L + W - w_s = \frac{\lambda}{4} + h \tag{3.1}$$

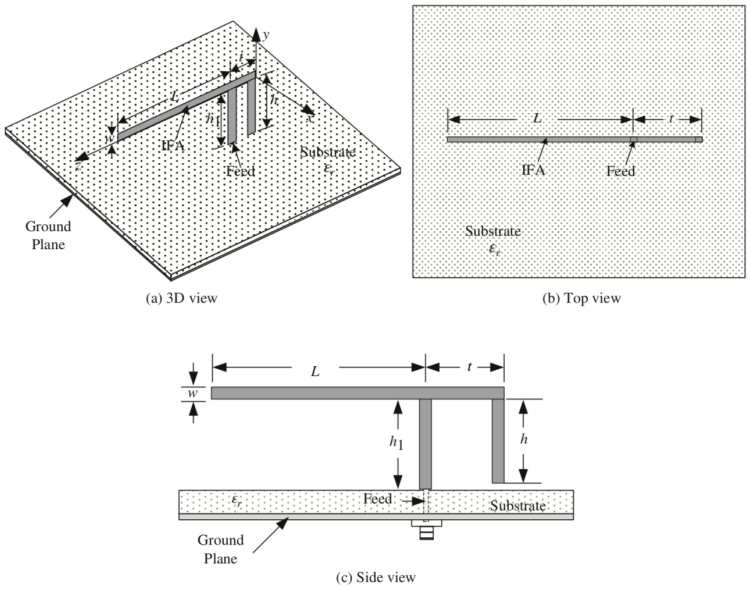

Figure 3.6: Inverted-F Antenna (Balanis, 2016)

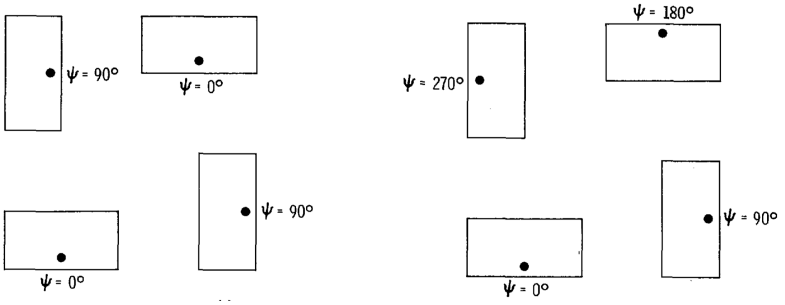

(a) For narrow-band applications

(b) For wide-band applications

Figure 3.7: Arrangement of 2x2 microstrip array that generate CP with LP elements (Huang, 1986)

If the width of the shorting pin, w_s is equal to the width of the patch, W then:

$$L = \frac{\lambda}{4} + h \tag{3.2}$$

$$f = \frac{v_0}{4(L + W - w_s - h)\sqrt{\epsilon_r}} \tag{3.3}$$

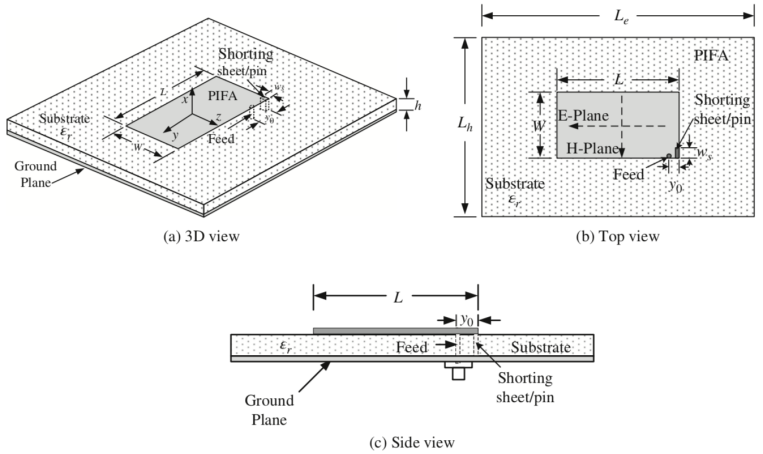

Figure 3.8: Planar Inverted-F Antenna (Balanis, 2016)

A $100 \times 100\text{mm}^2$ PIFA was designed by Telkom University in Indonesia for a low orbit nanosatellite ($10 \times 10 \times 20\text{cm}^3$). The design is shown in Figure 3.9. It operates at 2.35GHz with 107MHz bandwidth and circular polarization. They considered the helix antenna too long for the nanosatellite and found the PIFA to be a better alternative. The antenna is an array of 4 PIFA elements on a 1.6mm thick FR-4 substrate. The elements are arranged in a circle and a microstrip feed network divides the phase so that each element has a 90° consecutive phase difference.

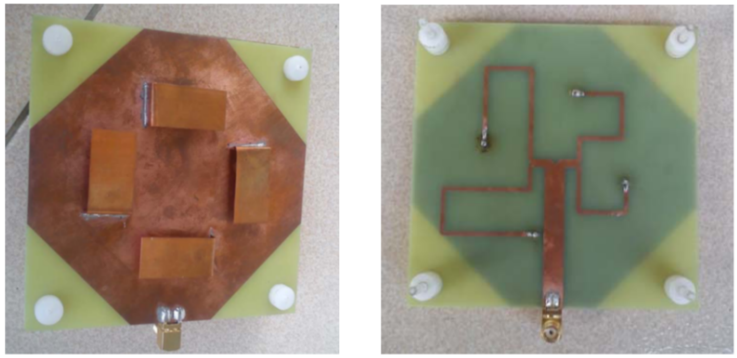

Figure 3.9: PIFA array by Kurnia et al. (2014)

The design was manufactured and the measurements show that the antenna has an axial ratio of 1.21, a return loss of -20.7dB at 2.35GHz and a gain of 4.78dBi. The gain was measured using the comparison method with a horn antenna as reference.

Another PIFA for Low Earth Orbit satellite communication has been designed in a collaboration between the University of Sheffield and King Abdulaziz City for Science and

Technology. It is a dual-band antenna operating at 135 MHz and 435 MHz. The dual band was implemented by adding a small parasitic element next to the PIFA as shown in Figure 3.10. The antenna is designed similarly to the one by Telkom University, with the elements arranged in a circle and excited with a 90° consecutive phase difference. The antenna was dimensioned for a $50 \times 50 \times 50\text{cm}^3$ satellite body, but the manufactured model was scaled down by a factor of 5.

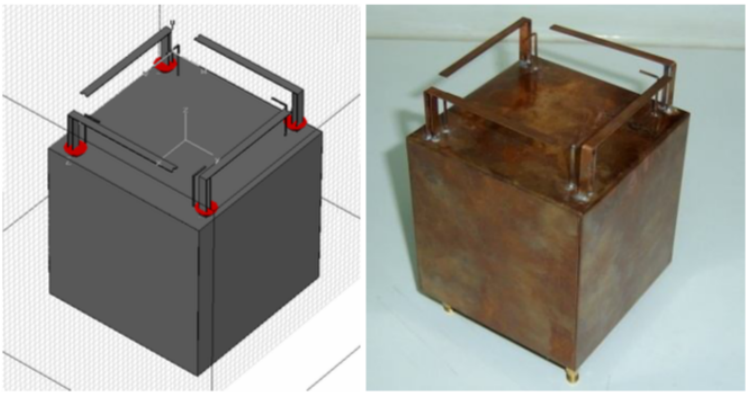

Figure 3.10: PIFA array by Amoudi and Langley (2009)

The radiation pattern of the manufactured model was never measured, but the results of the simulations in Figure 3.11 show a gain of 9.45dBi at 435MHz. The measurements were compared to a similar array, but of monopoles, and the results show that the gain of the PIFA is 1.65dBi higher. The height of the PIFA is also 3.6 times shorter than the monopole.

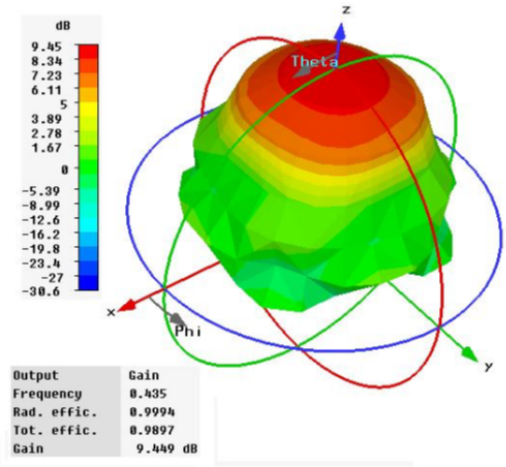

Figure 3.11: Radiation pattern of PIFA array by Amoudi and Langley (2009)

Although the author claims that the antenna design is a PIFA, it is questionable whether the antenna is not an IFA considering that the width of the element is relatively small. There exists an ambiguity in the literature with regards to the difference between the IFA and the PIFA, but in general, the IFA is a variety of the monopole and the PIFA is a shorted microstrip antenna defined by equation 3.1.

3.5 Helical Antennas

A helix antenna is made by wounding a metal wire-rod conductor in the form of a screw. If the dimensions of the antenna are large compared to the wavelength, the helix is said to be in axial mode and radiates with one major lobe in the direction of its axis as shown in Figure 3.12. If the dimensions are small compared to the wavelength, the helix is said to be in normal mode as shown in Figure 3.13 (Balanis, 2016).

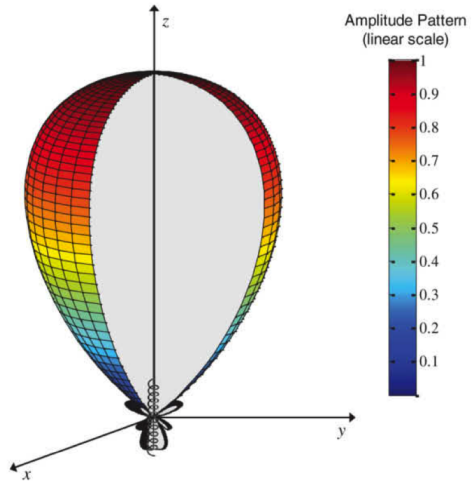

Figure 3.12: Axial mode of helix antenna (Balanis, 2016)

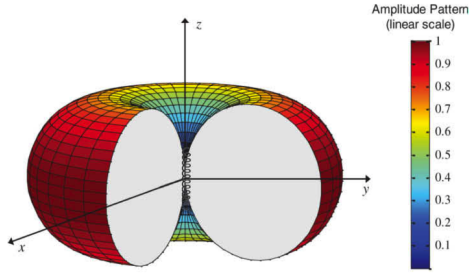

Figure 3.13: Normal mode of helix antenna (Balanis, 2016)

The axial mode is typical for satellite communications since it produces circular polarization. On the other hand, the radiation pattern is highly directional which is unfavourable when steering is not possible. In addition, they are often considered unpractical due to their size at lower frequencies.

The quadrifilar helix antenna (QHA) integrates four helical elements instead of just one, each rotated 90° with respect to one another. It achieves better performance in terms of gain, circular polarization purity and phase centre stability (Takacs, Aubert, Belot, and Diez, 2015). This makes it an increasingly popular antenna for mobile devices and small satellites, as Sowmya (2016) suggests in his paper where he presents a quadrifilar helix antenna designed at 250MHz for a small satellite. Both an open- and close-ended configuration is analysed. The designs and their results are shown in Figure 3.14 and 3.15. The gain is clearly better for the close-ended design, with a maximum of 2.18dBi. The maximum gain for the open-ended design reaches only -5.93dBi.

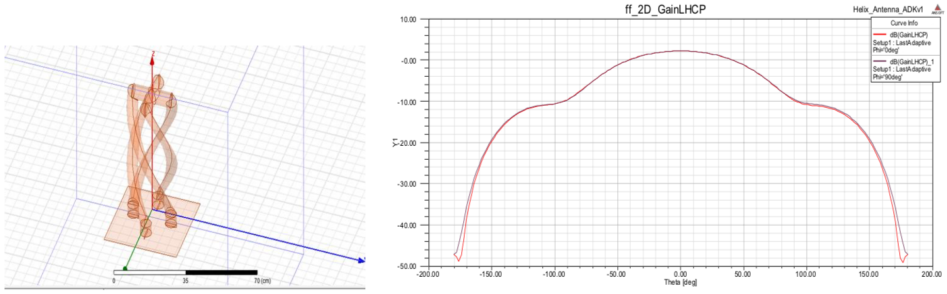

(a) Design model **(b)** 2D Radiation pattern for LHCP

Figure 3.14: Close-ended quadrifilar helix by Sowmya (2016)

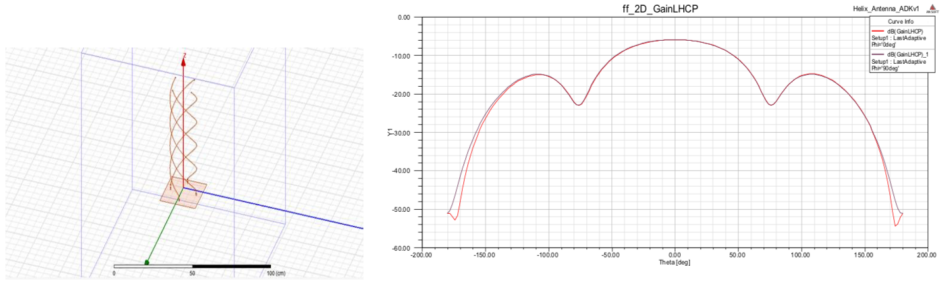

(a) Design model **(b)** 2D Radiation pattern for LHCP

Figure 3.15: Open-ended quadrifilar helix by Sowmya (2016)

Although the QHA designed by Sowmya (2016) did not perform well with regards to gain, others have demonstrated that better results are achievable. For example the QHA designed by McKerricher and Wight (2010) for RFID applications. It has similar performance indicators and limitations to those posed by this thesis; frequency of 900MHz, maximum output power of 1 Watt, circular polarization and peak gain of at least 3.5dBi when elevation angle is around 55°. A prototype of the antenna was built and the results are shown in Figure 3.16. Figure 3.16(c) shows that the gain of the prototype was reduced by as much as 5dBi compared to the simulated model. There exists methods to improve this such as adjusting the feed- and matching network. In general, the radiation pattern has an ideal shape.

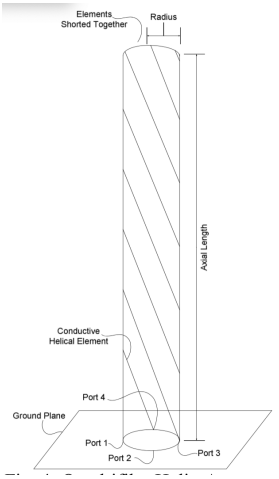

(a) Design model

(b) Prototype

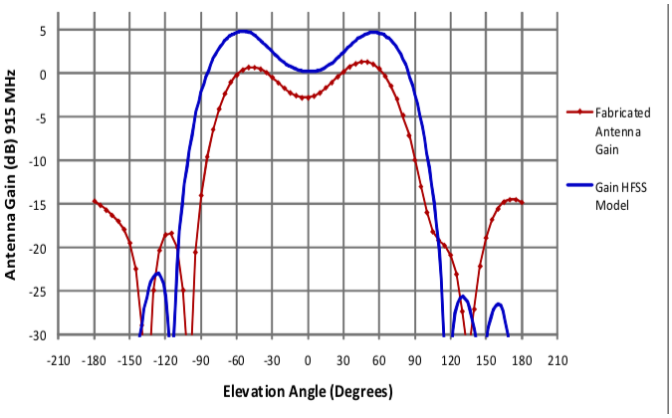

(c) Radiation pattern

Figure 3.16: Quadrifilar helix for RFID by McKerricher and Wight (2010)

The QHA design by McKerricher and Wight (2010) is based on parameters defined in a paper by Kilgus (1975) where r_0 is the radius in wavelengths, p is the pitch distance measured along the axis of the helix, N is the number of turns and L_{ax} the axial length of the helix. They are related by equation 3.4 and 3.5. Certain values of k and p give shaped-conical radiation patterns where the gain decreases from a maximum at the edge of the cone to a minimum at the center. This is precisely what the radiation pattern of the antenna on the sensor buoys should look like. The different patterns for different k and p values are shown in Figure 3.17.

$$k = \frac{r_0}{p} \tag{3.4}$$

$$L_{ax} = pN \tag{3.5}$$

To achieve the pattern in Figure 3.17(b), k must equal 0.038, N must equal 2 and p must equal 0.667λ. The radius of the helix at 400MHz thus becomes:

$r_0 = k \times p = 0.038 \times 0.667\lambda = 0.025\lambda$
$0.025 \times 0.75 = 0.019\text{m} = 1.9\text{cm}$

The axial length of the helix at 400MHz becomes:

$L_{ax} = pN = 0.667\lambda \times 2 = 1\text{m}$

These results are comparable to the design by McKerricher and Wight (2010): a 36cm long QHA at 900MHz with a radius of 1.27cm and 2 helical turns. All the performance indicators presented in Table 3.1 seem to be met, although the gain is somewhat low. The axial ratio was not measured for the antenna in McKerricher and Wight (2010), but according to Kilgus (1975) the AR of the circular polarization was generally excellent for the entire QHA data set, measuring 3 to 6 dB.

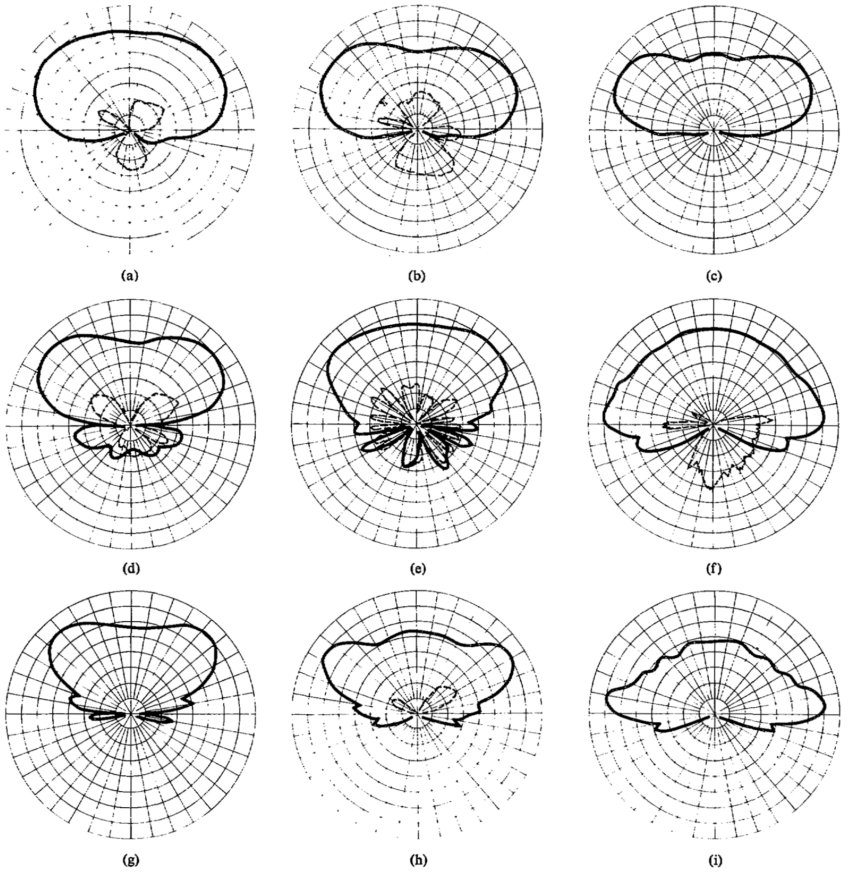

Circular polarization, 5 dB/division, measured radiation patterns (——— left-hand circular, – – – – – – right-hand circular). (a) 2 turns, $k = 0.083$, $p = 0.59$. (b) 2 turns, $k = 0.038$, $p = 0.667$. (c) 3 turns, $k = 0.083$, $p = 0.609$. (d) 3 turns, $k = 0.083$, $p = 0.600$. (e) 5 turns, $k = 0.164$, $p = 0.472$. (f) 5 turns, $k = 0.164$, $p = 0.707$. (g) 5 turns, $k = 0.083$, $p = 0.518$. (h) 5 turns, $k = 0.083$, $p = 0.579$. (i) 5 turns, $k = 0.083$, $p = 0.792$.

Figure 3.17: Radiation patterns for different k and p values on a backfire QHA (Kilgus, 1975)

3.6 Microstrip Antennas

A microstrip antenna is a thin metallic patch printed on a grounded dielectric substrate, as illustrated in Figure 3.18. Better efficiency and larger bandwidth is achieved using a thicker substrate with a low dielectric constant, but this will also increase the overall antenna size. The main lobe of the radiation pattern is usually normal to the patch, although end-fire radiation is also possible. The patch can be shaped into different geometries and sizes, making it applicable to various use cases. It is also relatively cheap and easy to fabricate. However its bandwidth is relatively narrow, it has a limited power capacity, spurious feed radiation, poor polarization purity and tolerance problems (Pozar, 1992).

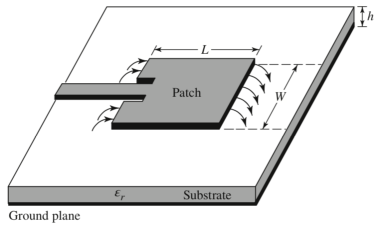

Figure 3.18: Illustration of microstrip antenna (Balanis, 2016)

Constantine G. Kakoyiannis and Philip Constantinou from the National Technical University of Athens, have designed and simulated a microstrip antenna at 436MHz suitable for picosatellites ($10 \times 10 \times 10\text{cm}^3$) (Kakoyiannis and Constantinou, 2008). As shown in Figure 3.19, the design is based on a technique that uses slits that are symmetrically placed at the perimeter of the patch. The slits increase the electrical length of the antenna as they disturb the currents flowing on the surface, forcing them to meander (Notis, Liakou, and Chrissoulidis, 2004). Circular polarization is ensured using a symmetric patch and a dual feed with signals in-phase quadrature.

The results of the simulations indicate a maximum directivity of 4.9dBi, but a maximum gain of only 0.7dBi due to low efficiency. The radiation pattern is shown in Figure 3.20. The dimensions of the final model are $170 \times 120 \times 100\text{mm}^3$. The paper points out that a higher gain is needed for small satellite communication, but this is very difficult with the size constraint of the picosatellite and a frequency of 436MHz. They suggest increasing the frequency to 0.9 or 2.4GHz since the dimensions are fixed.

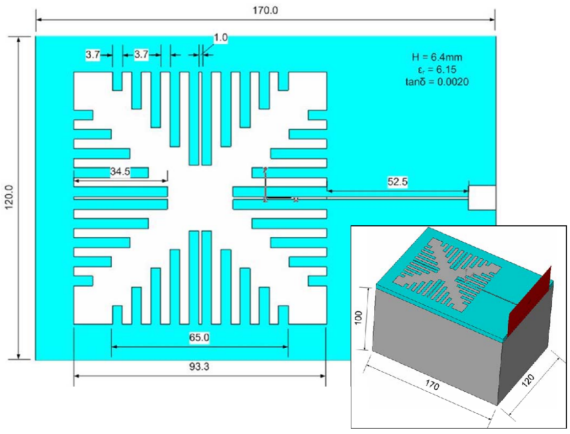

Figure 3.19: Microstrip antenna with tapered peripheral slits by Kakoyiannis and Constantinou (2008)

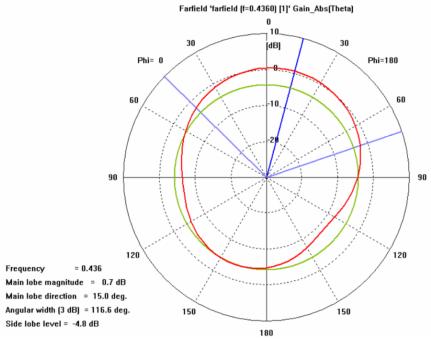

(a) Pattern cut at $\phi = 0°$

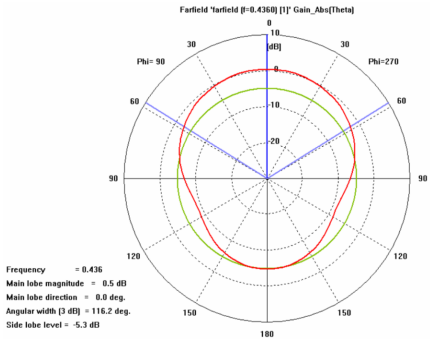

(b) Pattern cut at $\phi = 90°$

Figure 3.20: Radiation pattern of microstrip antenna with tapered peripheral slits by Kakoyiannis and Constantinou (2008)

3.7 Discussion

The linear wire antennas are simple and easy to manufacture, but the gain is low and circular polarization is not a given. On the other hand, the radiation pattern achieved by Schraml et al. (2017) is ideal. The IFA and PIFA seem to have good potential in terms of gain and circular polarization, and their small size makes them practical. The radiation patterns of the PIFAs that were studied are not perfectly ideal.

The QHA is circularly polarized and the simulations by Kilgus (1975) show good potential for an ideal radiation pattern. At 400MHz, the length of the antenna would be in the order of 1m which is rather large but within the requirement. The gain seems somewhat low at only 2.18dBi for the design by Sowmya (2016). Microstrip antennas can achieve good directivity, but due to low efficiency, the gain decreases drastically. On the other hand, they are small and practical antennas that can be customized perfectly for the use case presented. In addition, they can easily be designed to radiate circularly polarized waves.

A summary of the advantages and disadvantages of the antenna types with regards to the performance indicators in Table 3.1, is given in Table 3.2. In section 3.2, gain was identified as being the most important performance indicator. Without doubt, the PIFA (or IFA) by Amoudi and Langley (2009) has the highest gain of all those presented. It also seems possible to manufacture an IFA without too much difficulty. The radiation pattern is not ideal, but it should be possible to modify by, for example, changing the position of the elements on the ground plane. Whereas Amoudi and Langley (2009) had strict size constraints, the Arctic antenna is more flexible. Finally, the IFA is fairly flat and can be hidden in the Arctic snow.

	Gain	Polarization	Radiation Pattern	Size	Ease of fabrication
Dipole					
Monopole					
IFA					
Helix					
Microstrip					

Table 3.2: Pros and cons of the different antenna types. Green: good, orange: average and red: bad.

Antennas for satellite applications at NTNU have mostly been microstrip (Bolstad, 2009) or helix antennas (Stenhaug, 2011). An IFA was designed in 2008 but for a smoke detector (Lunde, 2008). Looking into the potential of IFA arrays will contribute to the field of research that concerns physically small antennas for satellite communication ground terminals.

Chapter 4

Design and Computer Simulations

This chapter describes how the antenna was designed using Computer Simulation Technology (CST) Studio Suite 2019; a high-performance 3D electromagnetic analysis software. The CST microwave transient solver is based on a finite integration technique (FIT). It consists of discretizing the integral form of Maxwell's equations by choosing geometrical grid objects as special integration domains. It is a suitable technique for computer simulations as the complexity of the continuous electric and magnetic field quantities is reduced to a finite number of well-defined discrete unknowns (Weiland, 2003).

4.1 Preliminary design

The IFA designed by Amoudi and Langley (2009) that was presented in section 3.4, is used as a baseline for the Arctic antenna design. The dimensions of the model they built was scaled down by 5, meaning the operating frequency of the antenna model is 725MHz instead of 145MHz. The dimensions at this frequency were given in the article and are listed in Table 4.1. They were scaled up by 1:1.81 to change the resonant frequency from 725MHz to 401MHz. The resulting dimensions used in the preliminary design of the Arctic antenna are also shown in Table 4.1.

	Amoudi and Langley (2009)	**Emilie Udnaes**
Frequency f (MHz)	725	401
Length L (mm)	70	127
Width W (mm)	5	9
Height H (mm)	26	47
Thickness T (mm)	1	2

Table 4.1: Design of IFA at 400MHz dimensioned after Amoudi and Langley (2009). Scale 1:1.81.

The spacing between the feed line and the shorting affects how well the antenna is matched. It was decided to choose an arbitrary value and sweep the parameter during optimization to the find the best value at 400MHz. The same goes for the spacing between the elements on the ground plane. A drawing of the preliminary design is shown in Figure 4.1. The figure also illustrates how the parameters are defined for future reference.

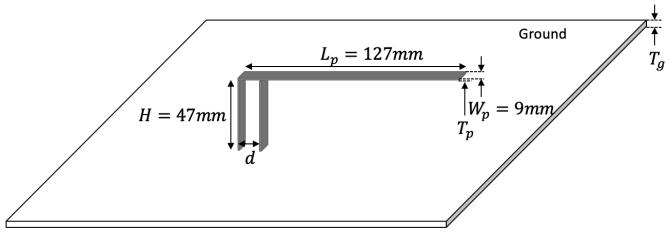

(a) Element

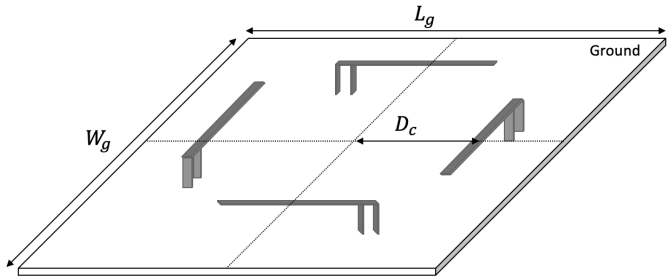

(b) Array

Figure 4.1: Preliminary design and definition of parameters

4.2 Optimization

The results of the preliminary design in CST indicated that an optimization of the design was needed. A detailed walk-through of this process is presented in Udnaes (2018). A more concise summary of this process will now be presented.

CST allows all the parameters that define the dimensions of the antenna to be swept. The designer chooses the beginning and end value, and how many steps in between. For each value, a new set of results is generated and saved. When the sweep is done, the results can be compared and the value that gives the most ideal result is selected to replace the old value.

Since there is an almost endless number of parametric combinations that can be swept, the process is highly experimental and time consuming. Not all combinations that were investigated will be presented, but the effect that the parameters have on the S11 parameters and the radiation pattern are illustrated.

The radiation pattern of an antenna is a two- or three dimensional spatial distribution of radiation properties such as power flux density, radiation intensity, field strength, directiviy, phase or polarization as a function of the observer's position along a path or surface of constant radius (Balanis, 2016). Figure 4.2 shows the coordinate system used in the analysis of such radiation patterns. The elevation angle that will be referred to later in the text, is in the negative Theta, θ direction.

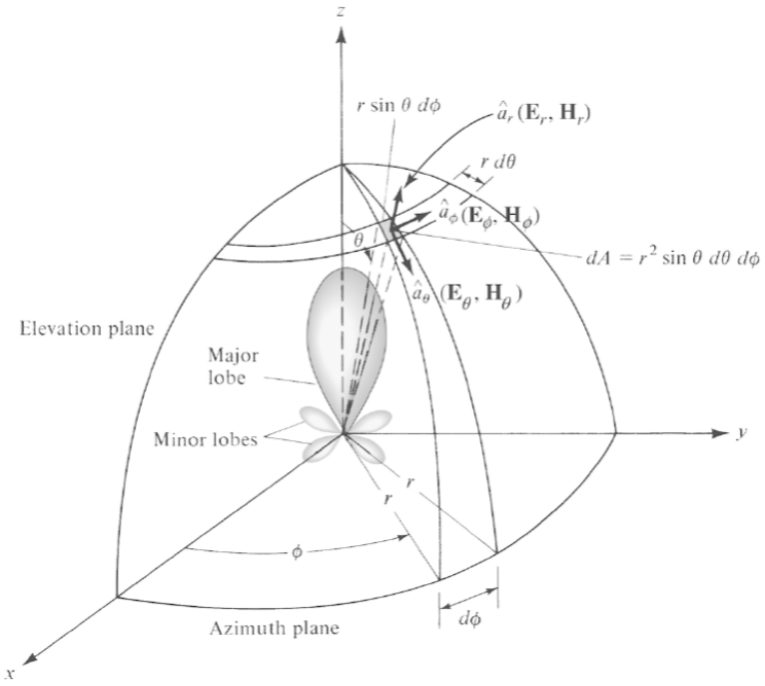

Figure 4.2: Coordinates of a radiation pattern (Balanis, 2016)

The realized gain has been selected as the radiation property of interest. CST defines it as the directivity times the total efficiency where total efficiency e_0 is the reflection (mismatch) efficiency, e_r times the dielectric efficiency, e_d times the conduction efficiency, e_c (equation taken from CST website). The efficiency is a value between 0 and 1.

$$G_0 = 10\log_{10}(e_0 D_0) \tag{4.1}$$

$$e_0 = e_r e_c e_d \tag{4.2}$$

4.2.1 Element

Firstly, the IFA element was optimized separately from the array, at 400MHz. Figure 4.3 shows a sweep of the parameter d. As can be seen, increasing the distance between the feed line and the shorting increases the frequency at which the element is best matched as well as the bandwidth.

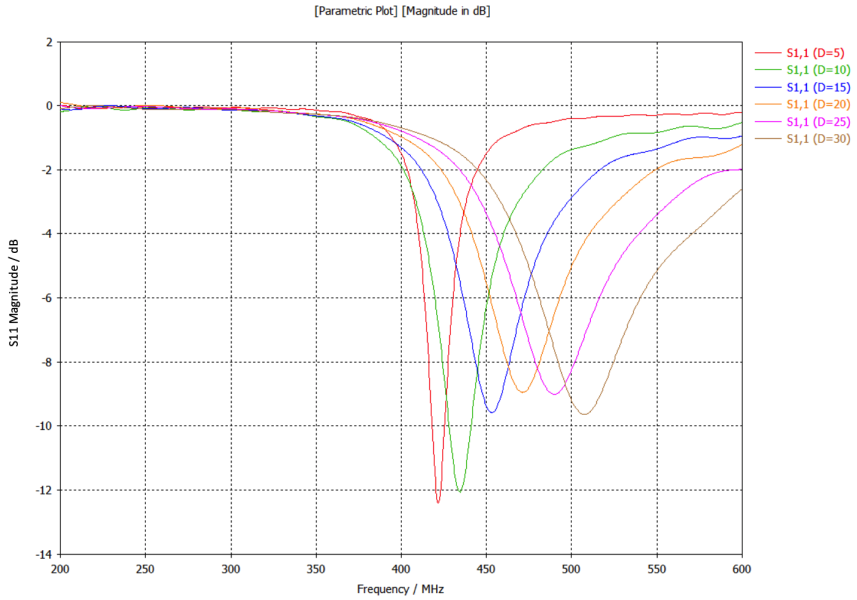

Figure 4.3: S11 parameter when distance between feed and shorting is swept from 5mm to 30mm ($L_p = 127$mm, $W_p = 9$mm, $T_p = 2$mm, $d =$variable, $H = 47$mm, $W_g = L_g = 400$mm)

Figure 4.4 shows that increasing the *length* of the antenna arm, L_p, while all the other parameters stay constant, increases the frequency at which the S11 parameter is the lowest. The S11 parameter drops significantly from -10dB when Lp=150mm, to -27dB when Lp=90mm. When the *height* of the IFA increases, the minimum S_{11} happens at a lower frequency as shown in Figure 4.5. S11 decreases from -8dB when H=35mm, to -13dB when H=55dB. It was found that the width of the arm has little effect on the S11 parameters, as shown in Figure 4.6. However it should be kept in mind that this parameter was swept only from 6mm to 12mm. If the width is increased more, then the design becomes more of a planar structure. Since the objective is to do a parametric study of an IFA, this was avoided.

The design after optimization is shown in Figure 4.7. The radiation pattern is shown in Figure 4.8. The maximum realized gain is 3.78dBi when $\theta = 30°$. Interestingly, the maximum is not in zenith. As was described in section 3.2, this is a wanted characteristic of the radiation pattern. Potentially, the maximum can be lowered even more to $\theta = 45°$. The S11 parameter of the element design at 400MHz is -12.2dB, as shown in Figure 4.9.

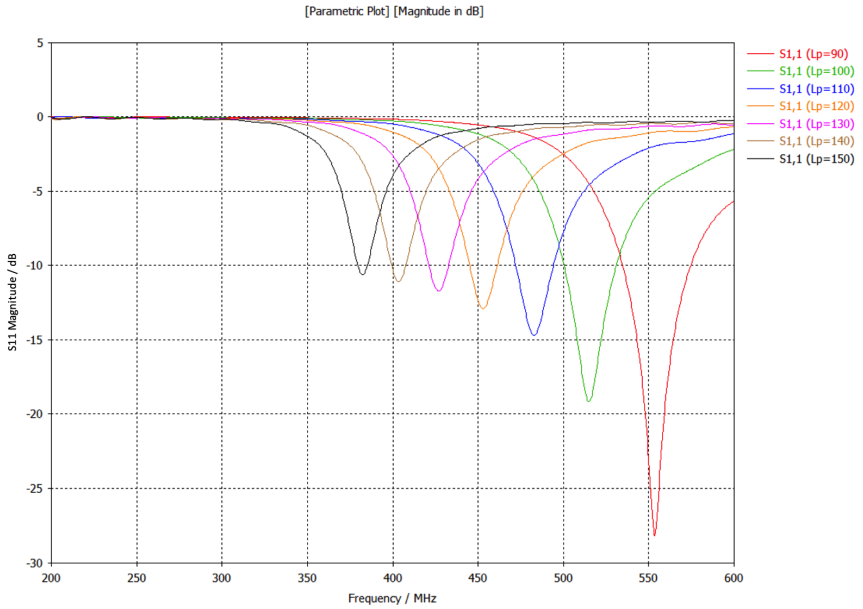

Figure 4.4: S11 parameter when the length of the IFA arm is swept from 90mm to 150mm (L_p = variable, W_p = 9mm, T_p =2mm, d = 10mm, H = 47mm, $W_g = L_g$ = 400mm)

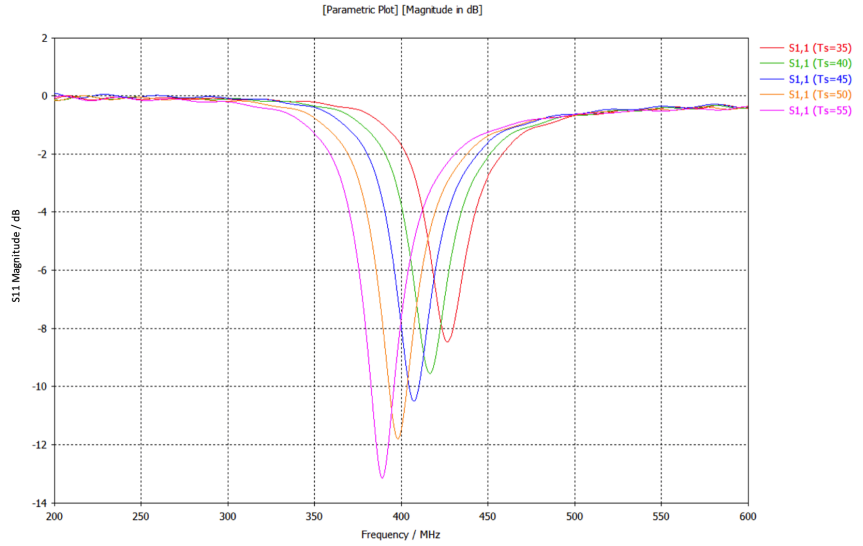

Figure 4.5: S11 parameter when the height of the IFA is swept from 35mm to 55mm (L_p =140mm, W_p = 9mm, T_p =2mm, d = 10mm, H = variable, $W_g = L_g$ = 400mm) (NB! $T_s = H$)

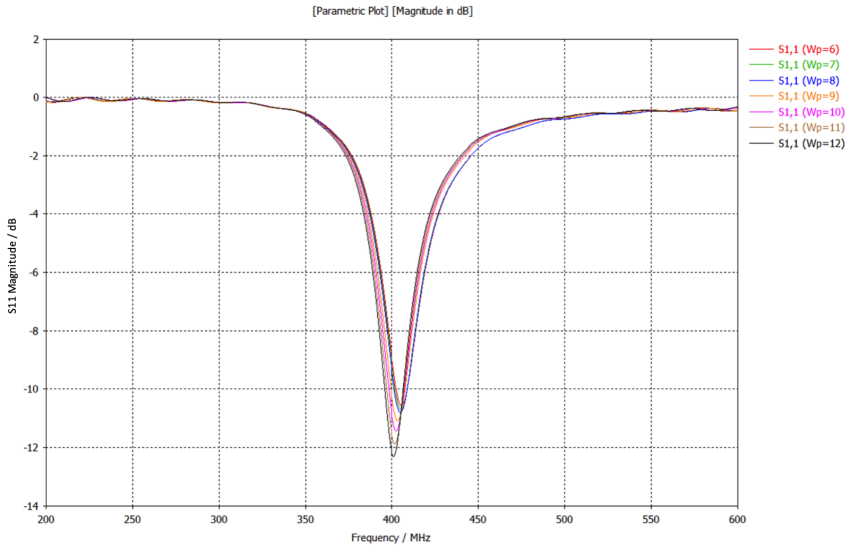

Figure 4.6: S11 parameter when the width of the IFA is swept from 6mm to 12mm (L_p =140mm, W_p =variable, T_p =2mm, d = 10mm, H = 47mm, $W_g = L_g$ = 400mm)

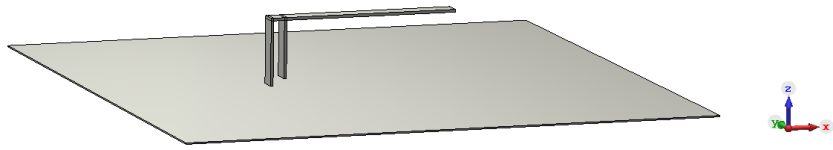

Figure 4.7: Element design (L_p =140mm, W_p =12mm, T_p =2mm, d = 10mm, H = 47mm, $W_g = L_g$ = 400mm)

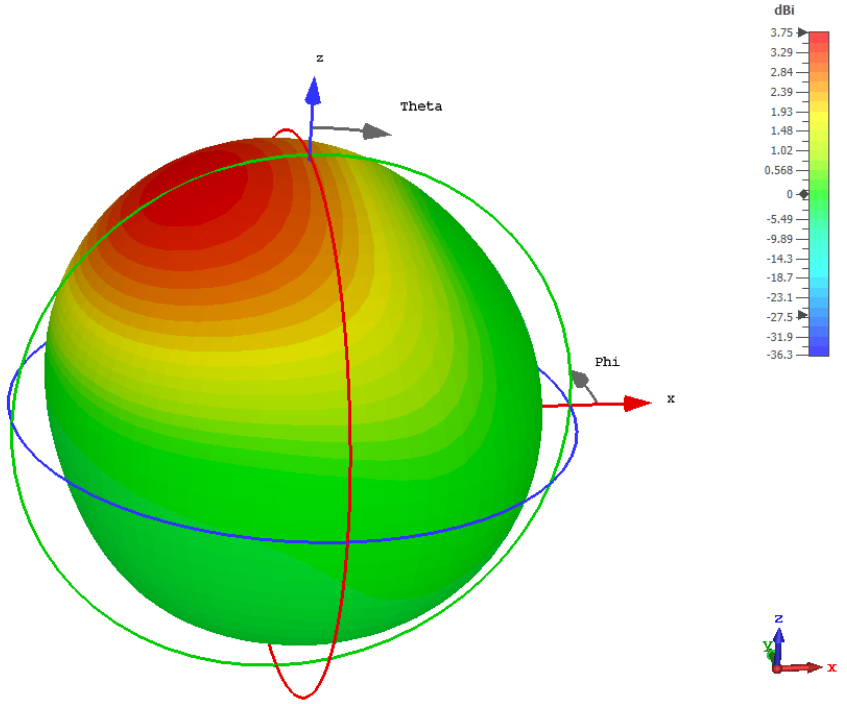

Figure 4.8: Realized gain of element design (L_p =140mm, W_p =12mm, T_p =2mm, d = 10mm, H = 47mm, $W_g = L_g$ = 400mm)

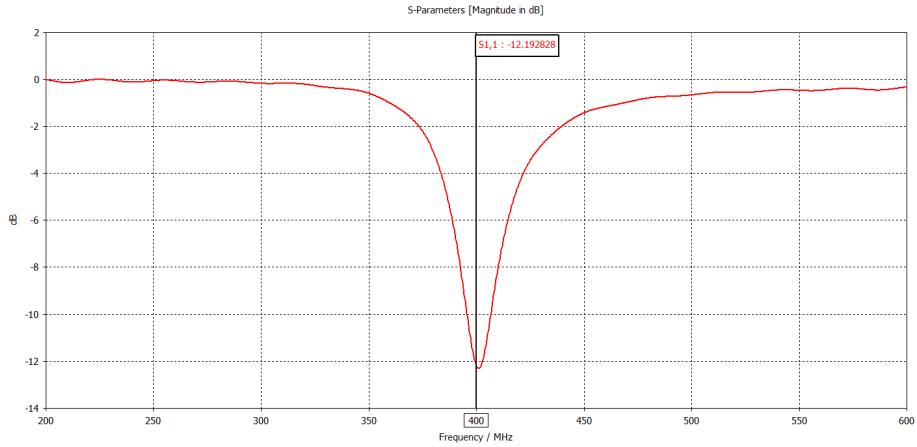

Figure 4.9: S11 parameter of element design (L_p =140mm, W_p =12mm, T_p =2mm, d = 10mm, H = 47mm, $W_g = L_g$ = 400mm)

4.2.2 Array

The design of the array introduced two new parameters: the size and shape of the ground plane and the placement of the elements on the ground plane. After thorough experimentation, the following conclusions were made:

- The greater the ground plane, the greater the gain.
- The further apart the elements are placed on the ground plane, the more directional the radiation pattern.
- The shape of the ground plane has little effect on the radiation pattern.

Some of the designs will now be presented. The focus is on the radiation pattern, as each design has been optimized for the return loss to be at least less than -10dB at 400MHz. The results used in the optimization of the element was used to guide the optimization of the array.

The first design consists of a circular ground plane and elements formed into arc-shaped wires as shown in Figure 4.10(a). Each element is fed with a 90° consecutive phase difference. The radiation pattern when the elements are placed such that D_c=160mm, is shown in Figure 4.12 and when they are placed such that D_c=240mm, in Figure 4.11. As can be seen, when the elements are placed further apart, the radiation pattern of each element can be seen distinctively. The maximum realized gain is then also higher since the pattern is more directive. Although the maximum realized gain is higher in Figure 4.11, the radiation pattern in Figure 4.12 is more ideal because it is more homogeneous in terms of Phi. Another circular design was tested where the ground plane remains circular, but the IFA elements are kept flat as the one shown in Figure 4.7. This did not affect the results very much. The radiation pattern is shown in Figure 4.13 and can be compared with Figure 4.12.

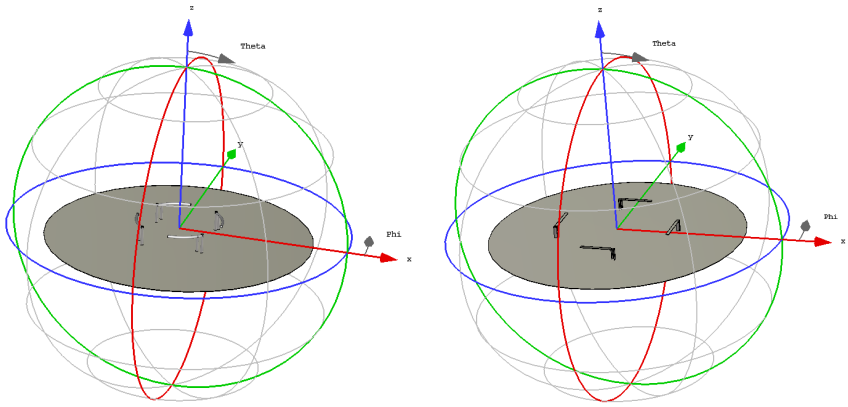

(a) Arced IFA elements **(b)** Standard IFA elements

Figure 4.10: Circular design of IFA array. Diameter of ground plane: 1000mm.

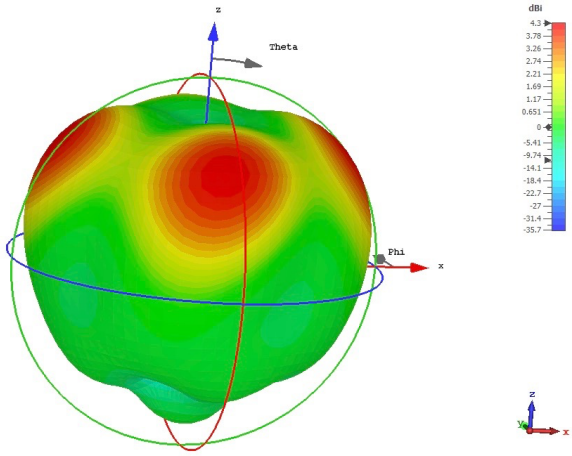

Figure 4.11: Radiation pattern and far field realized gain of circular IFA design, arced elements, D_c=240mm

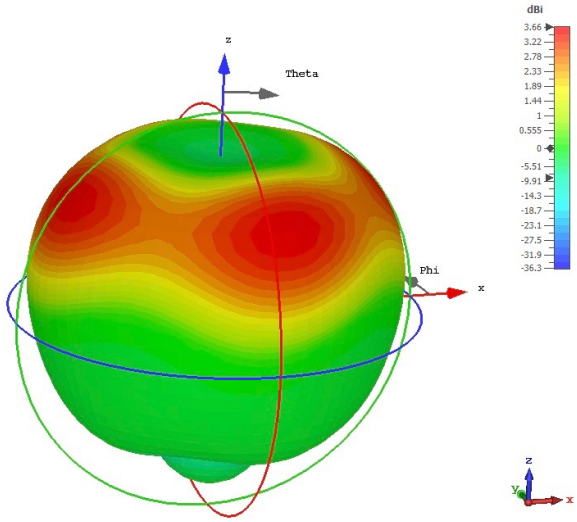

Figure 4.12: Radiation pattern and far field realized gain of circular IFA design, arced elements, D_c=160mm

The second design is an array of PIFA elements. The width of the elements was increased and a substrate was introduced, see Figure 4.14. This design did not give good results. Figure 4.15 shows the radiation pattern when D_c=150mm and Figure 4.16 shows the radiation pattern when D_c=300m. The design was dismissed since it did not resemble the ideal radiation pattern previously discussed.

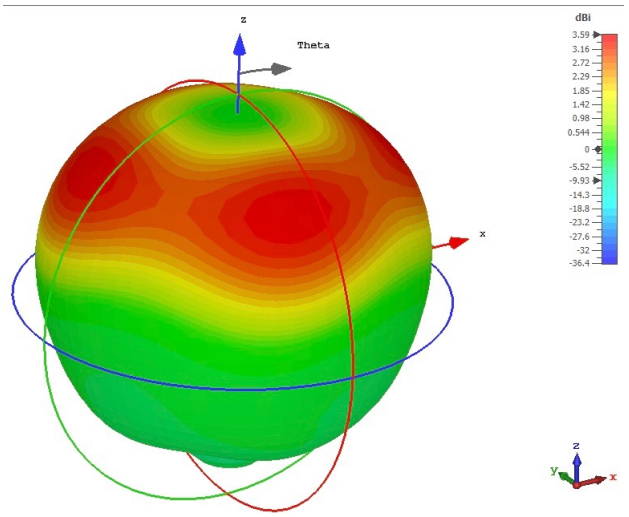

Figure 4.13: Radiation pattern and far field realized gain of circular IFA design, standard elements, D_c=160mm

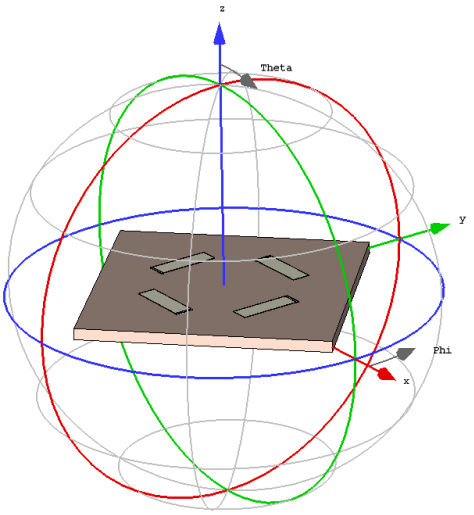

Figure 4.14: Design of PIFA array, $W_g = L_g = 500$mm

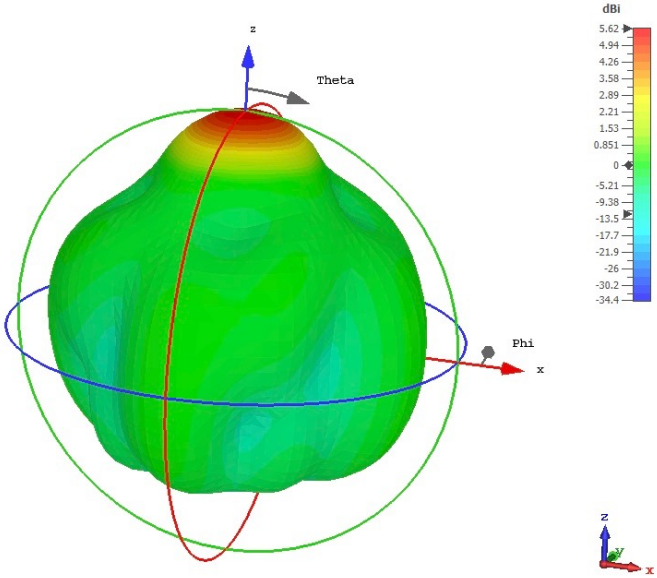

Figure 4.15: Radiation pattern and far field realized gain of PIFA array, $D_c = 150$mm

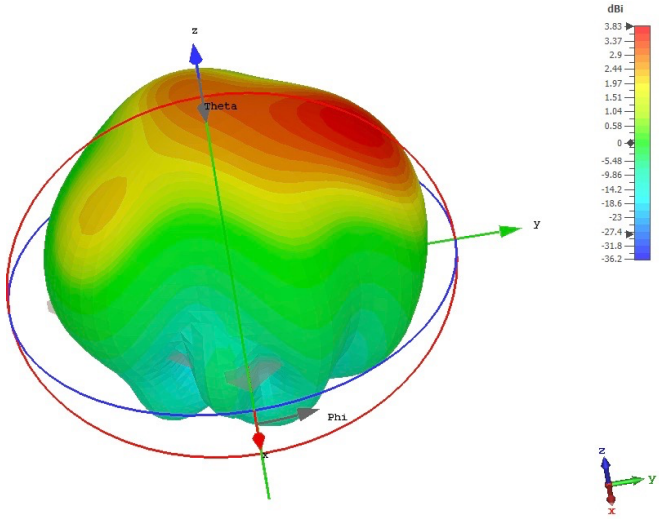

Figure 4.16: Radiation pattern and far field realized gain of PIFA array, $D_c = 300$mm

The third design is the most simple, with a square ground plane and standard IFA elements. It turns out that this simple design is in fact the most effective in terms of maximum realized gain and homogeneous partitioning of the gain in Phi direction. It was therefore decided to use this as the final design after careful optimization of all parameters. This final design is shown in Figure 4.17, the radiation pattern in Figure 4.18 and the S11 parameters in Figure 4.19.

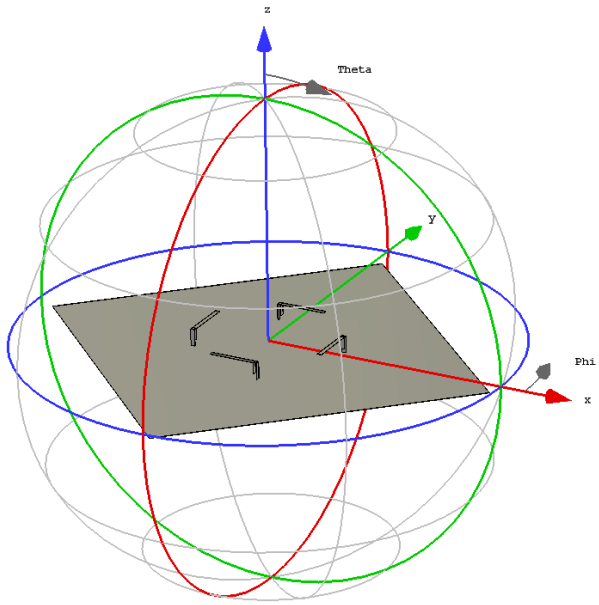

Figure 4.17: Final design of IFA array L_p =135mm, W_p =12mm, T_p =1mm, d = 8mm, H = 45mm, $W_g = L_g$ = 900mm, D_c = 188

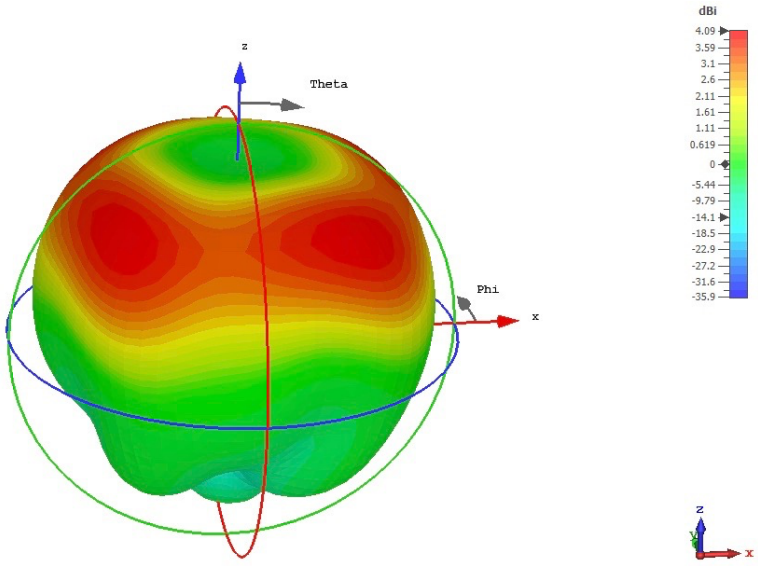

Figure 4.18: Radiation pattern and far field realized gain of final design of IFA array

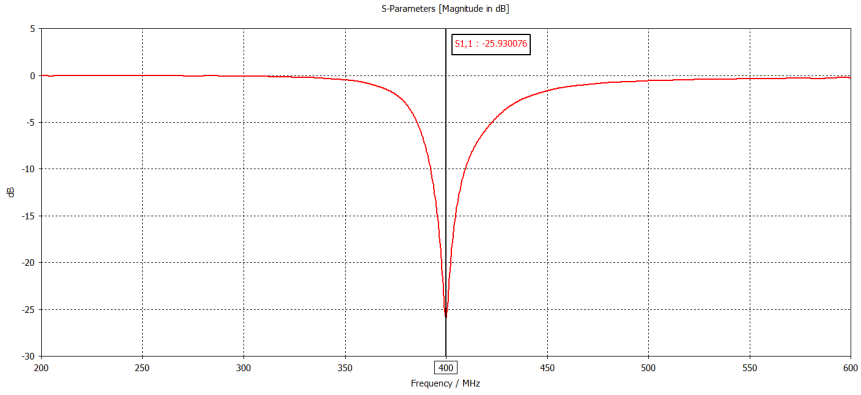

Figure 4.19: S11 parameters of final design of IFA array

4.3 Feed Network

In the CST simulations, each IFA element had a 90° consecutive phase difference at each port. To make this possible in practice, a special feed network was designed. There are many ways to implement phase difference between components, and for this project it was decided to use a four-way power splitter as well as cables that differ by $\lambda/4$ in length. An illustration of the system design is shown in Figure 4.20. The choice of components has already been discussed in Udnaes (2018).

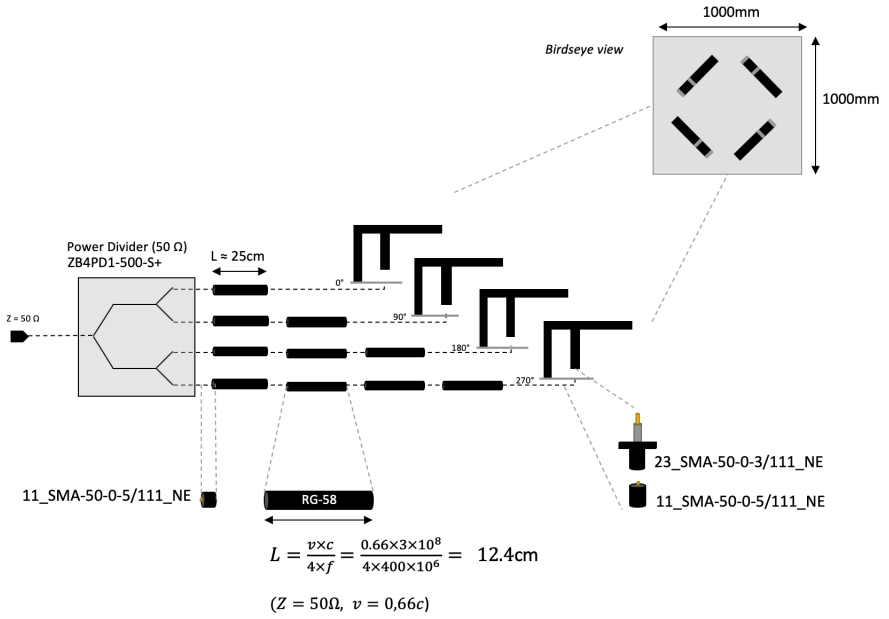

Figure 4.20: Feed network of IFA array

4.4 Discussion

In the optimization process of the design, it became clear that achieving a gain of 10dBi while staying within the size requirement of $1 \times 1 \times 1$ m^3 as well as ensuring that the radiation pattern is not too directive, is not possible. The maximum realized gain of the final design is 4dBi, but for some values of Phi at Theta constant, the gain drops by almost 1dB. See Figure 4.21(a) where the radiation pattern is shown at Phi=75°, and the maximum realized gain is dropped to 3.28dBi. The pattern is symmetrical for every Phi=Phi+90°.

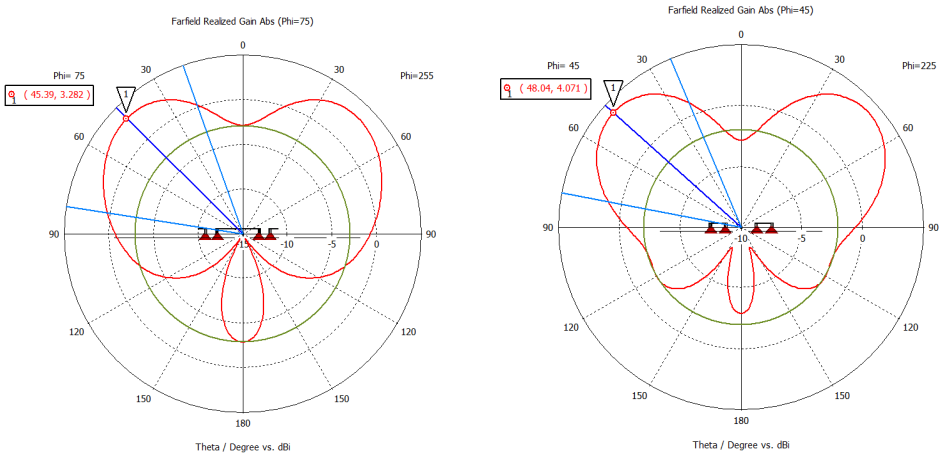

(a) Phi=75° **(b)** Phi=45°

Figure 4.21: 2D radiation pattern and far field realized gain of final IFA design

The link budget was used to calculate the data rate at different elevation angles depending on the gain of the transmitting antenna. All other variables were kept constant. Since the radiation pattern is not perfectly homogeneous in Phi direction, two cases were evaluated: Phi=45° and Phi=75°. In addition, two distinct cases were evaluated with regards to the link budget which is worst case scenario when ionospheric loss is 7dB and best case scenario when ionospheric loss is 1dB. The results are shown in Figure 4.22. Data points were taken every 5° for elevation angles between 30° and 90° (remark: an elevation angle of 30° corresponds to Theta=60°).

When ionospheric loss is low (i.e. 1dB), the data rate varies from ∼85kbit/s (zenith) to ∼240kbit/s (e=55°). When ionospheric loss is high (i.e. 7dB), the data rate is lower and more consistent, varying only from ∼20kbit/s (zenith) to ∼60kbit/s (e=55°). From e=70° on-wards, the curves start to converge. This is because the gain of the antenna at these angles is similar. The graph clearly shows that the data rate will not be constant during the orbital pass.

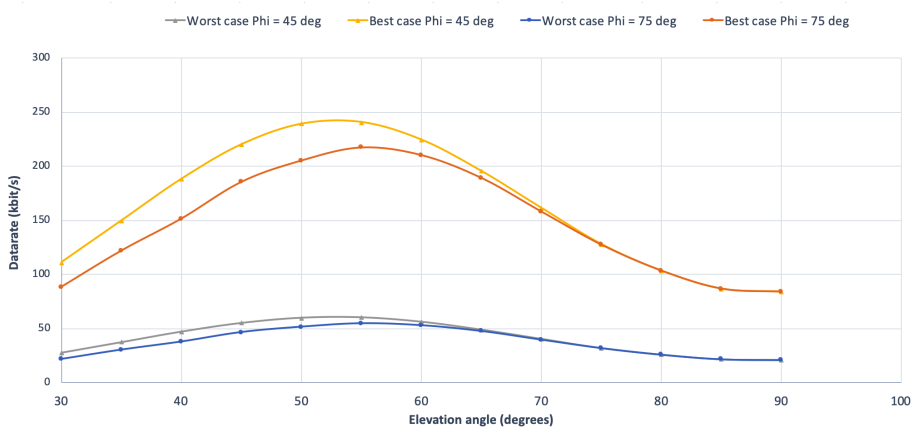

Figure 4.22: Data rate based on results of simulated IFA design

To evaluate whether the antenna would be good enough to use for Arctic satellite communication, the total data throughput in a year was calculated using data from Table 1.3. The method used to calculate the data throughput is described in section 2.9. The results are shown in Figure 4.23 using Phi=45° and an averaged data rate for a given elevation angle range. Depending on location, the minimum throughput is 2,3-3GB and maximum throughput is 9-11,7GB. The further north the sensor nodes are placed, the longer the access time and the greater the throughput.

As was stated in the introduction, the first generation of sensor buoys are expected to generate 2-3GB of data per year. This is expected to increase to hundreds of GB with new generations of sensor buoys. From the results of the simulations, it can be concluded that the IFA that has been designed can support satellite communication links for applications in the Arctic (locations above Longyearbyen) that generate 11GB or less per year.

	Longyearbyen				
		Worst case		Best case	
Elevation (deg)	Access time/year (sec)	Average datarate (kbit/s)	Throughput (GB)	Average datarate (kbit/s)	Throughput (GB)
30-45	303660	42	1,6	167,4	6,4
45-60	128520	58,1	0,9	231,2	3,7
60-75	46920	44,6	0,3	177,3	1,0
75-90	12960	35,3	0,1	100,6	0,2
			2,8		11,3

	GR_South				
		Worst case		Best case	
Elevation (deg)	Access time/year (sec)	Average datarate (kbit/s)	Throughput (GB)	Average datarate (kbit/s)	Throughput (GB)
30-45	265440	42	1,4	167,4	5,6
45-60	86880	58,1	0,6	231,2	2,5
60-75	35280	44,6	0,2	177,3	0,8
75-90	9840	35,3	0,0	100,6	0,1
			2,3		9,0

	GR_North				
		Worst case		Best case	
Elevation (deg)	Access time/year (sec)	Average datarate (kbit/s)	Throughput (GB)	Average datarate (kbit/s)	Throughput (GB)
30-45	257460	42	1,4	167,4	5,4
45-60	135600	58,1	1,0	231,2	3,9
60-75	92820	44,6	0,5	177,3	2,1
75-90	22800	35,3	0,1	100,6	0,3
			3,0		11,7

	Rossøya				
		Worst case		Best case	
Elevation (deg)	Access time/year (sec)	Average datarate (kbit/s)	Throughput (GB)	Average datarate (kbit/s)	Throughput (GB)
30-45	257580	42	1,4	167,4	5,4
45-60	136080	58,1	1,0	231,2	3,9
60-75	92820	44,6	0,5	177,3	2,1
75-90	22440	35,3	0,1	100,6	0,3
			3,0		11,7

Figure 4.23: Data throughput in Gigabyte at different locations in the Arctic (shown in Figure 1.4) when using the simulated IFA design (Phi=45°)

Chapter 5

Prototyping

When the design of the antenna was ready, a prototype of the antenna was built with the help of technical engineers at the NTNU Department of Electronic Systems. Detailed engineering drawings of the antenna and its dimensions were the starting point of the production. They can be seen in Figure 5.1. Some changes were made as the prototype was being built and will be discussed later in the chapter.

Components used in the production of the prototype are listed in Table 5.1. Originally, the idea was to use RG-223 coax cable as discussed in Udnaes (2018). However since RG-58 cable was already available at the university and the cable length needed was fairly long (1.74m), it was decided to use that instead in the prototype. The SMA connectors had to be changed accordingly to fit with the U7 cable type instead of U9. The RG-58 cable has a temperature range of -25°C to +85°C and is therefore not suited for the Arctic. However, it works for the purpose of testing the performance of the antenna.

Quantity	Description	Component ID number
4	Straight panel receptacle jack, flange mount (SMA)	23_SMA-50-0-3/111_NE
8	Straight cable plug (SMA)	11_SMA-50-3-5/111_NE
1	Power splitter (SMA)	ZB4PD1-500-S+
1,74 m	Coax cable	RG-58

Table 5.1: Components used in the antenna prototype

The material used for the antenna itself is brass. Brass is a copper-zinc alloy that is easy to shape. At the same time it is a relatively strong metal that does not bend too easily. It was a suitable choice of material for the production of the prototype considering that it was already available at the university. The details of the alloy are not known and therefore it is difficult to predict its behavior in low temperatures down to -40°C. This must be tested before an eventual use in the Arctic.

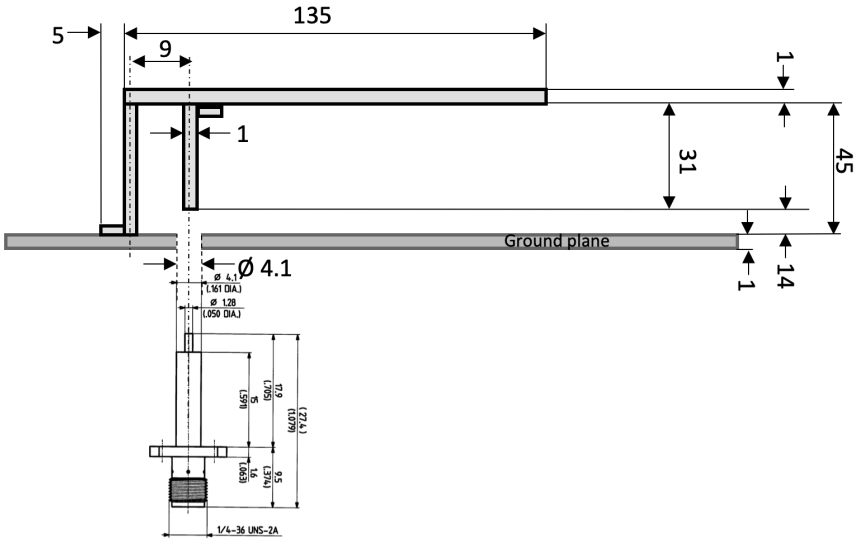

(a) Antenna element - side view

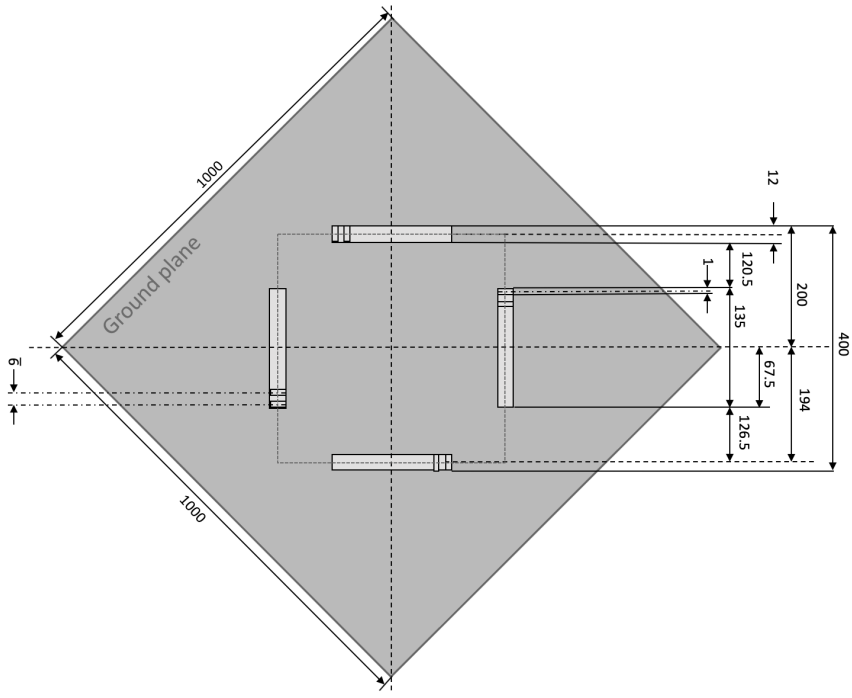

(b) Antenna array - top view

Figure 5.1: Dimensional drawings of antenna in mm

5.1 Ground Plane

The ground plane is a 900x900mm, 1mm thick brass plate. From the simulations it was found that the bigger the ground plane the greater the gain. Since 900mm was the greatest length available at the university, it was chosen to use this instead of 1x1m as intended in order to avoid any production delays.

The metal brass plate was mounted onto a 3cm thick Divinycell plate for stability. This material is easy to cut in, making it possible to make holes for cables and the power splitter. Four blocks of the same material were placed at the corners to lift the ground plane and allow space for the backside electronics. A picture of the prototype is shown in Figure 5.2.

(a) Back **(b)** Front

Figure 5.2: Prototype after production

5.2 Coax Cables and Power Splitter

Four RG-58 coax cables with different lengths were made with the help of Stein Olav Lund, Senior Engineer at NTNU. The lengths were calculated using the velocity factor specific to RG-58 which is 66%. Straight SMA cable plugs were crimped at both ends of each cable. The assembly instructions for SMA can be found in Appendix B.

The first cable has a length equal to the shortest distance possible between the first antenna element and the power splitter. This is a reference length that must be added to each of the other three cables. It was found that the most ideal position of the power splitter is at the center of the ground plane, making the reference cable 25cm long. The lengths of the four cables are as follows:

$L_1 = 25\text{cm}$
$L_2 = 25 + \frac{1\lambda}{4} = 25 + v \times \frac{c}{4f} = 25 + 0.66 \times \frac{3\times10^8}{400\times10^6} \times \frac{1}{4} = 25 + 12.4 = 37.4\text{cm}$
$L_3 = 25 + \frac{2\lambda}{4} = 25 + v \times \frac{2c}{4f} = 25 + 0.66 \times \frac{3\times10^8}{400\times10^6} \times \frac{2}{4} = 25 + 24.8 = 49.8\text{cm}$
$L_4 = 25 + \frac{3\lambda}{4} = 25 + v \times \frac{3c}{4f} = 25 + 0.66 \times \frac{3\times10^8}{400\times10^6} \times \frac{3}{4} = 25 + 37.1 = 62.1\text{cm}$

It amounts to 174.2cm of cable in total. The power splitter was simply screwed onto the Divinycell plate with each of the four output ports connected to the feed of each element through the coax cables. The antenna element can be taken off the larger ground plane to allow proper tightening of the SMA connector.

5.3 Element Design

Each IFA element was created as a separate antenna that can be completely removed from the larger ground plane. This makes it easier to transport the antenna array by allowing the more delicate structures to be packed separately. A guideline to mount the antenna after transportation is given in Appendix A. Instead of soldering the elements to the ground plane as was originally planned, they were screwed on. This allowed for more flexibility in the tuning process as is described in the next section.

The arm of the IFA is a piece of brass bent towards the ground plane. Brass is fairly rigid, meaning the bent structure does not sway unless it is touched. If the antenna will be part of a moving object, a stabilizing arrangement should be considered. This could be for example an electrically invisible material glued on between the bent structure and the ground plane.

5.4 Added Features

During the simulations it was noted that the distance between the feed and the shorting is sensitive and will affect the return loss of the antenna. Each element was therefore designed so that this distance can be varied within approximately one centimeter. A zoom in on this design feature can be seen in Figure 5.3. The straight panel SMA connector is not movable, but the shorting can be moved closer to the SMA, and the feed strip that is attached to the bent structure can be moved accordingly. This possibility to adjust was particularly useful in the testing and tuning of the prototype.

Another added feature is the possibility to adjust the position of the element on the ground plane. During the simulations it was found that by adjusting the position by as little as 1cm, the ”dip” at Theta=0° in the radiation pattern could be deepened by 1dBi. This feature was therefore added to the design to test whether the position of the element is really as sensitive as the simulations suggest, and if so allow the most optimal position to be used.

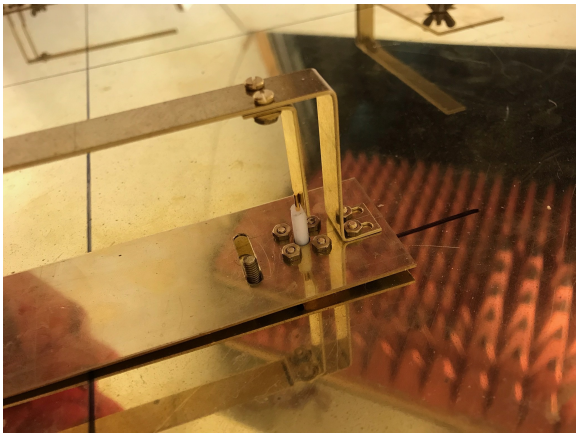

Figure 5.3: Picture of element design features

5.5 Physical Properties of Prototype

- Weight: 11.8 kg
- Height: 14 cm
- Diameter: 90x90 cm
- Interface: SMA
- Max power input: 1 Watt
- Impedance: 50 Ω

Chapter 6

Testing

This chapter explains how the testing of the prototype was planned and conducted. It is organized such that the requirement is first introduced before the setup is described and illustrated. Expected results and actual results are presented and discussed. The requirements are labeled as either pass or fail depending on the results of the measurements.

6.1 Return Loss

ID	Title	Requirement	Purpose
RL01	Return Loss	S11 < -10dB	Ensure that as little power as possible is reflected at the input of the antenna.

Table 6.1: Test requirement for the Return Loss at 400 MHz

According to Pozar (2012), there are three main reasons why impedance matching is important: 1) to ensure maximum power is delivered to the antenna, 2) to improve signal-to-noise ratio of the system and 3) to reduce amplitude and phase errors. Different techniques can be used to ensure good impedance matching including lumped elements, tapered lines, quarter-wave transformer, Chebyshev transformer or stubs. The inverted-F antenna can be properly tuned by varying the distance between the feed and the short-circuited stub.

Return loss is an effective measure to determine if there is an impedance mismatch. Return loss can also be referred to as the S11 parameter of a port. S-parameters relate amplitudes (magnitude and phase) of traveling waves incident and reflected from a microwave network (Pozar, 2012). The microwave network can consist of several ports, and the S-parameter will relate the voltage waves incident on the ports to those reflected from the ports. Considering an N-port network where V_n^+ is the amplitude of the voltage wave incident at port

n and V_n^- is the amplitude of the voltage reflected from port n, then the scattering matrix is given by:

$$\begin{vmatrix} V_1^- \\ V_2^- \\ . \\ . \\ V_n^- \end{vmatrix} = \begin{vmatrix} S_{11} & S_{12} & . & . & . & S_{1N} \\ S_{21} & . & . & . & . & . \\ . & . & . & . & . & . \\ . & . & . & . & . & . \\ S_{N1} & . & . & . & . & S_{NN} \end{vmatrix} \times \begin{vmatrix} V_1^+ \\ V_2^+ \\ . \\ . \\ V_n^+ \end{vmatrix}$$

A particular element of the S-matrix is defined by equation 6.1. S_{ii} is the reflection coefficient seen looking into port i when all other ports are terminated in matched loads. S_{ij} is the transmission coefficient from port j to port i when all other ports are terminated in matched loads (Pozar, 2012). The transmission coefficient T is often expressed in dB and referred to as the insertion loss IL.

$$S_{ij} = \left. \frac{V_i^-}{V_j^+} \right|_{V_k^+ = 0 \text{ for } k \neq j} \tag{6.1}$$

$$IL = -20\log|T|\text{dB} \tag{6.2}$$

For a system to be lossless, the scattering parameters must satisfy equation 6.3 and 6.4 (Pozar, 2012). In other words, the dot product of any column in the S-matrix with the conjugate of the same column, must give unity. The dot product of any column in the S-matrix with the conjugate of another column must give zero. The scattering parameters are properties only of the network itself assuming the network is linear and under the condition that all ports are matched. It should also be noted that the scattering matrix is symmetric for reciprocal networks (Pozar, 2012).

$$\sum_{k=1}^{N} S_{ki} S_{kj}^* = 0, \text{ for } i \neq j \tag{6.3}$$

$$\sum_{k=1}^{N} S_{ki} S_{ki}^* = 1, \text{ for } i = j \tag{6.4}$$

6.1.1 Setup

S-parameters are measured using a vector network analyzer (VNA). An illustration of the RL01 test setup can be seen in Figure 6.1. Equipment used in the setup include:

- Antenna Under Test (AUT)
- Power splitter ZB4PD1-500-S+ (datasheet in Appendix C)
- 4 phase shifting RG-58 cables (25cm, 37.4cm, 49.8cm and 62.1cm)
- Vector network analyzer Rohde & Schwarz ZVA50 10MHz..50GHz
- Cable between VNA and AUT
- Calibration kit 85052D4 3.5mm

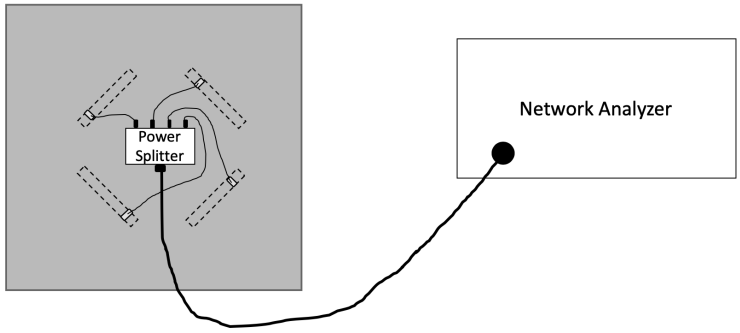

Figure 6.1: Test setup for tuning S11-parameters

The results from the VNA were exported as .s1p files and converted using MATLAB's "sparameters" function from the RF Toolbox. The full test procedure is given in Figure 6.2. MATLAB scripts can be found in Appendix E.

6.1.2 Calibration

To reduce systematic errors in the measurements, the VNA was calibrated using a Hewlett Packard 85052D4 3.5mm Calibration Kit. One-port calibration removes three systematic error terms including directivity, source match, and reflection tracking from reflection measurements (AgilentTechnologies, 2002). These errors are found by establishing three equations with three known calibration standards (ex. open, short and load). The VNA used in the test setup automatically solves the equation after the calibration procedure has been followed.

6.1.3 Expected Results

From the simulations made in CST, the S11 parameter is expected to be similar to that shown in Figure 4.19. In the CST simulations, each element was fed with a 90° consecutive phase difference. In the prototype, this phase difference is created using a power splitter and cables with a $\lambda/4$ consecutive length difference. The results of the simulations versus the test measurements are therefore likely to be somewhat different due to inaccuracies in the components as well as loss factors.

6.1.4 Test Procedure

<table>
<tr><th>Step</th><th>Description</th><th>Executed (sign)</th><th>Comment</th></tr>
<tr><td>1</td><td>Calibrate VNA</td><td></td><td></td></tr>
<tr><td>2</td><td>Measure S11 of each element and export results to .s1p file</td><td></td><td>
<table>
<tr><th></th><th>dB @ 400MHz</th><th>Min(dB) @ MHz</th></tr>
<tr><td>Port 1</td><td>-2.70</td><td>-32.42@426</td></tr>
<tr><td>Port 2</td><td>-2.83</td><td>-25.75@430</td></tr>
<tr><td>Port 3</td><td>-2.66</td><td>-33.38@432</td></tr>
<tr><td>Port 4</td><td>-3.08</td><td>-29.72@432</td></tr>
</table>
</td></tr>
<tr><td>3</td><td>Measure S11 at input of array and export results to .s1p file</td><td></td><td>-33.53 dB @ 446MHz (minimum)
-18.36 dB @ 400MHz</td></tr>
<tr><td>4</td><td>Tune each element to the same frequency, as close to 400MHz as possible and export results to .s1p file</td><td></td><td>
<table>
<tr><th></th><th>dB @ 400MHz</th><th>min(dB) @ MHz</th></tr>
<tr><td>Port 1</td><td>-3.91</td><td>-15.62@418</td></tr>
<tr><td>Port 2</td><td>-4.63</td><td>-13.53@422</td></tr>
<tr><td>Port 3</td><td>-3.41</td><td>-15.31@420</td></tr>
<tr><td>Port 4</td><td>-4.97</td><td>-16.10@425</td></tr>
</table>
</td></tr>
<tr><td>5</td><td>Measure S11 parameter at input of AUT and export results to .s1p file</td><td></td><td>-22.08 dB @ 400MHz</td></tr>
<tr><td>6</td><td>Re-tune elements if appropriate and export results to .s1p file</td><td></td><td>More tuning not possible</td></tr>
<tr><td>7</td><td>Convert .s1p files using MATLAB script:

<code>S1 = sparameters('file.s1p');
disp(S1)
rfplot(S1)</code></td><td></td><td></td></tr>
</table>

Figure 6.2: Test procedure for the Return Loss test (green indicating that the step was executed)

6.1.5 Results

ID	Requirement	Pass/Fail	Results
RL01	S11 < -10dB	Pass	S11 $= -22.1$dB

Table 6.2: Test results for the Return Loss at 400MHz

The S11 parameters before and after tuning are shown in Figure 6.3 and 6.4 respectively. The results are presented in both 2D plots and in Smith charts.

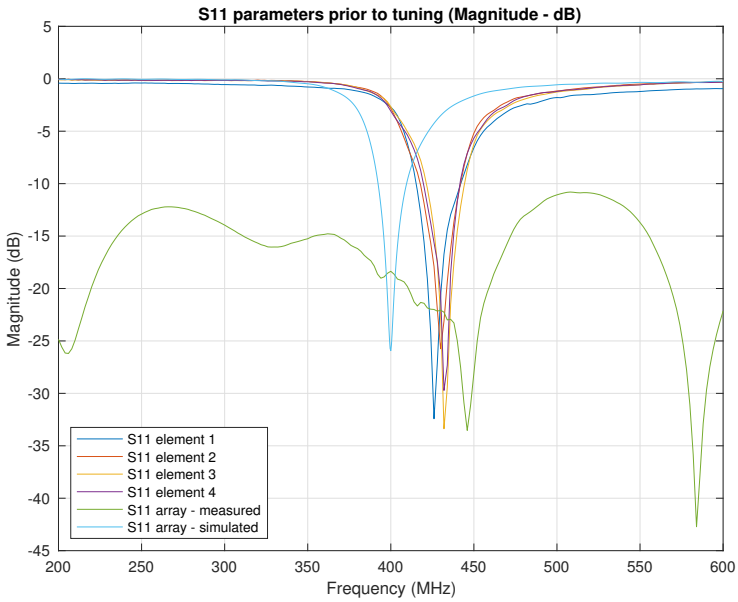

(a) 2D Plot

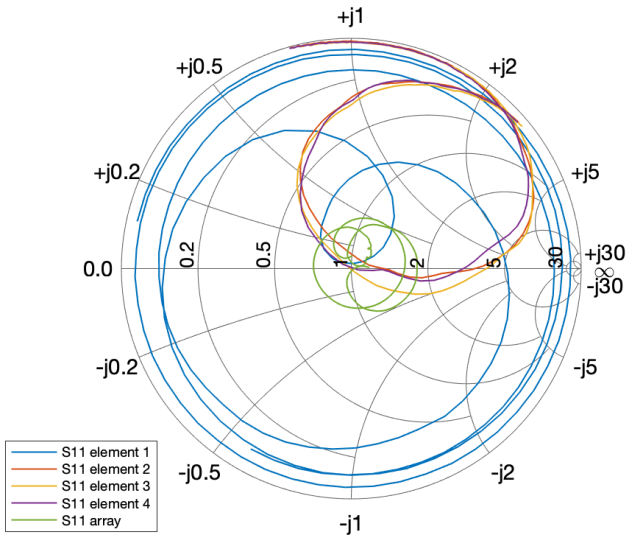

(b) Smith Chart

Figure 6.3: S11 parameters prior to tuning

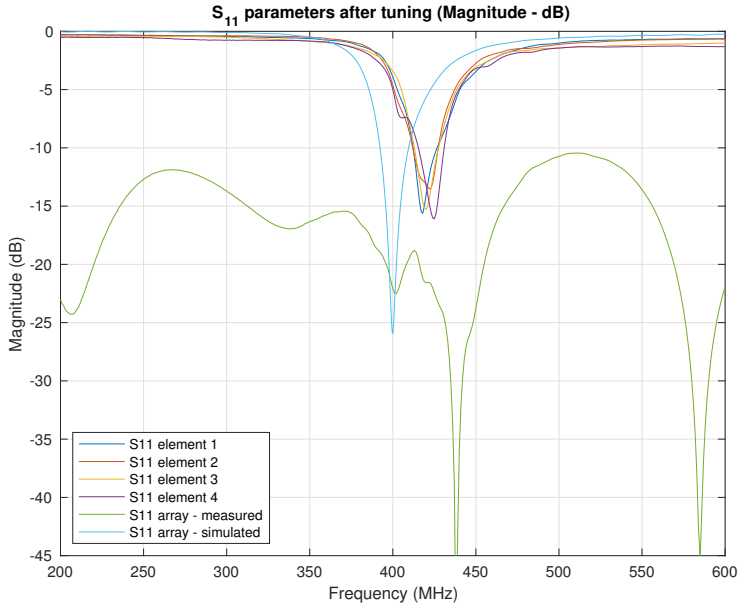

(a) 2D Plot

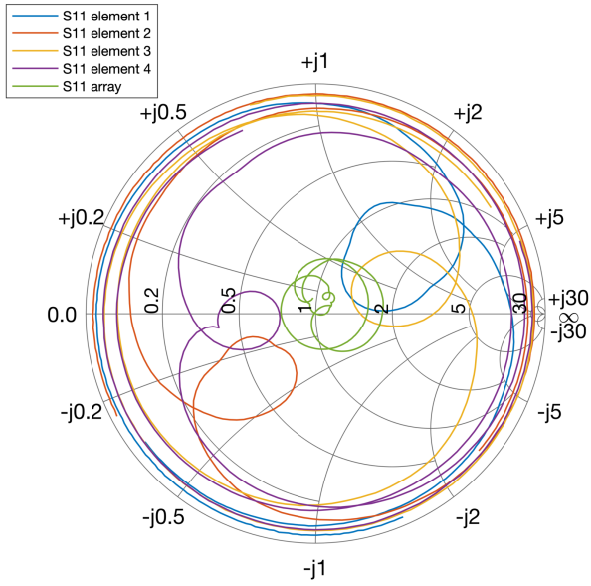

(b) Smith Chart

Figure 6.4: S11 parameters after tuning

6.1.6 Discussion

The results show that the antenna meets the RL01 test requirement for all frequencies between 200MHz and 600MHz. The S11 parameter stays below -10dB in the entire frequency range. As can be seen in the Smith charts, the S11 parameter stays close to the impedance matching point (50Ω reference) for all frequencies including 400MHz.

The apparent large bandwidth of the antenna can be explained using even-odd mode analysis of the Wilkinson Power Divider. The Wilkinson Power Divider is a passive component that divides an input signal into two or more equal or arbitrary output signals. It also works in the reverse direction to combine signals, meaning it is reciprocal. The divider used in the thesis is 4-way equal-split 50 Ω, as illustrated in Figure 6.5. The signal is evenly divided into amplitude and phase between the four output ports, and good isolation is achieved using resistors as absorbing loads for separating even and odd mode signals (Pozar, 2012). Isolation means that the signal at one port does not affect the signal at another port. The resistors ensure good matching at the ports.

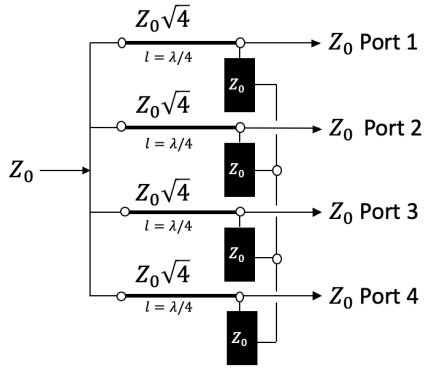

Figure 6.5: 5-port Wilkinson Power Divider

A two port Wilkinson power divider as shown in Figure 6.6 will now be considered. When the voltages at port 2 and 3 are equal, the excitation is said to be in even mode. When the voltages at port 2 and 3 are opposite, the excitation is said to be in odd mode. In the even mode, the symmetry line marks a virtual open and no current flows in the resistors between the two ports. In odd mode, the symmetry line marks a virtual short with a voltage null along the middle of the circuit. The quarter-wavelength transmission line shorted at port 1 looks like an open circuit when looking from port 2. Therefore all power is delivered to the Z_0 resistors between port 2 and 3, while none is going to port 1 (Pozar, 2012). Any reflection from loads at port 2 or 3 that appear as odd-mode excitation will be dissipated in the isolating resistors.

This is exactly what happens in the ZB4PD1-500-S+ power splitter: the reflections from each antenna element appear as odd-mode excitation since they differ by a quarter wave-

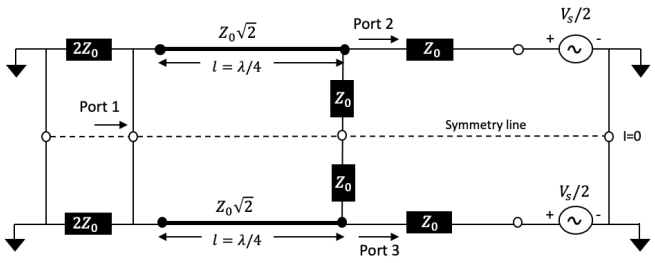

(a) Even-mode excitation

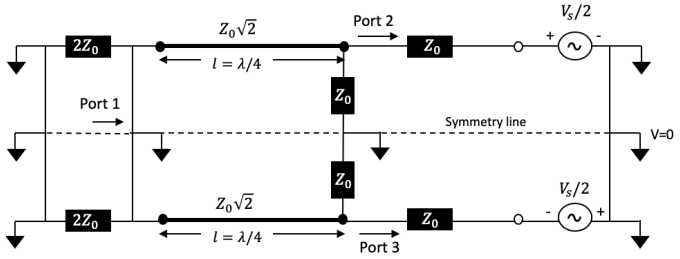

(b) Odd-mode excitation

Figure 6.6: Even-Odd Mode Analysis of Wilkinson Power Divider

length. The reflected power is thus dissipated in the power splitter and is not visible from the S11 measurements at the input of the splitter.

The power splitter contributes to what appears to be good matching over a large bandwidth, but according to Garg, Bhartia, Bahl, and Ittipiboon (2001) this may have a negative effect on the antenna efficiency. In addition, the tuning may have been based on inaccurate measurements since the measured return loss is not an accurate indication of what is actually reflected from each element. It should also be noted that although the return loss is low for frequencies between 200MHz and 600MHz, it does not mean that the antenna resonates well at all these frequencies. To understand the radiating characteristics of the antenna at 400MHz, it is necessary to conduct a radiation pattern test.

It should be noted that the detailed characteristics of the brass used in the prototype were not entered at the time of simulation, both because it was not known at the time that brass would be used but also because it would require extensive analysis of the material. Although not considered of great importance, the heterogeneousness of the material might have had an impact on the S11 parameters that was not accounted for during simulations.

6.2 Characterizing Cables and Power Splitter

ID	Title	Requirement	Purpose
Cab01	Phase characteristics of cables	$d\theta = 90° \pm 3°$	Ensure that each cable adds a consecutive λ /4 phase difference
Cab02	Loss characteristics of cables	$S21_{cab,i}$ <0.5dB/m	Measure how much loss each cable contributes
PS01	Phase characteristics of power splitter	$\theta = \theta_{ref} \pm 3°$	Ensure that phase difference between ports is minimal
PS02	Loss characteristics of power splitter	$S21_{avg} < 1$dB	Measure how much loss the splitter contributes

Table 6.3: Test requirements for the characterization of cables and power splitter at 400 MHz, i=[1..4]

To better understand the results of the RL01 test, a new test was set up to characterize each cable that was made specifically for this antenna as well as the power splitter. The parameters of interest in this test includes the phase shift at the output of each cable as well as the loss caused by their lengths. The phase and insertion loss at each port of the power splitter is also of interest to make sure this does not significantly impact the total phase shift and loss of the system. Although the power splitter is characterized in its datasheet (see Appendix C), it was considered necessary to verify in order to better understand what is going on in the system as well as for learning purposes.

As was described in section 6.1, S-parameters describe both magnitude and phase of traveling waves incident and reflected from a port. The S21 parameter is the transmission coefficient from port 1 to port 2. An incident wave is applied at port 1 and an outcoming wave is measured at port 2. By measuring this parameter using a VNA, one can determine the change in phase and magnitude as the wave travels between the ports, in for example a cable or through the power splitter. Since the the power splitter is reciprocal (can be used as both splitter and combiner), the scattering matrix is symmetric and either the S21 or S12 can be measured.

6.2.1 Setup

Cable measurements

A two-port network analyzer was used to measure the S-parameters. Since the shortest cable of 25cm was not long enough to connect port 1 to port 2 of the VNA, an additional cable had to be used. This additional cable can be considered ”invisible” in the results because it was included in the calibration. The female-female connector was also included in the calibration. An illustration of the setup can be seen in Figure 6.7. Equipment used:

- 4 phase shifting RG-58 cables (25cm, 37.4cm, 49.8cm and 62.1cm)
- Vector network analyzer Rohde & Schwarz ZVA50 10MHz..50GHz
- Extra cable and female-female SMA connector
- Calibration kit 85052D4 3.5mm

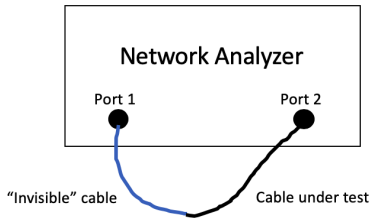

Figure 6.7: Test setup for characterizing cables

Power splitter measurements

A two-port network analyzer was used to measure the S-parameters. The input of the power splitter was directly connected to Port 2 of the VNA, while one of the output ports of the power splitter was connected to Port 1 of the VNA through an extra cable. The other three output ports of the power splitter were terminated with 50Ω loads. The setup is illustrated in Figure 6.8. The extension cable was included in the calibration and can therefore be considered ”invisible” in the results. Equipment used:

- Power splitter ZB4PD1-500-S+ (datasheet in Appendix C)
- $3\times$ 50Ω SMA loads
- Vector network analyzer Rohde & Schwarz ZVA50 10MHz..50GHz
- Extension cable from Port 1 to power splitter
- Calibration kit 85052D4 3.5mm

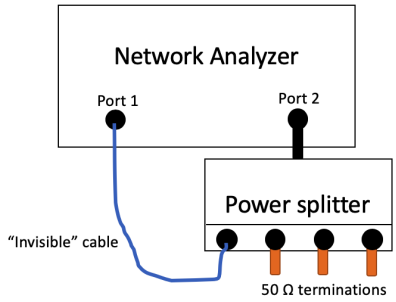

Figure 6.8: Test setup for characterizing the power splitter

6.2.2 Expected Results

Cable measurements

It is expected that there will be a 90°consecutive phase difference between the cables, assuming the calculations of the cable lengths are done correctly. A small error margin is expected due to random and human errors in the production of the cables. It is expected that the longer cables will be more lossy, but in total the loss should not exceed 1dB. According to the Huber+Suhner RG58 datasheet (see Appendix D), a nominal attenuation of 0,31dB/m is to be expected at 400MHz, assuming ambient temperature. This amounts to $0.31 \times 0.250 = 0.08$dB for cable 1, $0.31 \times 0.374 = 0.12$dB for cable 2, $0.31 \times 0.498 = 0.15$dB for cable 3 and $0.31 \times 0.621 = 0.19$dB for cable 4 which is in total 0.54dB. The results of the measurements will show higher numbers than this because of the additional connector loss.

Power splitter measurements

It is expected that the phase measured at each port is more or less equal. According to the ZB4PD1-500-S+ datasheet (see Appendix C), the maximum phase unbalance at 400MHz is 6°. A small insertion loss above the 6dB is expected. According to the datasheet, insertion loss at 400MHz is typically in the order of 0.9dB. The results of the measurements are likely to show higher numbers than this because of the additional connector loss.

6.2.3 Test Procedure

<table>
<tr><th>Step</th><th>Description</th><th>Executed (sign)</th><th>Comment</th></tr>
<tr><td>1</td><td>Calibrate VNA with extension cable</td><td></td><td></td></tr>
<tr><td>2</td><td>Measure S21 of each cable in both magnitude and phase format</td><td></td><td>@400MHz:
<table>
<tr><td></td><td>Magnitude (dB)</td><td>Phase (deg)</td></tr>
<tr><td>Cable1</td><td>-0.12</td><td>171</td></tr>
<tr><td>Cable 2</td><td>-0.17</td><td>83</td></tr>
<tr><td>Cable 3</td><td>-0.24</td><td>-5 (355)</td></tr>
<tr><td>Cable 4</td><td>-0.3</td><td>-97 (263)</td></tr>
<tr><td>Total</td><td>0.83</td><td>356</td></tr>
</table>
<table>
<tr><td></td><td>Phase difference (deg)</td></tr>
<tr><td>$d\theta_1$</td><td>171-83=88</td></tr>
<tr><td>$d\theta_2$</td><td>83+5=88</td></tr>
<tr><td>$d\theta_3$</td><td>97-5=92</td></tr>
<tr><td>$d\theta_4$</td><td>263-171=92</td></tr>
</table></td></tr>
<tr><td>3</td><td>Export results to .s2p file</td><td></td><td></td></tr>
<tr><td>7</td><td>Convert .s2p files using MATLAB script:
<pre>Cab1 = sparameters('file.s2p');
disp(Cab1)
rfplot(Cab2,1,1)
rfplot(Cab1,2,1,'angle')</pre></td><td></td><td></td></tr>
</table>

Figure 6.9: Test procedure for the characterization of cables (green indicating it was executed)

<table>
<tr><th>Step</th><th>Description</th><th>Executed (sign)</th><th>Comment</th></tr>
<tr><td>1</td><td>Calibrate VNA with extension cable</td><td></td><td></td></tr>
<tr><td>2</td><td>Measure S21 of each port in both magnitude and phase format. Every port that is not under test must be terminated with a 50 ohm load.</td><td></td><td>@400MHz:
<table>
<tr><td></td><td>Magnitude (dB)</td><td>Phase (deg)</td></tr>
<tr><td>Port 1</td><td>-6.70</td><td>-142</td></tr>
<tr><td>Port 2</td><td>-6.75</td><td>-143</td></tr>
<tr><td>Port 3</td><td>-6.71</td><td>-142</td></tr>
<tr><td>Port 4</td><td>-6.70</td><td>-142</td></tr>
</table></td></tr>
<tr><td>3</td><td>Export results to .s2p file</td><td></td><td></td></tr>
<tr><td>7</td><td>Convert .s2p files using MATLAB script:
<pre>PS1 = sparameters('file.s2p');
disp(PS1)
rfplot(PS1,1,1)
rfplot(PS1,2,1,'angle')</pre></td><td></td><td></td></tr>
</table>

Figure 6.10: Test procedure for the characterization of the power splitter (green indicating it was executed)

6.2.4 Results

ID	Requirement	Pass/Fail	Results
Cab01	$d\theta = 90° \pm 3°$	Pass	$d\theta = 90° \pm 2°$
Cab02	$S21_{cab,i}$ <0.5dB/m	Pass	$S21_{cab,i}$ <0.48dB/m
PS01	$\theta = \theta_{ref} \pm 3°$	Pass	$\theta = 142° \pm 1°$
PS02	$S21_{avg} < 1$dB	Pass	$S21_{avg} = 0.7$dB

Table 6.4: Test results for the characterization of the cables and power splitter at 400MHz, i=[1..4]

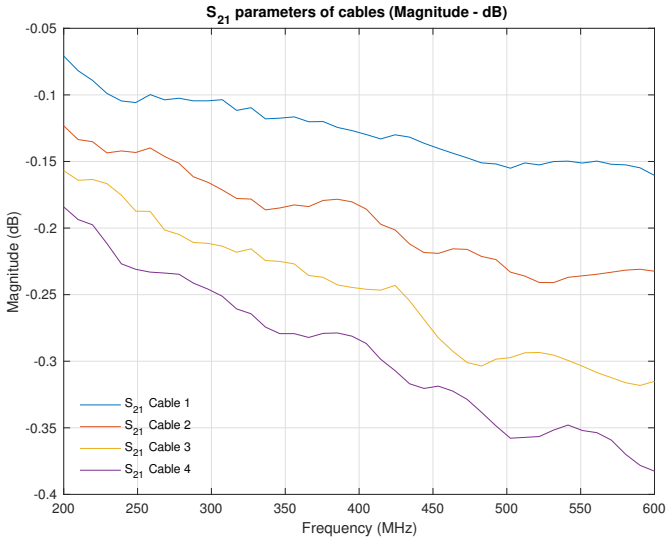

(a) Magnitude - dB

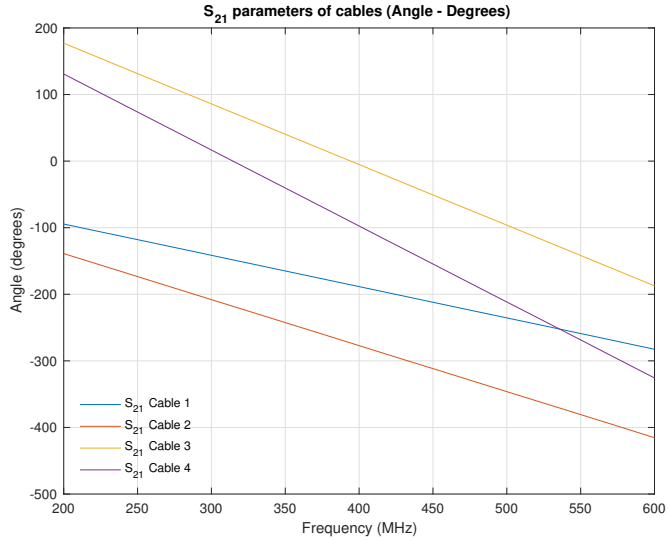

(b) Phase - degrees

Figure 6.11: S21 parameters of cables

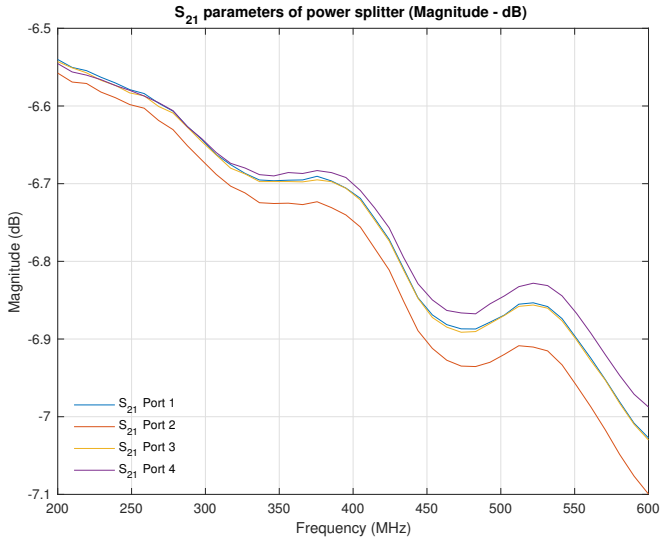

(a) Magnitude - dB

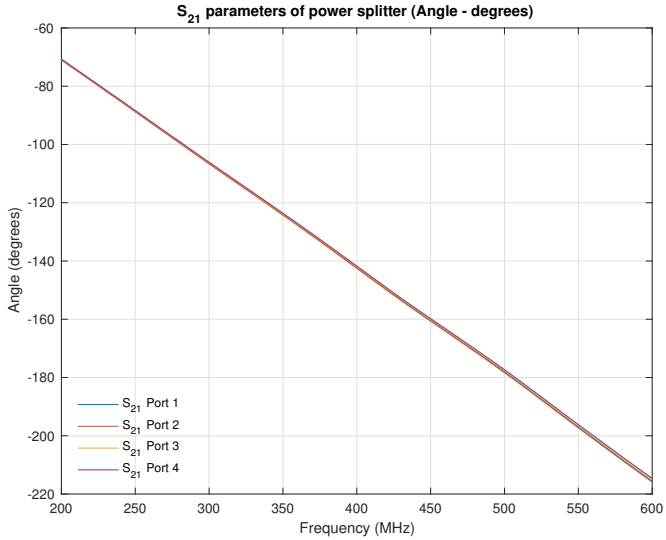

(b) Phase - degrees

Figure 6.12: S21 parameters of output ports of power splitter

6.2.5 Discussion

The results of the Cab01 test in Figure 6.11(b) show that the phase at the output of each cable differs by approximately 90°, as expected. The lengths of the cables have been calculated correctly, and the cables are effectively doing their job as phase-shifters.

The results of the Cab02 test in Figure 6.11(a) show that the four cables contribute with a loss of 0.12dB, 0.17dB, 0.24dB and 0.30dB respectively. The longest cable that contributes with the most loss of 0.3dB, is 62.1cm long and thus per unit length contributes with 0.48dB/m. As the signal travels through more medium, it is attenuated more. Since the attenuation from each cable is different, the strength of the signal arriving at the antenna elements also differs. Due to this difference, the antenna array will most likely generate an elliptical polarization rather than circular. The difference between the longest and shortest cable is 0.3-0.12=0.18dB. It is not considered critical, but the effect of this difference might be seen in the radiation pattern.

The PS01 test results show, as expected, that the phase at the output ports of the power splitter are very similar, with only the phase at port 2 differing by 1° from the other ports. As can be seen in Figure 6.12(b), it is almost impossible to distinguish one graph from another.

The results of the PS02 test in Figure 6.12(a) show that at each output port, there is a measured loss of 6.70dB, 6.75dB, 6.71dB and 6.70dB respectively. The power that enters the splitter is equally divided into the four output ports, and therefore we see a 6dB insertion loss at each port. The additional loss of around 0.7dB at each port is most likely coming from the dissipation of energy from the connectors and the splitter, as well as measurement inaccuracies. According to the datasheet of the power splitter, the insertion loss is typically in the order of 0.9dB. The test showed no anomalies to this expectation.

In general, the results of the tests are as expected. Undesired loss and phase shift are low and do not seen to explain the RL01 test results.

6.3 Radiation pattern

ID	Title	Requirement	Purpose
RAD01	Normalized radiation pattern	G_{max} at e=45°	Ensure that gain is highest at most critical elevation angles
RAD02	Normalized radiation pattern	G_{min} in zenith	Ensure that gain is lowest in least critical elevation angles

Table 6.5: Test requirements for the radiation pattern measurements at 400MHz

The objective of the radiation pattern test is to verify the directivity of the antenna, meaning in what direction it radiates/receives better or worse. The radiation pattern has been simulated computationally, and this test will determine whether the prototype has a pattern that resembles. The result will be normalized and therefore it will not be possible to read the gain. That would require another separate test with more careful calibrations.

6.3.1 Setup

The radiation pattern test was set up in the 10x6x4m^3 anechoic chamber at NTNU. The chamber is for frequencies between 1-20GHz, but since this project is time and resource limited it was deemed good enough. An illustration of the setup is shown in Figure 6.13 and pictures are shown in Figure 6.14. To mount the antenna on the rotating disk, a hole was drilled in the middle of a thin wooden plate. The antenna was put perpendicular to the wooden plate by fastening the legs using a press tool.

The reference transmit antenna, a Yagi-Uda type antenna, was mounted such that it faced the AUT. It was connected to port 2 of the VNA with an amplifier in between. The Yagi-Uda was rotated by 90 °to change between vertical and horizontal polarization, see Figure 6.14. A python script developed by Jens Abraham, Ph.D. candidate at NTNU, was used to command the motion controller and process the results from the VNA. MATLAB scripts used to plot the results are found in Appendix E. Equipment used in the setup include:

- Anechoic chamber for 1-20 GHz with rotating disk
- Newport XPS Q8 motion controller
- Vector network analyzer Rohde & Schwarz ZVA50 10MHz..50GHz
- Yagi-Uda reference antenna
- Broadband amplifier HP 87422A
- AUT with necessary mounting equipment
- Computer with AntennChamberCLI.py script

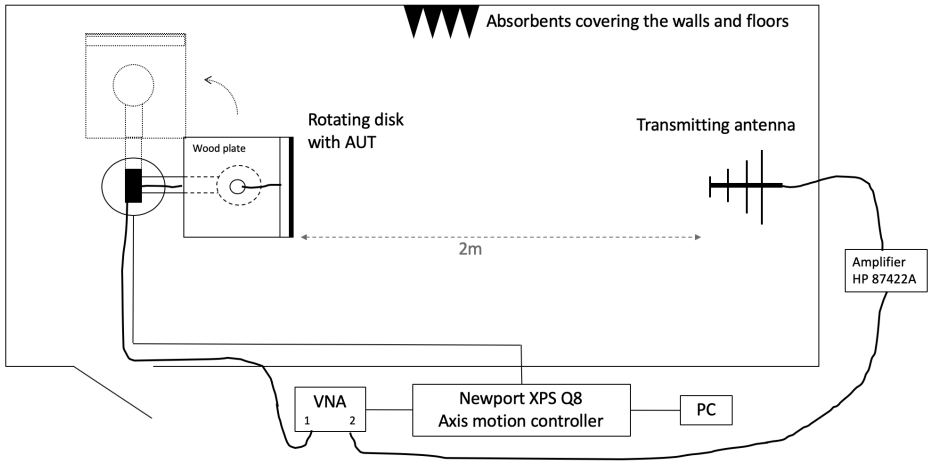

Figure 6.13: Test setup for the radiation pattern measurements

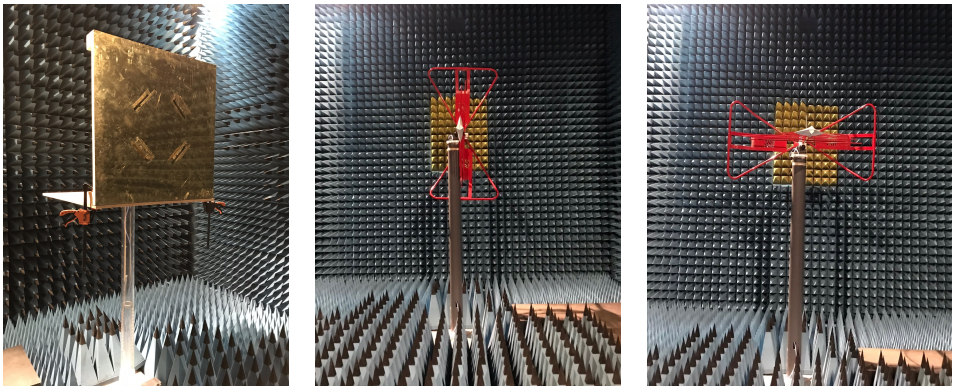

(a) AUT **(b)** Yagi-Uda, vertical **(c)** Yagi-Uda, horisontal

Figure 6.14: Antenna setup in anechoic chamber

6.3.2 Expected Results

The expected result for the radiation pattern is shown in Figure 6.15. There should be a minima at zenith and a maxima at ϕ=45°.

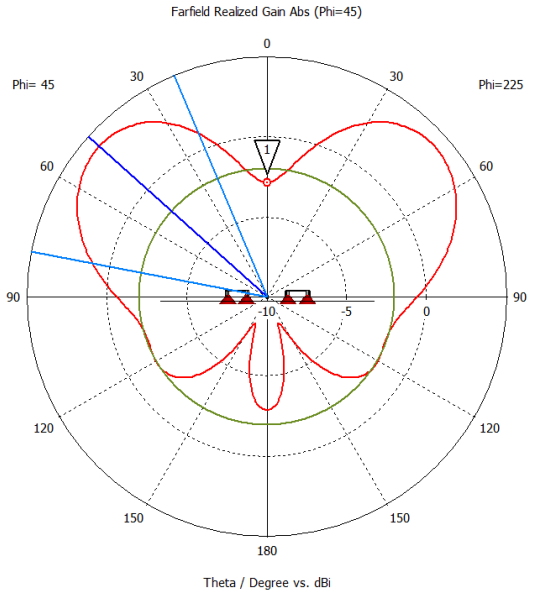

Figure 6.15: Expected radiation pattern at 400MHz and Phi=45°

6.3.3 Test Procedure

In the test procedure given in Figure 6.16, the antenna elements are placed in two different positions: $D_{c,min}$=17,3cm and $D_{c,max}$=18,6cm. The difference in these two positions is illustrated in Figure 6.17. D_c is measured from the center of the ground plane to the first border of the element's ground plane.

Step	Description	Executed (sign)	Comment
1	Mount transmit reference antenna on fixed disk, in vertical position		
2	Connect reference antenna to VNA using coax		
3	Mount AUT on rotating disk with $d_c = min$		
4	Connect AUT to VNA using coax		
5	Open pre-programmed script on computer		
6	Enter frequency		
7	Run script and save file		Filename: 20190424_102615
8	Mount AUT on rotating disk with $d_c = max$		
9	Run script and save file		Filename: 20190424_104047
10	Rotate reference antenna by 90 degrees to put it into horizontal position		
11	Run script and save file		Filename: 20190424_104435
12	Mount AUT on rotating disk with $d_c = min$		
13	Run script and save file		Filename: 20190424_105041
14	Process data and plot results		

Figure 6.16: Test procedure for measuring the radiation pattern

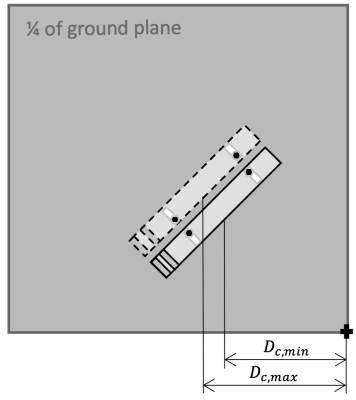

Figure 6.17: The two possible positions of an element on the ground plane. Dc,min=173mm and Dc,max=186mm.

6.3.4 Results

ID	Requirement	Pass/Fail	Results
RAD01	G_{max} at e=45°	Fail	See figures 6.18 and 6.19
RAD02	G_{min} at zenith	Fail	See figures 6.18 and 6.19

Table 6.6: Test results for the radiation pattern measurements at 400MHz

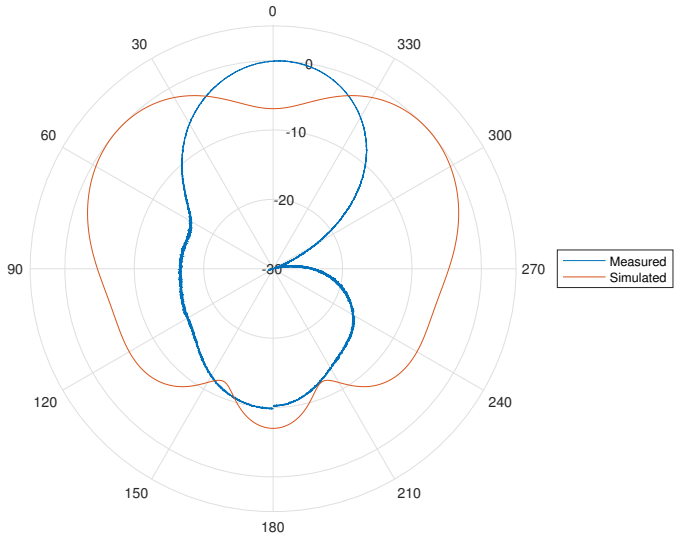

(a) D_c=max

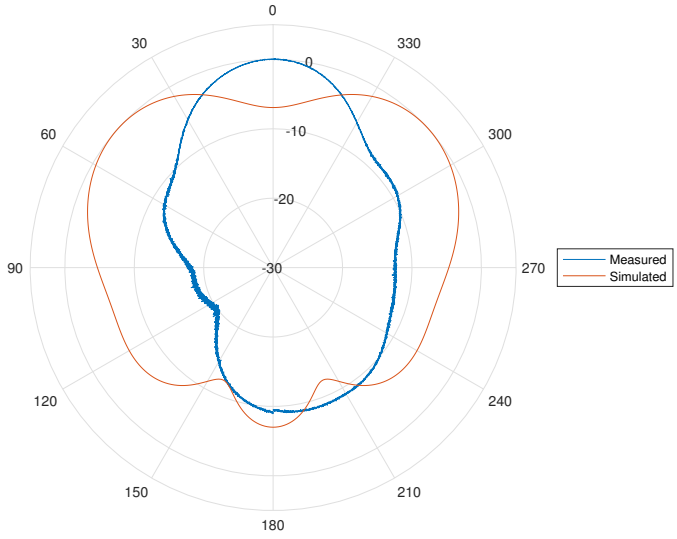

(b) D_c=min

Figure 6.18: Normalized radiation pattern of AUT when reference antenna is vertically polarized

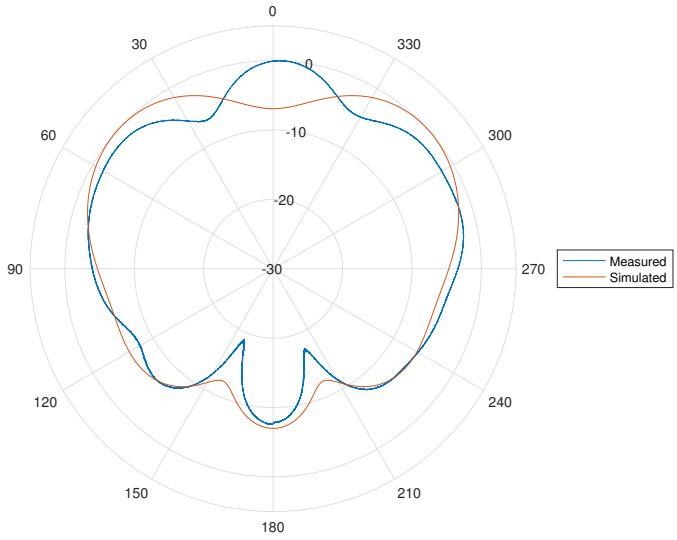

(a) D_c=max

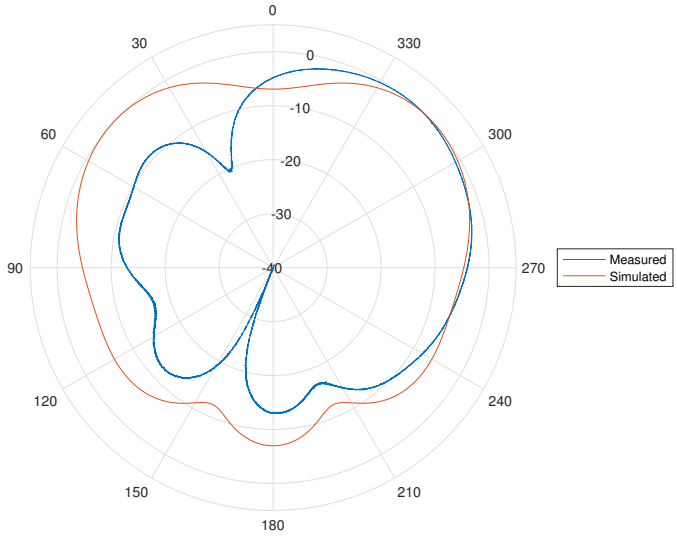

(b) D_c=min

Figure 6.19: Normalized radiation pattern of AUT when reference antenna is horizontally polarized

6.3.5 Discussion

The results of the RAD tests failed the requirement of having maximum gain at an elevation angle of 45° and minimum in zenith. The reference transmitting antenna is a Yagi-Uda antenna which transmits either vertically or horizontally polarized waves depending on its position relative to the receiving antenna. Since the reference antenna can be put in two different positions, the measured radiation pattern of the IFA array has two different results shown in Figure 6.18 and 6.19 respectively. The measured radiation patterns have been compared with the results of the simulations, but such a comparison is not really fair because of the Yagi-Uda being used as a reference. This is considered a limitation of the results presented.

It can be seen in the results that the position of the antenna element on the ground plane, either $D_{c,min}$=17,3cm or $D_{c,max}$=18,6cm affects the radiation pattern significantly. This was not expected. In the simulations, the position of the elements only changed the depth of the dip in zenith, as well as the magnitude of the main lobes. The reason for the deviation could be due to a certain inaccuracy in the positions of the elements. Due to some mechanical difficulties in adjusting their positions, the elements were not perfectly aligned. Although having the flexibility to adjust their positions was interesting for testing purposes, it also caused inaccuracies.

An anechoic chamber is a room made up of special walls that absorb reflections of electromagnetic waves at a given frequency. The chamber available at NTNU is made for the frequency range 1-20GHz. Since the RAD tests were done at 400MHz, the resulting radiation patterns may have been influenced by reflections in the room. Redoing the tests in a more suitable chamber could improve the results.

Chapter 7

Discussion and Future Work

The results of the link budget, the evaluation of antenna types, the simulations and the testing of the prototype have already been discussed in detail. It is now time to come back to the objective of the thesis and evaluate whether it has been met. The reader is reminded that the main objective of the thesis is *"To evaluate whether a feasible and practical antenna can be designed and implemented for the retrieval of 2-200GB of data from sensor nodes in the Arctic using small satellites, at Ultra-High Frequencies"*.

According to the link budget, the amount of data that an Arctic satellite communication system can support is heavily dependent on the gain of the antennas on both the receiving and transmitting side. A lot of effort has been put into analysing the trade-offs that maximize antenna gain. After reviewing HYPSO's orbit it was concluded that the gain of the ground antenna should be directed not towards zenith but towards lower elevation angles where the satellite appears most often. In the evaluation of different antenna types, it was found that having the necessary radiation properties whilst at the same time remaining small and practical, is a challenge. Typically, large paraboles are used as ground terminals in satellite communication systems but such installations require heavy logistics and antenna pointing mechanisms.

Based on a project by Amoudi and Langley (2009), it was expected that an array of 4 IFAs could reach a gain of about 9-10dBi. However after simulating several IFA array configurations at 400MHz, it was not deemed possible to achieve more than a realized gain of 4dBi within the given restrictions of the use cases. The ground plane had to be almost $1m^2$ to achieve this gain. Although smaller than the typical parabolic antennas that communicate with satellites, $1m^2$ may be too large for certain types of sensor nodes. It will not be possible to integrate it with microelectronics on smaller sensors in for example an "Internet of Things" network. Weighing more than 10kg, it can even be difficult to integrate it with Arctic ABC's sensor buoys considering that their total weight will dramatically change. It could be interesting in future work to investigate if the radiation pattern keeps its shape when the frequency is increased and the size reduced.

Although the gain of the simulated design was lower than expected, the conical shape of the radiation pattern is ideal. The results are relevant for any application that requires communication from different angles. This includes not only ground terminals of satellite communication systems, but also RFID and other mobile connectivity nodes. When incorporating the simulation results in the link budget, it was found that depending on ionospheric loss from the atmosphere, the data throughput in one year could be anywhere between 2GB and 11GB in Longyearbyen. This is not in the order of hundreds of GB needed by the next generation of sensor nodes. It may however, be enough for certain applications. This is to be evaluated by the potential users of the satellite communication system, including Arctic ABC.

It is important to acknowledge that the results coming from the link budget are based on a number of assumptions (see section 2.8). For example, the data rate has been calculated assuming that the E_b/N_0 equals the required E_b/N_0, with no margin. Atmospheric loss is assumed to be zero and ionospheric loss either 7dB or 1dB. These are simplifications of a much more complex system. The results should therefore not be accepted blindly, but may be used as an indication of the level of performance that can be expected under a certain set of circumstances.

A prototype was built and tested, but since the gain was not measured it is difficult to assess its performance. It would have been useful to have more test results to compare the prototype with the simulated design. Tests to determine gain, temperature tolerance and polarization characteristics would have helped to evaluate whether the antenna could be deployed in the Arctic. These tests are suggested for further work, as well as building a radome that protects the antenna. Although only the IFA was chosen for further analysis from the evaluation of antenna types, the QHA could be a good alternative. It is suggested to try the design method by Kilgus (1975) and compare it with the results of the IFA design at 400MHz.

Chapter 8

Conclusion

An array of four Inverted-F Antennas was designed using CST and the results of the simulations indicate a maximum realized gain of 4dBi. By plotting the gain of the antenna at different elevation angles into the link budget, it was found that a maximum of $\sim$10GB of data can be collected from sensor nodes located north of Longyearbyen, using the NTNU HYPSO small satellite. More realistically, the data throughput will be somewhere between 2GB and 11GB depending on the ionospheric activity in the atmosphere as well as other loss factors. A prototype of the antenna was manufactured and tested using facilities and equipment available at NTNU. The Return Loss at 400MHz after tuning the antenna was measured to be -22dB. The radiation pattern was not as similar to the simulations as expected. Future work to test the gain, temperature tolerance and polarization characteristics of the antenna prototype is suggested in order to validate whether the antenna could be suitable for implementation in the Arctic.

Bibliography

AgilentTechnologies, 2002. Agilent AN 1287-3 Applying Error Correction to Network Analyzer Measurements Application Note. Tech. rep., Agilent Technologies, Inc.

Amoudi, A. A., Langley, R., 2009. Design of an Inverted F Antenna for Low Earth Orbit (LEO) satellite application. 2009 3rd European Conference on Antennas and Propagation, 1896–1899.

Aurbakken, E. F., 2015. Link Budget Parameters for CAMOS. Master's thesis, Norwegian University of Science and Technology.

Balanis, C. A., 2016. Antenna Theory, Analysis and Design, 4th Edition. John Wiley and Sons.

Birkeland, R., May 2014. An Overview of Existing and Future Satellite Systems for Arctic Communication.

Birkeland, R., 2018. NTNU Small Satellite Lab Website.
URL `https://www.ntnu.edu/ie/smallsat`

Birkeland, R., January 2019. On the Use of Micro Satellites as Communication Nodes in an Arctic Sensor Network. Ph.D. thesis, Norwegian University of Science and Technology (NTNU).

Blues, D. S., 2019. Kongsberg Satellite Services.
URL `https://www.svalbardblues.com/svalbard/bedrifter/kongsberg-satellite-services/`

Bolstad, A. J., 2009. Development of a Patch Antenna Array between 2-6 GHz with Phase Steering Network for a Double CubeSat. Master's thesis, Norwegian University of Science and Technology.

Cao, Y., Cheung, S., Yuk, T., 2014. Circularly Polarized Monopole Antenna Using CRLH TL Feed Network. 2014 Loughborough Antennas and Propagation Conference (LAPC), 259–262.

Garg, R., Bhartia, P., Bahl, I., Ittipiboon, A., 2001. Microstrip Antenna Design Handbook. Artech House.

Grøtte, M., September 2018. Mission Analysis Report for HYPSO, unpublished.

Haykin, S., Moher, M., 2010. Communication Systems, 5th Edition. John Wiley and Sons.

Huang, J., 1986. A Technique for an Array to Generate Circular Polarization with Linearly Polarized Elements. IEEE Transactions on Antennas and Propagation, 1113–1124.

Kakoyiannis, C. G., Constantinou, P., 2008. A Compact Microstrip Antenna with Tapered Peripheral Slits for CubeSat RF Payloads at 436MHz: Miniaturization techniques, design & numerical results. IEEE International Workshop on Satellite and Space Communications.

Kashihara, S., Kuroki, F., 2009. J-Shaped Monopole Antenna Array As an Antenna for Terrestrial Digital Broadcasting at UHF Band. 2009 IEEE MTT-S International Microwave Symposium Digest, 293–296.

Kilgus, C. C., 1975. Shaped-Conical Radiation Pattern Performance of the Backfire Quadrifilar Helix. IEEE Transations on Antennas and Propagation, 392–397.

Kurnia, G. F., Nugroho, B. S., Prasetyo, A. D., 2014. Planar Inverted-F Antenna (PIFA) Array with Circular Polarization for Nano Satellite Application. Proceedings of ISAP 2014.

Løge, L., 2008. A satellite system for broadband communications to polar areas. Master's thesis, Norwegian University of Science and Technology.

Lunde, V., 2008. Design av PCB antenne for 433 MHz. Master's thesis, Norwegian University of Science and Technology.

Maini, A. K., Agrawa, V., 2010. Satellite Technology: Principles and Applications, 2nd Edition. Wiley and Sons.

Marholm, S., 2012a. Antenna Systems for NUTS. Master's thesis, Norwegian University of Science and Technology.

Marholm, S., January 2012b. Semester Project: Antenna Systems for NUTS.

McKerricher, G. I., Wight, J. S., 2010. Quadrifilar Helix Antenna for UHF RFID. 2010 IEEE Antennas and Propagation Society International Symposium.

Mendez, B. L. E., 2013. Link Budget for NTNU Test Satellite. Master's thesis, Norwegian University of Science and Technology.

Notis, D. T., Liakou, P. C., Chrissoulidis, D. P., 2004. Dual Polarized Microstrip Patch Antenna, Reduced in Size by Use of Peripheral Slits. European Conference on Wireless Technology, 273–276.

Paxal, V., 2016. Space Technology I Lecture - Communication via Satellite, norwegian University of Science and Technology.

Pozar, D. M., 1992. Microstrip Antennas. Proceedings of the IEEE, 79–91.

Pozar, D. M., 2012. Microwave Engineering, 4th Edition. Wiley and Sons.

Schraml, K., Narbudowicz, A., Chalermwisutkul, S., Heberling, D., Ammann, M. J., 2017. Easy-to-Deploy LC-Loaded Dipole and Monopole Antennas for Cubesat. 11th European Conference on Antennas and Propagation (EUCAP), 2303–2306.

Sowmya, R. R., 2016. Quadrifilar Helix Antenna for Small Satellites. International Conference on Recent Issues in Engineering, Science and Technology-ICRIEST '16, 251–255.

Stenhaug, B. H., 2011. Antenna system for a ground station communicating with the NTNU Test Satellite (NUTS). Master's thesis, Norwegian University of Science and Technology.

Takacs, A., Aubert, H., Belot, D., Diez, H., 2015. Miniaturization of Compact Quadrifilar Helix Antennas for Telemetry, Tracking and Command Applications. Progress In Electromagnetics Research 2016, 125–136.

Thompson, P. T., 2013. Satellite Communications Modulation and Multiplexing. In: Jan Fagerberg and David C. Mowery and Richard R. Nelson (Ed.), Handbook of Satellite Applications. Springer, Ch. 14, pp. 326–358.

Udnaes, E., December 2018. Semester Project: Antenna Design for UHF Satellite Communication from Sensor Buoys in the Arctic, Norwegian University of Science and Technology.

Vita, P. D., 2012. AN4190 Application note - Antenna selection guidelines. Tech. rep., STMicroelecronics.

Vogedes, D., 2019. Mare Incognitum - mission statement.
URL `http://www.mare-incognitum.no/index.php`

Weiland, T., 2003. Finite Integration Method and Discrete Electromagnetism. Springer.

Zhang, Z., 2011. Antenna Design for Mobile Devices. John Wiley and Sons Asia.

Zolich, A., Torre, P. R. D. L., Rodwell, S., Geoffroy, M., Johnsen, G., Berge, J., October 2018. An ice-tethered buoy for fish and plankton research, 1–7.

Appendix A

Prototype Guidelines

In the case that the antenna should be disassembled in order to be transported safely, a step-by-step guideline on how to reassemble it properly is described next.

1. Connect one of the antenna elements to cable 1 that is 25cm long, using a torque. Fasten the element to the ground plane in position 1 or 2 as illustrated in figure 6.18. The cable should be going through the hole in the ground plane. On the backside of the ground plane, connect the cable to port 1 of the power splitter.

2. Repeat step 1 with the next antenna element following a clockwise direction. Use cable 2 that is 37.4cm long, and connect to port 2 on the power splitter. Always use a torque to tighten correctly.

3. Repeat step 1 again with the third antenna element, following a clockwise direction. Use cable 3 that is 49.8cm long and connect to port 3 of the power splitter.

4. Repeat step 1 again with the last antenna element, following a clockwise direction. Use cable 4 that is 62.1cm long and connect to port 4 of the power splitter.

5. All the elements should now be fastened onto the ground plane and connected to the power splitter. The input of the antenna is the input of the power splitter. Any radio or test setup can be connected keeping in mind that maximum power input is 1 Watt and the impedance is 50 Ω.

6. The antenna should be laid flat on the ground, except if another position is required for testing. The antenna elements will start wobbling if exposed to harsh movement. Low-frequency movements of the antenna from for example long waves is not considered problematic, but the antenna should not be used in harsh weather without a protective radome. It will not withstand any type of weight and the area around it should be cleared for potential dangers such as falling objects.

It should be noted that the prototype has not been built for Arctic conditions. The materials used may not behave the same in temperatures below 0°C as in room temperature.

For testing in more severe environmental conditions, the antenna will need a radome as suggested in section 3.1.

Appendix B

SMA Assembly Instructions

C	19.09.05	4186/MAP

Assembly instruction Series SMA No. 3069

Tools and materials required :

Soldering iron
Solder
Scissors, blade (74 Z-0-0-68)
Contact holder No. W 54
Locator tool No. W 14 "F" and "M"
Crimp tool : A insert for ...SMA-50-2-...
B insert for ...SMA-50-3-...

Straight connectors for flexible cables

Cable entry : crimped

Connector types : (e.g.)		Cable : (e.g.)
	21 SMA 50 - 2 - 5	RG 188 A/U
	21 SMA 50 - 2 - 6	K 02252-d
11 SMA 50 - 3 - 5	21 SMA 50 - 3 - 5	RG 141 A/U
11 SMA 50 - 3 - 6	21 SMA 50 - 3 - 6	RG 142 A/U

This connector is supplied in 3 parts

Centre contact : soldered

Braid : cavity A für ..SMA-50-2... / B für ...SMA-50-3...

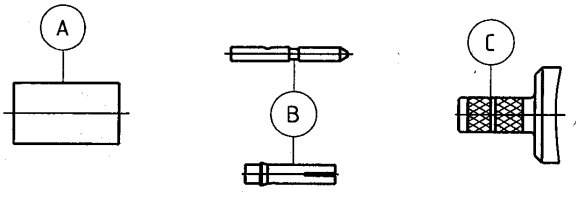

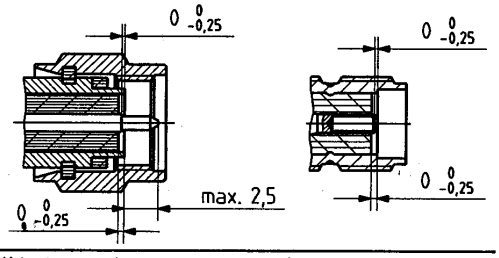

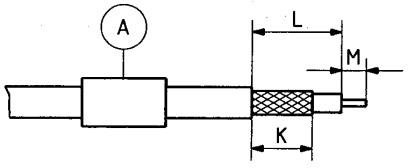

If required, slide taper sleeve or heat-shrink sleeve onto cable (not illustrated). Prepare cable acording to diagram.

Type :	K	L	M
11 SMA-50-2-...	5 mm	8,5 mm	2 mm
21 SMA-50-2-...	5 mm	7,5 mm	2 mm
. . .SMA-50-3-...	8 mm	10,5 mm	2 mm
24 SMA-50-2-...	5 mm	12,5 mm	2 mm

Slide ferrule A onto cable.

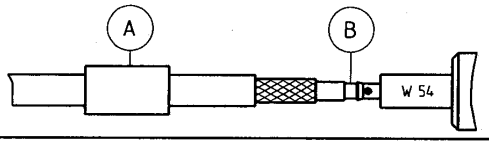

Push contact B onto contact holder W 54.
Heat contact B using a dry soldering iron.
Flow small amount of solder into bore hole of contact, insert inner conductor of cable and solder to contact.
Clean contact B and cable dielectric, remove excess solder.

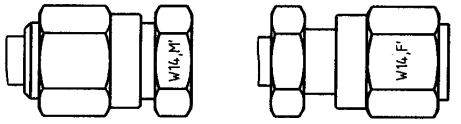

Mount locator tool W 14 onto connector body C
("M" for male,"F" for female.)

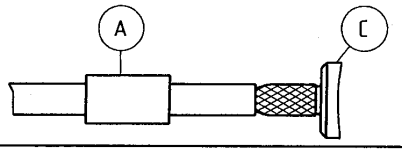

Splay out braid and insert carefully prepared cable fully into connector body C.
Ensure that braid lies above the crimp neck.

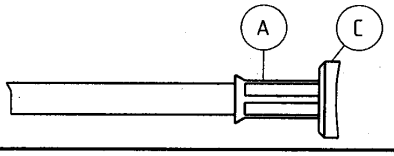

Slide ferrule A over braid to about connector body C and crimp as close to connector body C as possible.
Remove locator tool and check interface dimensions.

SUHNER's skilled staff and specialised equipment are available to carry out complete R.F.lead-assembly on your behalf.We mount your connectors on cables at economic prices! Please contact our representative for further details of this service.

HUBER + SUHNER AG CH-9100 HERISAU

Deutscher Text siehe Rückseite

Appendix C

ZB4PD1-500+ Data Sheet

Coaxial

Power Splitter/Combiner

ZB4PD1-500+

4 Way-0° 50Ω 5 to 500 MHz

SMA version shown

CASE STYLE: UU188

Connectors	Model
BNC	ZB4PD1-500+
SMA	ZB4PD1-500-S+
N-TYPE	ZB4PD1-500-N+

+RoHS Compliant

The +Suffix identifies RoHS Compliance. See our web site for RoHS Compliance methodologies and qualifications

Maximum Ratings

Operating Temperature	-55°C to 100°C
Storage Temperature	-55°C to 100°C
Power Input (as a splitter)	1W max.
Internal Dissipation	0.250W max.

Permanent damage may occur if any of these limits are exceeded.

Coaxial Connections

SUM PORT	S
PORT 1	1
PORT 2	2
PORT 3	3
PORT 4	4

Features

- wideband, 5 to 500 MHz
- high isolation, 34 dB typ.
- rugged, shielded case

Applications

- VHF/UHF
- receivers/transmitters

Outline Drawing

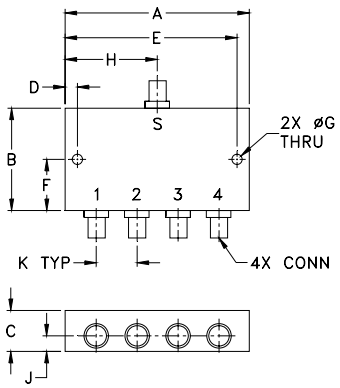

Outline Dimensions (inch / mm)

A	B	C	D	E	F
3.50	2.13	.88	.150	3.350	1.06
88.90	54.10	22.35	3.81	85.09	26.92

G	H	J	K	wt
.125	1.75	.44	.89	grams
3.18	44.45	11.18	22.61	260

Electrical Specifications

FREQ. RANGE (MHz)	ISOLATION (dB)						INSERTION LOSS (dB) ABOVE 6.0 dB						PHASE UNBALANCE (Degrees)			AMPLITUDE UNBALANCE (dB)		
	L		M		U		L		M		U		L	M	U	L	M	U
f_L-f_U	Typ.	Min.	Typ.	Min.	Typ.	Min.	Typ.	Max.	Typ.	Max.	Typ.	Max.	Max.	Max.	Max.	Max.	Max.	Max.
5-500	34	20	34	20	28	20	0.4	1.0	0.5	0.9	0.9	1.5	1	3	6	0.2	0.2	0.4

L = low range [f_L to 10 f_L] M = mid range [10 f_L to f_U/2] U = upper range [f_U/2 to f_U]

Typical Performance Data

Freq. (MHz)	Total Loss[1] (dB)				Amp. Unbal. (dB)	Isolation (dB)			VSWR S	VSWR 1	VSWR 2	VSWR 3	VSWR 4
	S-1	S-2	S-3	S-4		1-2	2-3	3-4					
5.00	6.34	6.35	6.33	6.33	0.01	52.83	40.68	50.23	1.08	1.12	1.12	1.13	1.13
30.00	6.32	6.32	6.31	6.32	0.01	46.48	40.23	44.89	1.05	1.09	1.09	1.09	1.09
50.00	6.34	6.34	6.34	6.35	0.01	43.68	39.45	41.92	1.05	1.09	1.09	1.09	1.10
100.00	6.39	6.39	6.39	6.38	0.01	38.83	37.13	36.88	1.07	1.09	1.10	1.10	1.10
130.00	6.44	6.43	6.43	6.43	0.01	36.86	35.97	34.90	1.05	1.09	1.08	1.08	1.08
150.00	6.47	6.46	6.47	6.46	0.01	35.87	35.35	33.83	1.05	1.08	1.08	1.08	1.08
180.00	6.44	6.44	6.43	6.43	0.01	34.55	34.35	32.40	1.08	1.08	1.09	1.10	1.10
200.00	6.50	6.51	6.49	6.48	0.03	33.82	33.88	31.75	1.08	1.07	1.07	1.09	1.09
230.00	6.53	6.54	6.52	6.51	0.03	32.96	33.12	30.74	1.06	1.06	1.04	1.05	1.05
250.00	6.55	6.56	6.55	6.53	0.03	32.54	32.76	30.22	1.08	1.06	1.06	1.06	1.06
290.00	6.59	6.59	6.59	6.58	0.02	31.75	32.00	29.34	1.10	1.05	1.05	1.07	1.07
350.00	6.63	6.64	6.62	6.60	0.04	31.02	31.24	28.37	1.11	1.03	1.04	1.04	1.04
400.00	6.69	6.72	6.68	6.67	0.05	30.73	30.84	27.85	1.10	1.02	1.01	1.03	1.03
450.00	6.69	6.72	6.71	6.67	0.05	30.66	30.70	27.53	1.14	1.01	1.01	1.03	1.03
500.00	6.77	6.81	6.79	6.75	0.06	30.85	30.77	27.37	1.11	1.01	1.02	1.01	1.02

1. Total Loss = Insertion Loss + 6dB splitter loss.

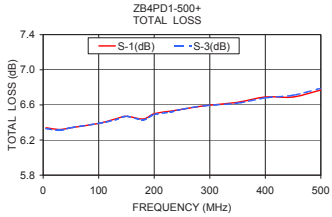

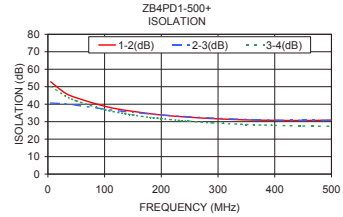

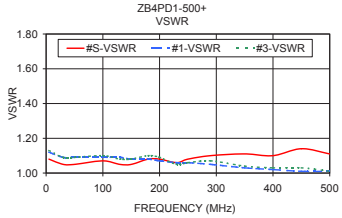

electrical schematic

Notes

A. Performance and quality attributes and conditions not expressly stated in this specification document are intended to be excluded and do not form a part of this specification document.

B. Electrical specifications and performance data contained in this specification document are based on Mini-Circuit's applicable established test performance criteria and measurement instructions.

C. The parts covered by this specification document are subject to Mini-Circuits standard limited warranty and terms and conditions (collectively, "Standard Terms"); Purchasers of this part are entitled to the rights and benefits contained therein. For a full statement of the Standard Terms and the exclusive rights and remedies thereunder, please visit Mini-Circuits' website at www.minicircuits.com/MCLStore/terms.jsp

Appendix D

RG58 Data Sheet

Data Sheet

Flexible RF cable
RG_58_C/U

Description

RG: RG type RF cables

RG58, 50 Ohm, 1 GHz, 85°C, ø4.95 mm, PVC jacket

Technical Data

Construction

	Material	Detail	Diameter
Centre conductor	Copper, Tin plated	Strand-19	0.9 mm
Dielectric	PE (Polyethylene)		2.95 mm
Outer conductor	Copper, Tin plated	Braid, 96%	3.6 mm
Jacket	PVC II (low migration)	RAL 9005 - bk	4.95 mm +/- 0.15

Print: HUBER+SUHNER RG 58 C/U 50 Ohm (PA no.)

Electrical Data

Impedance	50 Ω +/- 2
Operating Frequency	1 GHz
Capacitance	101 pF/m
Velocity of signal propagation	66 %
Signal delay	5.03 ns/m
Insulation resistance	≥ 1 x 10^8 MΩm
Min. screening effectiveness	≥ 38 dB (up to 1 GHz)
Max. operating voltage	≤ 2.5 kV_{rms} (at sea level)
Test voltage	5 kV_{rms} (50 Hz/1 min)

Mechanical Data

Weight		3.7 kg/100 m
Min. bending radius	static	25 mm
	repeated (for ≤ 50 bendings)	50 mm

Environmental Data

Temperature range	-25 °C... +85 °C
Installation temperature	-20 °C... +60 °C
2011/65/EU (RoHS)	compliant

Additional Information

Ordering Information

Order as	RG_58_C/U

Remarks

(For details refer to the HUBER+SUHNER RF CABLES GENERAL CATALOGUE or contact your nearest HUBER+SUHNER partner)

Suitable Connectors

Cable group	U7 3 mm / 50 Ohm

Data Sheet

Flexible RF cable
RG_58_C/U

Matrix typical Attenuation [formula: (a*f^0.5 + b*f)] and maximum Power CW [formula: (p/f^0.5)]
Coefficients:

a = 0.3455	b = 0.2373	f_{max} = 1	P at 1GHz = 105

Frequency (GHz)	Nom. attenuation (dB / m) sea level 25° C ambient temperature	Nom. attenuation (dB / ft) sea level 25° C ambient temperature	Max. CW power (watt) sea level 40° C ambient temperature
0,05	0,09	0,027	470
0,1	0,13	0,041	332
0,15	0,17	0,052	271
0,2	0,2	0,062	235
0,25	0,23	0,071	210
0,3	0,26	0,079	192
0,35	0,29	0,088	177
0,4	0,31	0,096	166
0,45	0,34	0,103	157
0,5	0,36	0,111	148
0,55	0,39	0,118	142
0,6	0,41	0,125	136
0,65	0,43	0,132	130
0,7	0,46	0,139	125
0,75	0,48	0,145	121
0,8	0,5	0,152	117
0,85	0,52	0,159	114
0,9	0,54	0,165	111
0,95	0,56	0,171	108
1,0	0,58	0,178	105

Appendix E

MATLAB Scripts

S11 Parameters prior to tuning

```
S1 = sparameters('/Volumes/UDNAES/Sparam/10.s1p');
disp(S1)
rfplot(S1)

hold on

S2 = sparameters('/Volumes/UDNAES/Sparam/2.s1p');
disp(S2)
rfplot(S2)

hold on

S3 = sparameters('/Volumes/UDNAES/Sparam/3.s1p');
disp(S3)
rfplot(S3)

hold on

S4 = sparameters('/Volumes/UDNAES/Sparam/4.s1p');
disp(S4)
rfplot(S4)

hold on

S5 = sparameters('/Volumes/UDNAES/Sparam/11.s1p');
disp(S5)
rfplot(S5)

hold on

s11freq=s11sim.Frequency;
s11dB=s11sim.dB;
plot(s11freq,s11dB);

hold off

title('S11 parameters prior to tuning (Magnitude - dB)');
legend({'S11 element 1','S11 element 2','S11 element
 3', 'S11 element 4', 'S11 array - measured', 'S11 array -
 simulated'}, 'Location','southwest');
```

S11 parameters after tuning

```
Cab1 = sparameters('/Volumes/UDNAES/Sparam/AT_e1wc.s1p');
disp(Cab1)
rfplot(Cab1,1,1)


hold on

Cab2 = sparameters('/Volumes/UDNAES/Sparam/AT_e2wc.s1p');
disp(Cab2)
rfplot(Cab2,1,1)

hold on
Cab3 = sparameters('/Volumes/UDNAES/Sparam/AT_e3wc.s1p');
disp(Cab3)
rfplot(Cab3,1,1)

hold on

Cab4 = sparameters('/Volumes/UDNAES/Sparam/AT_e4wc.s1p');
disp(Cab4)
rfplot(Cab4,1,1)

hold on

AT000 = sparameters('/Volumes/UDNAES/Sparam/AT_02.s1p');
disp(AT000)
rfplot(AT000,1,1)

hold on

s11freq=s11sim.Frequency;
s11dB=s11sim.dB;
plot(s11freq,s11dB);

hold off
ylim([-45 0])

title('S_{11} parameters after tuning (Magnitude - dB)')
legend({'S11 element 1','S11 element 2','S11 element
 3', 'S11 element 4', 'S11 array - measured', 'S11 array -
 simulated'}, 'Location','southwest' );
```

S21 parameters (magnitude) - cables

```
Cab1 = sparameters('/Volumes/UDNAES/Sparam/Cab1.s2p');
disp(Cab1)
rfplot(Cab1,2,1)

hold on

Cab2 = sparameters('/Volumes/UDNAES/Sparam/Cab2.s2p');
disp(Cab2)
rfplot(Cab2,2,1)

hold on
Cab3 = sparameters('/Volumes/UDNAES/Sparam/Cab3.s2p');
disp(Cab3)
rfplot(Cab3,2,1)

hold on
Cab4 = sparameters('/Volumes/UDNAES/Sparam/Cab4.s2p');
disp(Cab4)
rfplot(Cab4,2,1)

hold off

title('S_{21} parameters of cables (Magnitude - dB)')
legend({'S_{21} Cable 1','S_{21} Cable 2','S_{21} Cable 3', 'S_{21}
 Cable 4'}, 'Location','southwest' );
legend('boxoff');
```

S21 parameters (phase) - cables

```
Cab1 = sparameters('/Volumes/UDNAES/Sparam/Cab11.s2p');
disp(Cab1)
rfplot(Cab1,2,1,'angle')

hold on

Cab2 = sparameters('/Volumes/UDNAES/Sparam/Cab21.s2p');
disp(Cab2)
rfplot(Cab2,2,1,'angle')

hold on
Cab3 = sparameters('/Volumes/UDNAES/Sparam/Cab31.s2p');
disp(Cab3)
rfplot(Cab3,2,1,'angle')

hold on
Cab4 = sparameters('/Volumes/UDNAES/Sparam/Cab41.s2p');
disp(Cab4)
rfplot(Cab4,2,1,'angle')

hold off

title('S_{21} parameters of cables (Angle - Degrees)')
legend({'S_{21} Cable 1','S_{21} Cable 2','S_{21} Cable 3', 'S_{21}
 Cable 4'}, 'Location','southwest' );
legend('boxoff');
```

S21 parameters (magntitude) - power splitter

```
PS1 = sparameters('/Volumes/UDNAES/Sparam/PS1.s2p');
disp(PS1)
rfplot(PS1,2,1)

hold on
PS2 = sparameters('/Volumes/UDNAES/Sparam/PS2.s2p');
disp(PS2)
rfplot(PS2,2,1)

hold on
PS3 = sparameters('/Volumes/UDNAES/Sparam/PS3.s2p');
disp(PS3)
rfplot(PS3,2,1)

hold on
PS4 = sparameters('/Volumes/UDNAES/Sparam/PS4.s2p');
disp(PS4)
rfplot(PS4,2,1)

hold off

title('S_{21} parameters of power splitter (Magnitude - dB)')
legend({'S_{21} Port 1','S_{21} Port 2','S_{21} Port 3', 'S_{21} Port
 4'}, 'Location','southwest' );
legend('boxoff');
```

S21 parameters (phase) - power splitter

```
PS1 = sparameters('/Volumes/UDNAES/Sparam/PS1.s2p');
disp(PS1)
rfplot(PS1,2,1,'angle')

hold on
PS2 = sparameters('/Volumes/UDNAES/Sparam/PS2.s2p');
disp(PS2)
rfplot(PS2,2,1,'angle')

hold on
PS3 = sparameters('/Volumes/UDNAES/Sparam/PS3.s2p');
disp(PS3)
rfplot(PS3,2,1,'angle')

hold on
PS4 = sparameters('/Volumes/UDNAES/Sparam/PS4.s2p');
disp(PS4)
rfplot(PS4,2,1,'angle')

hold off

title('S_{21} parameters of power splitter (Angle - degrees)')
legend({'S_{21} Port 1','S_{21} Port 2','S_{21} Port 3', 'S_{21} Port
 4'}, 'Location','southwest' );
legend('boxoff');
```

Radiation pattern (dc=max, vertical ref)

```
h5disp('/Volumes/UDNAES/radpattern/20190424_104047_418922.h5ant');
angles = h5read('/Volumes/UDNAES/
radpattern/20190424_104047_418922.h5ant','/angles');
Rangles = deg2rad(angles);
RTheta = deg2rad(Theta1);
start = [1 1];
count = [1 9531];
powers = h5read('/Volumes/UDNAES/
radpattern/20190424_104047_418922.h5ant','/powers',start,count);
powers_n=powers-max(powers); %normalize gain (measurement)
y = linspace(0,360,361); %to make polar plot exported from CST
 symmetric
Theta1=y(:); %to convert from row to column
RTheta = deg2rad(Theta1); %convert to radians
NGain = pplotCST.Gain-max(pplotCST.Gain); %normalize gain (simulation)
figure
pax = polaraxes;
polarplot(Rangles,powers_n);
hold on
polarplot(RTheta,NGain);
pax.ThetaZeroLocation = 'top';
rlim([-30 5]);
legend('Measured','Simulated');
```

Radiation pattern (dc=max, horizontal ref)

```
h5disp('/Volumes/UDNAES/radpattern/20190424_104435_110460.h5ant')
angles = h5read('/Volumes/UDNAES/
radpattern/20190424_104435_110460.h5ant','/angles');
Rangles = deg2rad(angles);
start = [1 1];
count = [1 9662];
powers = h5read('/Volumes/UDNAES/
radpattern/20190424_104435_110460.h5ant','/powers',start,count);
y = linspace(0,360,361); %to copy symmetric polar plot exported from
 CST
Theta1=y(:) %to convert from row to column
RTheta = deg2rad(Theta1);
NGain = pplotCST.Gain-max(pplotCST.Gain); %to normalize data
figure
pax = polaraxes;
polarplot(Rangles,powers);
hold on
polarplot(RTheta,NGain);
pax.ThetaZeroLocation = 'top';
rlim([-30 5]);
legend('Measured','Simulated');
```

Radiation pattern (dc=min, horizontal ref)

```
h5disp('/Volumes/UDNAES/radpattern/20190424_105041_012000.h5ant')
angles = h5read('/Volumes/UDNAES/
radpattern/20190424_105041_012000.h5ant','/angles');
Rangles = deg2rad(angles);
start = [1 1];
count = [1 9681];
powers = h5read('/Volumes/UDNAES/
radpattern/20190424_105041_012000.h5ant','/powers',start,count);
powers_n=powers-max(powers);
y = linspace(0,360,361); %to copy symmetric polar plot exported from
 CST
Theta1=y(:); %to convert from row to column
RTheta = deg2rad(Theta1);
NGain = pplotCST.Gain-max(pplotCST.Gain); %to normalize data
figure
pax = polaraxes;
polarplot(Rangles,powers_n);
hold on
polarplot(RTheta,NGain);
pax.ThetaZeroLocation = 'top';
rlim([-40 5]);
legend('Measured','Simulated');
```

Radiation pattern (dc=min, vertical ref)

```
h5disp('/Volumes/UDNAES/radpattern/20190424_102615_437522.h5ant')
angles = h5read('/Volumes/UDNAES/
radpattern/20190424_102615_437522.h5ant','/angles');
Rangles = deg2rad(angles);
start = [1 1];
count = [1 9568];
powers = h5read('/Volumes/UDNAES/
radpattern/20190424_102615_437522.h5ant','/powers',start,count);
y = linspace(0,360,361); %to copy symmetric polar plot exported from
 CST
Theta1=y(:); %to convert from row to column
RTheta = deg2rad(Theta1);
NGain = pplotCST.Gain-max(pplotCST.Gain); %to normalize data
figure
pax = polaraxes;
polarplot(Rangles,powers);
hold on
polarplot(RTheta,NGain);
pax.ThetaZeroLocation = 'top';
rlim([-30 5]);
legend('Measured','Simulated');
```

Emilie Udnæs

Antenna Design for UHF Satellite Communication from Sensor Nodes in the Arctic

NTNU
Norwegian University of
Science and Technology